

Holocene variations in atmospheric circulation in the North Atlantic region reconstructed from lake sediments

Marthe Gjerde



Dissertation for the degree of philosophiae doctor (PhD)
at the University of Bergen

2016

Dissertation date: 17.06.2016

© Copyright Marthe Gjerde

The material in this publication is protected by copyright law.

Year: 2016

Title: Holocene variations in atmospheric circulation in the North Atlantic region reconstructed from lake sediments

Author: Marthe Gjerde

Print: AiT Bjerch AS / University of Bergen

Scientific environment

This dissertation was carried out at the Department of Earth Science, University of Bergen and at the Bjerknes Centre for Climate Research, Bergen, Norway, in affiliation with Centre for Climate Dynamics at the Bjerknes Centre. Parts of the research were conducted at the University Centre in Svalbard, Norway. This thesis constitutes the PhD project AMOVIND and contributes to, and has received funding from, the project SHIFTS (Shifting Climate States of the Polar Regions) funded by the Norwegian Research Council. The main supervisor of this dissertation is Professor Jostein Bakke (University of Bergen), and the co-supervisors are Professor Atle Nesje (University of Bergen), Associate Professor Anne Hormes (University Centre in Svalbard/University of Gothenburg, Sweden) and Professor Raymond S. Bradley (University of Massachusetts, USA).



Department of Earth Science

Faculty of Mathematics and Natural Science

University of Bergen



Centre for Climate Dynamics

Bjerknes Centre for Climate Research



Department of Arctic Geology

University Centre in Svalbard

Acknowledgements

First I would like to thank my supervisors Jostein Bakke, Atle Nesje, Anne Hormes and Raymond Bradley for all their support and for sharing their expertise with me. Jostein Bakke is thanked in particular for designing this project, and for excellent choice of study sites where he also participated in the field work.

Big thanks go to Kristian Vasskog who has been both co-author, field assistant and provided great support and advice in writing. Thanks to my colleagues and friends at the Department of Earth Science for the great scientific and social environment, especially Hella E. Wittmeier, Lea T. Oppedal, Willem van der Bilt, Torgeir O. Røthe, Sædis Ólafsdóttir, and Eivind W. N. Støren. Everyone who helped with field work is thanked, and especially Tom Thorsen and Bjørn André Skjæret provided excellent help at Andøya and Ålfotbreen, respectively. I would also like to thank everyone who has helped with laboratory work.

Finally, I would like to thank my family and friends for all their support and love over the years, and special thanks goes to Anne Gjerde and Nina Norberg who did their best for keeping me fed and keeping my head sane over the last few weeks. Bjørn André is thanked for his remarkable patience and love.

Bergen, March 2016.

Marthe Gjerde

*Fjell lokkar ikkje meg lenger.
Eg har levt lenge nok millom kalde breddar.
Enno leitar eg meg fram i skogane, lyder
til haustvinden, stoggar ved tjørnane,
fylgjer elvane. Endå seint på året
kan du finna bær der.
Fjell lyt du yver skal du koma lenger.
Nutane fær stå der dei stend méd.*

- Olav H. Hauge

Abstract

Holocene variations in atmospheric circulation in the North Atlantic region have been reconstructed, based on three individual lake sediment studies from sites along the coast of Norway and Svalbard. This thesis contributes with new palaeoclimatic reconstructions revealing variability in wind and precipitation patterns in the northeastern North Atlantic.

In Paper I, we present a new record of Holocene glacier variability of Ålfotbreen ice cap in western Norway. By applying a novel approach of calibrating lake sediments with instrumental glacier mass-balance measurements we are able to extend glacier mass-balance variability as reflected in equilibrium-line altitude (ELA) changes for the last 1400 years. Our data suggest that deglaciation of Ålfotbreen occurred ~9700 cal yr BP, and the ice cap was subsequently absent or very small until a short-lived glacier event is seen in the lake sediments ~8200 cal yr BP. The ice cap was most likely completely melted until a new glacier event occurred around ~5300 cal yr BP. Ålfotbreen was thereafter absent (or very small) until the onset of the Neoglacial period ~1400 cal yr BP. The Little Ice Age (LIA) ~650-50 cal yr BP was the largest glacier advance of Ålfotbreen since deglaciation, with a maximum extent at ~400-200 cal yr BP, when the ELA was lowered approximately 200 m relative to today. The late onset of the Neoglacial at Ålfotbreen is suggested to be a result of its low altitude relative to the regional ELA. Further, we apply a known relationship between summer temperature and ELA variations at 10 glaciers in Norway (including Ålfotbreen) to reconstruct winter precipitation during the last 1400 years.

In Paper II, we present a lake record from lake Hakluytvatnet at Amsterdamøya island, the northwesternmost island on Svalbard. The lake sediment archive reveals large environmental changes that have taken place at Hakluytvatnet since the Late Glacial, as detected by multi-proxy analyses including physical sediment properties and diatom analysis. A robust chronology has been established for the lake sediment core through 28 AMS radiocarbon (^{14}C) ages, and this gives an exceptionally well-constrained age control for a lake at this latitude (79.5°N) that is not varved. The

sedimentary archive recorded the last ~13,000 years of climate change, and is the first lake record going back to the Late Glacial at this site. Our findings indicate that a local glacier was present during the Younger Dryas (YD), and we estimate YD equilibrium-line altitude (ELA) lowering. Further, we construct a new time-series reflecting precipitation-based detrital sediments entering Hakluyvatnet (i.e., runoff) covering the period from ~5000-1300 cal yr BP. We discuss our runoff record and the internal productivity of the lake towards a record of varying sea ice extent in the Fram Strait acting as a moisture source area for Hakluyvatnet.

In Paper III, a late-Holocene record of storminess in Arctic Norway is reconstructed from aeolian sediment input into the coastal lake Måvatnet, Andøya island. The study site is situated at the extreme west coast of Arctic Norway; a sensitive location for changes in North Atlantic westerly winds. Through a novel approach, combining monitoring of wind-blown lake sedimentation in sediment traps with multi-proxy analyses of lake sediments we quantify the input of wind-blown sand from a west-facing beach acting as source area into lake Måvatnet during the late-Holocene. We further assess the validity of this record to represent variations in the strength of the westerlies (i.e., storminess). The high-resolution record reveals an abrupt increase in storminess synchronously with the onset of the Little Ice Age (LIA), ca. 600 cal yr BP, coeval with increased winter precipitation at Ålftobreen (Paper I) and a strengthening of the persistent low-pressure west of Iceland (Icelandic Low) that exerts a strong effect on North Atlantic storm tracks. Further, the timing of the onset of the LIA along the coast of Norway appears to be linked to the dynamics of the large-scale atmospheric circulation systems in the North Atlantic.

List of publications

- Paper I: Gjerde, M., Bakke, J., Vasskog, K., Nesje, A., Hormes, A. (2016). Holocene glacier variability and Neoglacial hydroclimate at Ålfotbreen, western Norway. *Quaternary Science Reviews*, 133. pp 28-47. doi:10.1016/j.quascirev.2015.12.004
- Paper II: Gjerde, M. Bakke, J., D'Andrea, W., Balascio, N.S., Bradley, R.S., Vasskog, K., Ólafsdóttir, S., Røthe, T.O., Perren, B., Hormes, A.: Late Glacial and Holocene multi-proxy environmental reconstruction from Lake Hakluytvatnet, Amsterdamøya Island, Svalbard (79.5°N). *Submitted to Special Issue: 'Post-glacial/Holocene conditions on Amsterdamøya Island', Quaternary Science Reviews.*
- Paper III: Gjerde, M., Bakke, J.: Increased storminess at Andøya (Arctic Norway) during the Little Ice Age reconstructed from lake sediments. *Submitted to Quaternary Research.*

The published paper (Paper I) is reprinted with permission from Quaternary Science Reviews. All rights reserved.

Contents

SCIENTIFIC ENVIRONMENT	3
ACKNOWLEDGEMENTS	4
ABSTRACT	7
LIST OF PUBLICATIONS	9
CONTENTS	10
OUTLINE	11
INTRODUCTION	12
RESEARCH OBJECTIVES	13
BACKGROUND.....	14
STUDY AREA	17
METHODOLOGICAL APPROACH	20
PAPER I – GLACIER RECONSTRUCTION (WESTERN NORWAY).....	28
PAPER II – RUNOFF RECONSTRUCTION (NORTHWEST SVALBARD).....	30
PAPER III – STORMINESS RECONSTRUCTION (ARCTIC NORWAY)	32
SYNTHESIS AND FUTURE PERSPECTIVES	34
REFERENCES	37
PAPER I	45
PAPER II	79
PAPER III	119

Outline

This thesis consists of an introduction and three individual papers. In the introduction, I present a short overview of the scientific background and the main research objectives of the study. The study areas and the methodological approaches are thereafter presented. The three papers are introduced, and the palaeoclimatic implications that can be drawn from the results are discussed and I assess potential future research that can build on the findings from this thesis.

The second part contains the three papers that form the Ph.D. thesis. In Paper I, a new record of Holocene glacier variability of the ice cap Ålfotbreen in western Norway is presented. Further, a novel approach coupling lake sediments with instrumental glacier mass-balance measurements allows for calibration of our lake record that is used to extend glacier mass balance variability reflected in equilibrium-line altitude (ELA) changes back in time. Finally, we apply a known relationship between summer temperature and ELA variations at 10 glaciers in Norway (including Ålfotbreen) to reconstruct winter precipitation during the last 1400 years. In Paper II, we perform multi-proxy analyses of lake sediments to reconstruct climate at Amsterdamøya, Svalbard. The robustly dated high-Arctic record reveals the large environmental changes impacting lake sedimentation that have taken place since the Late Glacial. Further, we construct a new time-series reflecting precipitation-based sedimentation (i.e., runoff) covering the last ~5000 years, and we discuss our record towards a sea ice extent record. In Paper III, we quantify the input of wind-blown sand from a beach into a lake during the late-Holocene at Andøya, Arctic Norway, and assess the validity of this record to represent variations in storminess. Through a novel approach, combining monitoring of wind-blown lake sedimentation in sediment traps with multi-proxy analyses of the lake sediments, we are able to construct a storminess record that indicates a strengthened wind climate in northern Norway at the onset of the Little Ice Age (LIA, 600 years ago), coeval with the onset of increased winter precipitation at Ålfotbreen.

Introduction

Only palaeoclimatic reconstructions offer the possibility to extend earth system observations beyond the instrumental time period. Such reconstructions are especially important in the Arctic (defined here as north of 60°N) because the rate of on-going change is unprecedented within Common Era observations, and the changes we see today are urgently needed to be put into a longer time perspective. Our knowledge of natural climate variability in the Arctic is limited due to the scarcity of data and the relatively short period of observation. Projected anthropogenic forcing on climate (IPCC, 2013) will be superimposed on these natural variations, which might result in fundamental changes to internal climate feedback mechanisms, influencing the timing and amplitude of future climate. This leads to a critical emerging question in the scientific community: how will the effects of global warming be manifested in the Arctic? To make meaningful climate projections at the regional scale and to evaluate model simulations of future climate, we need a longer perspective than the short instrumental period provides. Palaeoclimate data yield a longer-term perspective on climate system variability, and on the interaction between climate systems and associated feedbacks that further modify the forcing (Bradley, 2000). New methodologies and improved techniques allow for high-resolution palaeoclimate reconstructions, and this thesis aims to employ both recently developed and traditional lake sediment techniques to produce high-resolution time-series of past changes in climate. The novel palaeoclimate records are thereafter assessed in a palaeoclimatic context, and the implications and contributions from this thesis are synthesized. Finally, a proposal for future research building on this thesis is outlined.

Research objectives

In light of the introduction to the significance of palaeoclimatic research, the scientific rationale behind this PhD thesis can be formulated in the following research question:

To what extent can analyses of physical and geochemical lake sediment properties be used to quantify earth surface processes such as wind, runoff and glacier activity, and how it is possible to upscale these processes to large-scale atmospheric variability in the North Atlantic region?

This main research question is thereafter approached at three distinct study sites, applying both comparable and alternative methods where the common denominator is the focus on investigating and detecting atmospheric circulation variability as reflected in lake sediments. Thus, the objectives of this thesis are:

- Apply quantitative glacier reconstructions and winter precipitation reconstructions from the maritime ice cap Ålfotbreen in western Norway as a proxy for winter hydroclimate
- Resolve which sedimentary properties can be used as a proxy for runoff in a high-Arctic lake catchment on Svalbard through a multi-proxy approach
- Investigate the relationship between grain-size distribution and aeolian transport in an Arctic lake in Northern Norway
- Decipher the natural variability and rate of change in the strength and spatial patterns of the westerlies in Arctic Norway and Svalbard during the late-Holocene

Background

The northeastern (NE) North Atlantic region is a key area in climate research, as the dynamic properties of the prevailing atmospheric and oceanic systems can change in a rapid pace, both spatially and temporally, and have done so in the past (e.g. Bianchi and McCave, 1999). This thesis is based on work from three sites chosen on a south-north transect across coastal Norway and Svalbard to explore past atmospheric circulation changes and hydroclimate variability as recorded in lake sediments. The three study sites are targeted on the basis of their potential to record past changes in atmospheric circulation patterns reflected in precipitation- and wind-induced sedimentation to the lakes. A common focus of the three papers has been to understand the impact of changing atmospheric circulation on earth surface processes and their sedimentary signature in the lake sediments.

Large-scale implications of projected climate warming (IPCC, 2013) can only be assessed when considering complex teleconnection patterns that are affecting the climate system, and to infer future climate change we rely on climate models that build on palaeoclimate data and instrumental data. Data on past variability of atmospheric circulation patterns are urgently needed in global climate models, as the future warmer climate will likely affect precipitation patterns and storm tracks (IPCC, 2013), which in turn will impact human societies manifested in e.g. increasing numbers of floods and droughts. Globally, there are numerous palaeoclimate reconstructions produced, encompassing various proxies in records from e.g. ice cores, peat bogs, marine sediments, tree-rings, speleothems, and lake sediments; all of which can be used to improve our knowledge on past natural climate variability and enhance the robustness of future projections in climate models. However, seasonal reconstructions from various proxies in palaeoclimate archives is not straightforward. Reconstructions of summer season climate (e.g. July temperature from pollen or chironomids) are copious due to the biological and faunal productivity seasons occurring mostly during spring/summer. Winter season climate reconstructions are subsequently limited in numbers, although a few direct winter season proxies are recognized, such as isotopes reflecting permafrost variability (e.g.

Meyer et al., 2015), and glacier reconstructions from glaciers reflecting mainly winter season signal as well as winter precipitation reconstructions (Dahl and Nesje, 1996; Nesje et al., 2001; Nesje and Matthews, 2012). As this thesis focuses on proxies mostly reflecting winter season climate, it therefore opts to offer a seasonal contribution to the endeavour of the palaeoclimate community.

Late Glacial and Holocene climate in the northeastern North Atlantic – a climatic and chronological framework

The last remnants of the northern hemisphere (NH) ice-sheets disintegrated after the Last Glacial Maximum (LGM, ~20 ka), and the Younger Dryas (YD: 12.9-11.7 ka; Rasmussen et al., 2006) marked the final readvance of the Scandinavian Ice Sheet before complete deglaciation. NH summer season solar insolation was at its maximum during the early Holocene (Berger and Loutre, 1991), and the early Holocene climate was punctuated by cooling induced by meltwater pulses from remnants of the decaying ice sheets, leading to unstable climate in the North Atlantic (Fleitmann et al., 2008; Kleiven et al., 2008). The succeeding warmer period termed the Holocene Thermal Maximum (HTM) was especially pronounced in the high-Arctic (Renssen et al., 2009), and might therefore serve as an important reference period for future warmer climate and the consequence for high-Arctic and polar areas reflected in e.g. diminishing sea-ice, vegetation changes, and glacier melt. The mid- to late-Holocene climate in the NE North Atlantic can be explained in the context of a decreasing trend of summer insolation forcing a summer season cooling (Vinther et al., 2006), superimposed by mechanisms and feedback processes such as solar activity and volcanic forcing further modulating the climate (Wanner et al., 2008). Around 4 ka, the NH cooling led to a weaker meridional overturning circulation and the southward displacement of the Intertropical Convergence Zone (ITCZ) (Haug et al., 2001; Mayewski et al., 2004); intensifying the westerlies over the North Atlantic which is illustrated by increased glacier activity in the region (i.e. the 'Neoglacial'; e.g. Nesje, 2009; Solomina et al., 2015). In Scandinavia, numerous glacier reconstructions reveal a consistent pattern, with larger glacier activity since the onset

of the Neoglacial and the glacier reconstructions point to a combination between external forcing factors (i.e., solar insolation) and regional weather modes as the dominant control of glacier activity (Nesje, 2009). The transition from the warmer HTM into the colder and wetter late Holocene occurred in concert with an increased dominance of Atlantic water along the western coast of Norway (Risebrobakken et al., 2003). The Little Ice Age (LIA) (~600-100 cal yr BP) was a relatively cold period with glacier advances at several sites globally (Grove, 2001; Matthews and Briffa, 2005) and intensification of NE North Atlantic wind climate (Lamb, 1979). However, the climate dynamics explaining the LIA are not yet fully understood and neither is the full extent spatially or temporally (e.g. Bradley and Jones, 1993; Nesje and Dahl, 2003; Mann et al., 2009). This thesis aims to provide insight into the timing of the LIA at two sites in Norway as well as the palaeoclimatic inferences that can be drawn from the reconstructions, thereby presenting a framework for future studies to investigate the LIA in a context of storminess and glacier advances imposed by variations in westerly winds along the coast of Norway.

Study area

The three lakes investigated are all situated in the northeastern sector of the North Atlantic, covering almost twenty degrees of latitude from 61°-79°N (Fig. 1). The coastal setting implies that the climate at all sites is strongly affected by the relatively warm North Atlantic Current (NAC), the northern continuation of the Gulf Stream; and their downwind position of the associated westerly winds that transport warmer air masses northwards. The study areas are consequently characterised by relatively warm winters despite their high-latitude location.

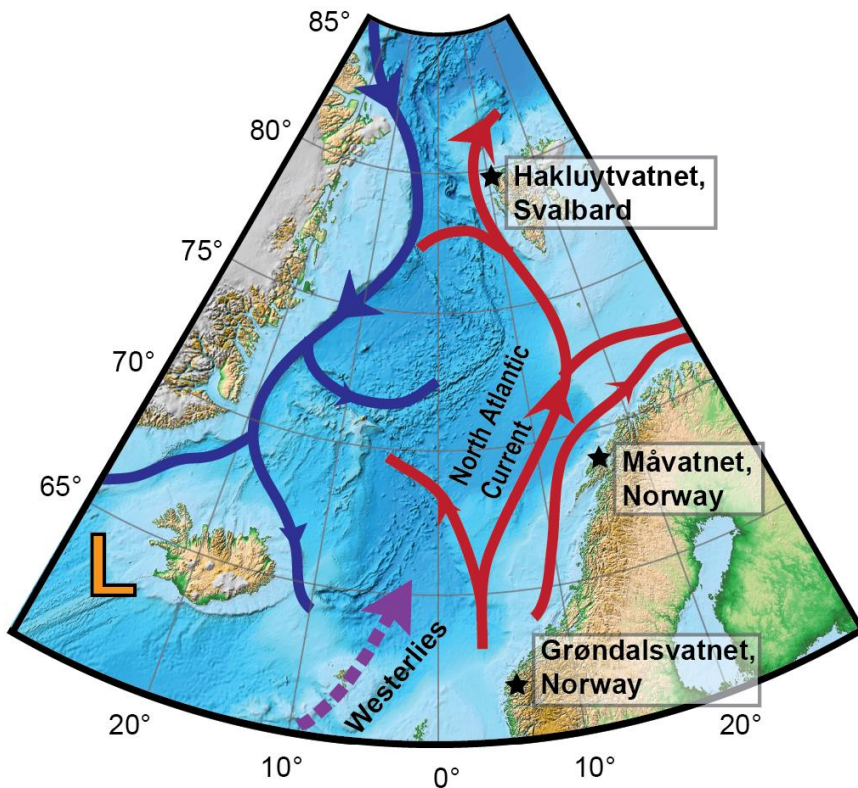


Figure 1: Overview of study sites (black asterisks) in the northeastern North Atlantic region (bathymetric data: ETOPO1 Global Relief Model, NOAA). Warmer Atlantic currents in red, colder Arctic waters in blue. Dashed purple arrow illustrates westerly winds; orange ‘L’ denotes position of the persistent low-pressure system west of Iceland (Icelandic Low) that exerts a strong effect on North Atlantic storm tracks.

Atmospheric circulation in the northeastern North Atlantic

The Arctic Oscillation (AO) and the North Atlantic Oscillation (NAO) constitute the most prominent modes of winter climate variability in the northern hemisphere (Wanner et al., 2001), transporting atmospheric masses from the mid-latitudes to high-latitudes in the North Atlantic with a shared winter storm track between the NE North Atlantic and the Arctic (Rogers and McHugh, 2002). The AO/NAO modes are quantified by variations in the sea level pressure gradient, which is reflected in the strength and position of the westerly winds. The bimodal pattern of the AO constitutes the shifting state of the annular pattern of higher air-pressure over the NH polar region where the associated temperature and polar jet stream shift concurrent with air pressure oscillations. During positive AO (AO+), the pattern of the AO is sustained annular in shape by a strong high-pressure system preserved by strong upper-stratospheric level winds manifested in the jet stream marking the transition between Arctic and warmer air masses south of the Arctic and the outer extent of the AO, thereby allowing warmer air masses from the south to reach further north. During a negative phase of the AO (AO-), a weaker high-pressure system over the polar region allows for cold polar air to penetrate further south, and induces a more ‘wobbly’ extent of the jet stream, which is also weakened, allowing for cold polar air masses to reach further south. Analogous to the AO, the North Atlantic Oscillation is considered the dominant winter-season mode of atmospheric variability in the North Atlantic (e.g. Marshall et al., 2001; Pinto and Raible, 2012), responsible for the meridional atmospheric heat transport from the tropics to the Arctic latitudes (Fig. 2). The NAO is often defined as an index based on mean sea level pressure (SLP) differences between Stykkisholmur, Iceland, where a persistent low-pressure system (Icelandic Low, Fig. 1) is situated, and a high-pressure system situated at the Azores (Azores High). Though, the position of the NAO centres of action may shift over space and time (Pinto and Raible, 2012). The difference in SLP between these two indexed sites tend to vary as such that when the low-pressure outside Iceland is lower than average, the high-pressure system at the Azores is higher than average, and vice versa; if the Icelandic Low is less pronounced, the Azores High is lower than average. This implies that the meridional pressure gradient is larger when the index is high

(positive NAO; NAO+), thereby transporting warmer air accompanied by stronger meridional (westerly) winds and steering winter storms and precipitation to northern Europe (Fig. 2A), and simultaneously resulting in sunny, dry conditions in mid- and southern Europe. The wintertime westerlies over southern Norway are closely linked with the NAO (e.g. Nordli et al., 2005) and a positive NAO often leads to high accumulation of mass in Norwegian glaciers (Hurrell, 1995). As the AO/NAO are most pronounced during winter, we opt to test if our winter season reconstructions reflect variability in North Atlantic atmospheric modes and in particular the NAO which may further reflect the westerly winds that hold a key position in modulating the amount of precipitation that reaches the coast of Norway and Svalbard. A potential for detecting changes in the position and strength of the westerlies (e.g. Bakke et al., 2008) lies in investigating the south-north transect presented in the three papers.

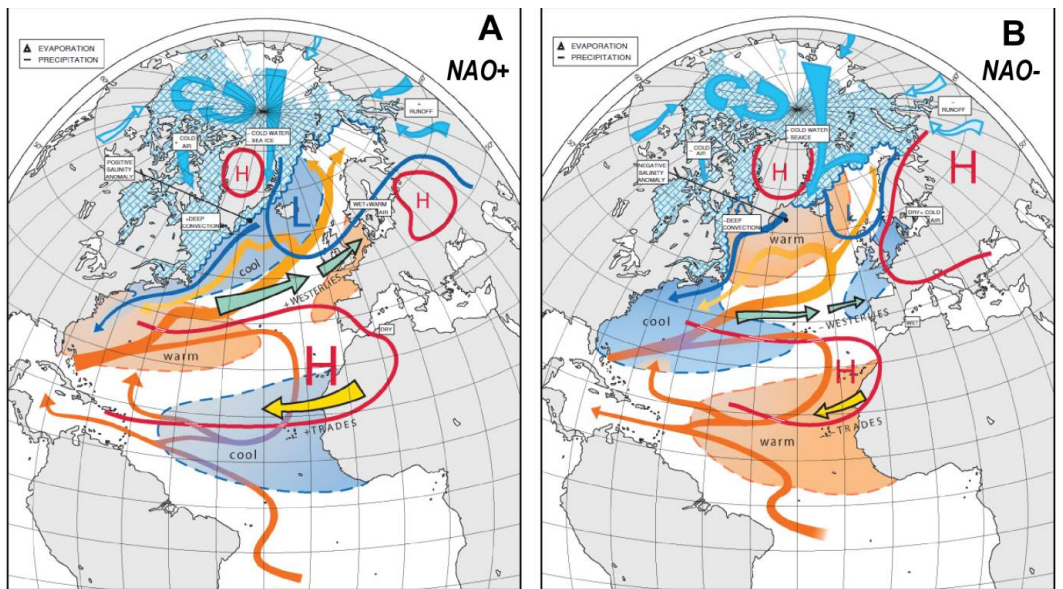


Figure 2: This figure adapted from Pinto and Raible (2012) and Wanner et al. (2001) illustrates schematically the states of the NAO and the implications for North Atlantic climate following the interplay between the two states: A) positive NAO (NAO+), B) negative NAO (NAO-).

Methodological approach

Lakes act as archives for recording climate variations by continuously recording autochthonous (internally produced) and allochthonous (from outside the lake) sediment accumulation. There are several processes affecting lake sedimentation, and in order to utilize lake sediments as climate archives we must evaluate and fingerprint different sedimentary sources to assess climatic impact as well as local catchment processes affecting sediment accumulation. In this thesis, a combined approach based on geomorphological mapping of the catchment areas with lake sediment analysis allow for robust inferences on how climate variability has affected sediment accumulation in the lakes. Geomorphological mapping allows for inferences on modern catchment sedimentation processes (e.g. Bakke et al., 2005a; Berntsson et al., 2015) and can be particularly helpful when combining with lake sediment analyses to avoid misinterpretation (Ballantyne, 2002). By performing a combined echo sounding and ground-penetrating radar (GPR) survey of the lake bathymetry and sediment thickness prior to coring at all sites, we attempted to detect suitable coring sites that held relatively thick sedimentary sequences (i.e., higher sediment accumulation rates allowing for high-resolution analysis), and without mass-movement deposits protruding into the coring site thereby perturbing the stratigraphic resolution. This approach has been followed at all coring sites and is suggested to be applied as a standard method before coring lake sediments. Coring a combination of longer piston cores (Nesje, 1992) and shorter gravity cores (HTH/UWITEC) enable a continuous sedimentary archive to be extracted, including the sediment-water interface containing modern sediment accumulation that can be age-determined by e.g. ^{210}Pb dating for calibration with instrumental data such as glacier mass-balance measurements. The short core(s) can thereafter tentatively be coupled with the longer piston core(s) and the sedimentary record can thus be extended.

Analyses of lake sediments

The interplay between autochthonous and allochthonous sediments and their relative contribution to lake sediment accumulation vary over time and space, and disentangling these factors are crucial in order to make robust palaeoenvironmental interpretations. A range of laboratory methods were applied at all three sites, and are briefly explained below. The site-specific applications of the different proxies employed are thereafter described as the lake settings are contrasting and distinct proxies had to be applied to infer palaeoclimate from the individual sites.

Magnetic properties may inform on changes in detrital sediment in-wash from the catchment, and are therefore widely applied in lake sediment studies (Thompson et al., 1975; Snowball et al., 1999). Various processes transporting minerogenic input to a lake basin are responsible for bringing different types of allochthonous sediments into a lake, and distinct magnetic signatures can be detected when combining lake sediments with sediment soil samples from the various sources in a catchment to infer relative contribution to detrital input variability back in time (Vasskog et al., 2012; Wittmeier et al., 2015). X-ray fluorescence scanning (XRF) using an ITRAX scanner (Croudace et al., 2006) enables rapid, non-destructive qualitative geochemical profiling, and provides high-resolution elemental results that are frequently applied in lake sediment studies (Croudace and Rothwell, 2015). In all three papers, we have applied high-resolution XRF scanning as a tool for inferring variability in sedimentary input to the lake sediments (Davies et al., 2015). Weight loss-on-ignition (LOI,%), dry bulk density (DBD, g/cm³), and water content (WC,%) (Dean, 1974; Heiri et al., 2001) comprise frequently applied physical sediment parameters that have been analysed at all sites. LOI acts as an indicator of organic content, whereas DBD reflects the mass of dry solids in a given bulk volume (Brady and Weil, 1996). As DBD reflects detrital input it has been found to show a close relationship with e.g. glacier equilibrium-line changes as increased glacier erosion during periods with larger glacier extent enhances glacial sediment in-wash to lake sediment accumulation (e.g. Bakke et al., 2005a; Bakke et al., 2010). Relative changes in grain-size distribution (GSD) may reveal changes in catchment processes that have been

induced by earth surface processes, and GSD changes can allow for identification of the relative contribution of different sediment sources in a catchment and how they have varied over time. Further, grain-size analysis can be used to validate e.g. a detrital signal from DBD and can identify whether a large discrepancy in DBD, LOI or other physical parameters originate from mass-wasting deposits (see below). Recent studies also point out the possibility of high-resolution grain-size analysis in combination with modelling to infer process-specific variability in catchments (Dietze et al., 2012). To further differentiate between the various sedimentary impacts on lake sedimentation, and to explore the multivariate datasets consisting of large amounts of qualitative and quantitative data we employed Principal Component Analysis as a statistical tool.

Episodic sediment input complicate continuously deposited sediments and may perturb sediment accumulation rates (Rubensdotter and Rosqvist, 2009). These short lived 'event' layers can result from several processes such as floods (Støren et al., 2010; Schillereff et al., 2014), avalanches (Nesje et al., 2007), debris flows and other gravitational processes (Sletten et al., 2003), or as a combination of several processes (Nesje et al., 1995; Vasskog et al., 2011). Identification of these short-lived events in the sedimentary sequence may further enable climatic interpretation (Støren et al., 2012; Støren and Paasche, 2014). In all three papers, we have aimed at detecting any visible event layers and subsequently omitted them from age-depth models. We examined various statistical approaches (e.g. Støren et al., 2010) and geochemical ratios (e.g. Vasskog et al., 2011; Wittmeier et al., 2015) but found no significant universal proxy that could be applied to detect event layers at all sites, and we therefore visually inspected the cores and critically evaluated any inferred event layer before omitting from age-depth modelling. A final, important remark regarding use of lake sediments as palaeoenvironmental archives include a thorough assessment of potential anthropogenic influence on lake sedimentation that may cause misinterpretation of the sediment record (Augustsson et al., 2013), and we have aimed at identifying any possible human-induced sedimentary source of error.

Finally, to contextualize and compare our findings with other records a chronological framework must be established. Chronological control is arguably the most important parameter when constructing palaeoclimate time-series, and in this thesis a particular focus has been on constructing robust chronological age-depth relationships and evaluating model output. By omitting event layers and unreliable radiocarbon ages we have aimed at constructing as robust age-depth relationships as possible. The age-models applied are chosen based on the prior knowledge from individual ^{14}C radiocarbon ages and ^{210}Pb ages obtained, and from several runs and subsequent validations of the age-model output.

Assessing the uncertainties and potential pitfalls in lake sediment analyses, a combination of geomorphological mapping and thorough pre-coring analyses are suggested to ensure suitable coring sites for high-resolution continuous lake sediment studies. Further, a comprehensive understanding of past and modern sedimentation processes affecting lake sedimentation is essential for elucidating climatically forced versus local catchment impact on lake sedimentation. Figure 4 shows a selection of catchment processes affecting lake sedimentation, and highlights the importance of careful selection of coring locations prior to palaeoclimatic inferences.

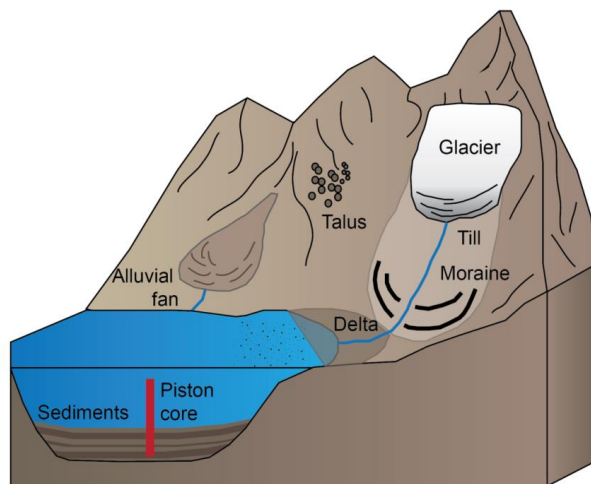


Figure 3: Conceptual figure showing selected catchment processes affecting lake sedimentation.

Utilizing distal glacier-fed lake sediments for quantitative reconstructions of glacier fluctuations and winter precipitation

Glaciers are sensitive indicators of climate change; however, as they integrate both ablation-season (summer) temperature and accumulation-season (winter) precipitation signals, the very nature of glaciers makes it difficult to separate between the main controlling factors in records of past glacier activity. Distal glacier-fed lakes act as traps for glacially eroded sediments that are transported by glacial meltwater streams down-valley, and by quantifying the influx of glacial sediment to these lakes it is possible to reconstruct continuous changes in upstream glacial erosion and hence glacier size through time. Pioneering work on distal glacier-fed lake sediments introduced the methodology where LOI was used as an inverse indicator for glacier activity (Karlén, 1976). This methodology, however, encounters the problem that there will always be some part of the minerogenic sediments that does not originate from glacial erosion (Jansson et al., 2005). Consequently, novel proxies and methodologies have been developed and applied to glacier-fed lake sediments in order to better quantify the actual contribution from upstream glacial erosion to the lake sediments (e.g. Karlén, 1981; Nesje et al., 1991; Dahl and Nesje, 1992; Karlén and Matthews, 1992; Dahl and Nesje, 1994; Leemann and Niessen, 1994; Nesje et al., 1995; Matthews et al., 2000; Nesje et al., 2000; Nesje et al., 2001; Dahl et al., 2003; Lie et al., 2004; Rosqvist et al., 2004; Bakke et al., 2005a; Bakke et al., 2005b; Osborn et al., 2007; Shakesby et al., 2007; Bakke et al., 2010; Vasskog et al., 2012; Bakke et al., 2013; Røthe et al., 2015; Wittmeier et al., 2015). Some of these records present only relative changes in glacial input to the lakes, but in cases where dated moraine ridges are available to reconstruct the glacier extent at specific points in time, lake records can be calibrated to produce continuous reconstructions of changes in equilibrium-line altitude (ELA) (e.g. Nesje et al., 2001; Dahl et al., 2003; Bakke et al., 2010; Røthe et al., 2015).

Lake Grøndalsvatnet (Paper I) is a distal glacier-fed lake in western Norway, and has previously been investigated by Nesje et al. (1995). However, their coring location situated in front of a colluvial fan was not optimal due to numerous mass movement

deposits found in the core that obstructed continuous glacier sediment accumulation. A vital part of this project was therefore to carefully select coring sites in order to avoid obtaining cores containing event layers by performing a thorough GPR survey of the lake bathymetry and sediment thickness prior to coring. The age of the moraines situated in front of Ålfotbreen ice cap representing previous larger glacier extents are unknown, and we therefore tentatively applied the mass-balance measurements going back to CE1963 to calibrate with our proxy record for glacier eroded-material (high-resolution XRF titanium count rates). If an independent record of summer temperature is available, estimates of past winter precipitation can be extracted from continuous ELA reconstructions (e.g. Dahl and Nesje, 1996; Bjune et al., 2005) through the so-called ‘Liestøl equation’ described by O. Liestøl in Sissons (1979); a mathematical expression based on the empirical relationship between annual precipitation and summer temperature at the ELA of ten Norwegian glaciers (including Ålfotbreen; Fig. 4). The ‘Liestøl equation’ was therefore applied in Paper I by implementing our ELA reconstruction covering the last ~1400 years with a temperature reconstruction from Mann et al. (2009) that we calibrated with instrumental summer temperatures from Bergen, Norway. Our novel approach of calculating ELA and winter precipitation is suggested to be applied at other sites where lack of (dated) moraines complicates the accurate timing and extent of past glacier advances, although this requires instrumental measurements of ELA.

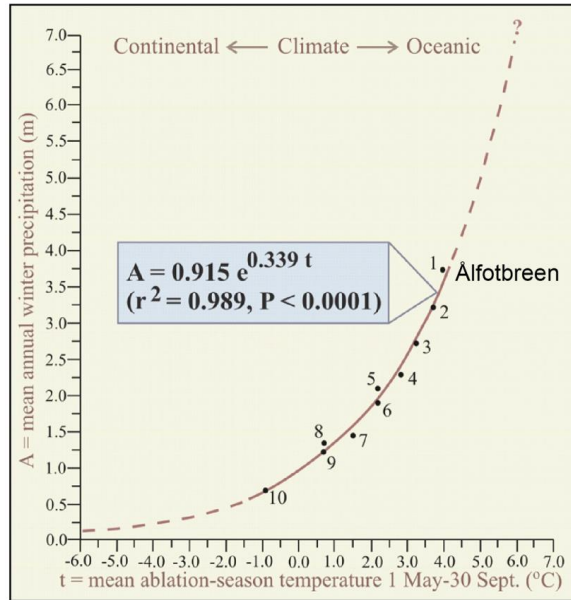


Figure 4: The exponential relationship between temperature and precipitation at the ELA of 10 glaciers in Norway. This relationship implies that if the former ELA is known, it is possible to calculate how the other parameters have fluctuated, and is applied in Paper I. Figure adapted from Bakke (2004), based on Liestøl in: Sissons (1979).

Reconstructing precipitation-induced detrital sedimentation (runoff) in lake sediments

Lake Hakluytvatnet, Amsterdamøya island (Svalbard), was cored in an attempt of reconstructing precipitation-induced runoff to the (presently) non-glaciated catchment (Paper II). By high-resolution grain-size analysis, we aimed at identifying the sediment reaching lake Hakluytvatnet as runoff; i.e. precipitation-induced detrital input. The lack of glacier-meltwater entering the lake over (at least) the last 5000 years along with geomorphic mapping of the flat valley bed implies that the dominant source for minerogenic input to lake Hakluytvatnet over the last 5000 years was silt-sized sediment originating from precipitation and/or spring melt from the catchment.

Multi-proxy analysis of the lake sediments including diatom and high-resolution geochemical XRF scanning further revealed the large environmental shifts that have taken place since the Late Glacial at Amsterdamøya island, which in turn strongly affected lake sedimentation. Also, the strikingly high organic content of the sediment representing ~5000-1300 cal yr BP at this latitude (79.5°N) was explored in an attempt of constructing a high-resolution radiocarbon chronology of the lake sediment fill and the results indicate that high-resolution age-depth relationships are possible even in non-varved high-Arctic lakes by careful selection of sites. Thus, we were able to construct a new high-resolution time-series of inferred precipitation-induced detrital in-wash to the lake.

Fingerprinting the aeolian member of lake sedimentation

In Paper III, we present a novel methodological approach employing sediment trap monitoring and lake sediment analyses of Måvatnet lake, Andøya (Arctic Norway) in order to identify the aeolian component of lake sedimentation as a proxy for past extreme wind activity (i.e., storminess). Understanding the surrounding catchment processes in conjunction with sea-level changes is a vital part of explaining past sediment accumulation in Måvatnet. Utilizing sediment traps as a methodological approach to detect aeolian sedimentation is examined in several studies (e.g. Lancaster, 2002), and a few studies have combined sediment trap monitoring with sediment core studies (and hydrological data) (e.g. Schillereff et al., 2015). Studies from peat bogs in southwest Sweden have used grain-size analysis for aeolian sediment fingerprinting, and suggest increased sand content in peat cores as a proxy for increased wind activity (Björck and Clemmensen, 2004; de Jong et al., 2006; de Jong et al., 2007; de Jong et al., 2009). At Måvatnet we attempted a similar approach using grain-size distribution as a proxy for aeolian sedimentation in the lake. We further statistically determined higher-resolution geochemical (XRF) proxies that reflected the aeolian grain-size member and could thus produce a high-resolution storminess record covering the late-Holocene.

Paper I – Glacier reconstruction (western Norway)

Glaciers and small ice caps respond rapidly to climate perturbations (mainly winter precipitation, and summer temperature), and the mass-balance of glaciers located in western Norway is governed mainly by winter precipitation (Pw). Records of past Pw can offer important insight into long-term changes in atmospheric circulation, but few proxies are able to accurately capture winter climate variations in Scandinavia. Reconstructions of equilibrium-line-altitude (ELA) variations from glaciers that are sensitive to changes in Pw therefore provide a unique opportunity to quantify past winter climate in this region. Here we present a new, Holocene glacier activity reconstruction for the maritime ice cap Ålfotbreen in western Norway, based on investigations of distal glacier-fed lake sediments and modern mass balance measurements (1963-2010). Several lake sediment cores have been subject to a suite of laboratory analyses, including measurements of physical parameters such as dry bulk density (DBD) and loss-on-ignition (LOI), geochemistry (XRF), surface magnetic susceptibility (MS), and grain-size distribution, to identify glacial sedimentation in the lake. Both radiocarbon (AMS ^{14}C) and ^{210}Pb dating was applied to establish age-depth relationships in the sediment cores. A novel approach was used to calibrate the sedimentary record against a simple ELA model, which allowed reconstruction of continuous ELA changes for Ålfotbreen during the Neoglacial (when Ålfotbreen was present, i.e. the last ~1400 years). Furthermore, the resulting ELA variations were combined with an independent summer temperature record to calculate Neoglacial Pw using the 'Liestøl'-equation. The resulting Pw record is of higher resolution than previous reconstructions from glaciers in Norway and shows the potential of glacier records to provide high-resolution data reflecting past variations in hydroclimate. Complete deglaciation of Ålfotbreen occurred ~9700 cal yr BP, and the ice cap was subsequently absent or very small until a short-lived glacier event is seen in the lake sediments ~8200 cal yr BP. The ice cap was most likely completely melted until a new glacier event occurred around ~5300 cal yr BP, coeval with the onset of the Neoglacial at several other glaciers in southwestern Norway. Ålfotbreen was thereafter absent (or very small) until the onset of the

Neoglacial period ~1400 cal yr BP. The ‘Little Ice Age’ (LIA) ~650-50 cal yr BP was the largest glacier advance of Ålfotbreen since deglaciation, with a maximum extent at ~400-200 cal yr BP, when the ELA was lowered approximately 200 m relative to today. The late onset of the Neoglacial at Ålfotbreen is suggested to be a result of its low altitude relative to the regional ELA. A synthesis of Neoglacial ELA fluctuations along the coast of Norway indicates a time-transgressive trend in the maximum extent of the LIA, which apparently seems to have occurred progressively later as we move northwards. We suggest that this trend is likely due to regional winter precipitation differences along the coast of Norway.

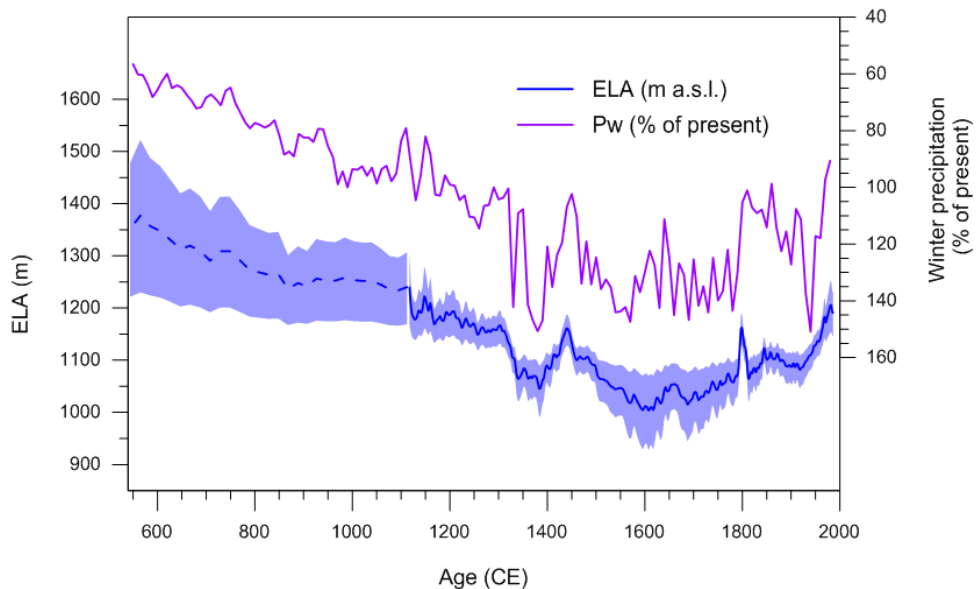


Figure 5: Reconstructed ELA and winter precipitation (% of present, inverted) from Ålfotbreen (Paper I). Note the co-variance of the two parameters, reflecting the close relationship between winter precipitation and annual glacier mass balance ($R^2 = 0.71$) (glacier mass balance data: Kjølmoen, 2011).

Paper II – Runoff reconstruction (northwest Svalbard)

Robust records of past climatic changes are sparse and poorly resolved in the Arctic due to low organic production that restricts the use of radiocarbon dating and challenging logistics that make data collection difficult. Here, we present a new lake record from lake Hakluytvatnet at Amsterdamøya island (79.5°N), the northwesternmost island on Svalbard. Multi-proxy analyses of lake sediments in combination with geomorphological mapping reveal large environmental shifts that have taken place at Amsterdamøya since the Late Glacial. A robust chronology has been established for the lake sediment core through 28 AMS radiocarbon (¹⁴C) ages, and this gives an exceptionally well-constrained age control for a lake at this latitude. The sedimentary archive recorded the last ~13,000 years of climate change, and is the first lake record going back to the Late Glacial at this site. Our findings indicate that a local glacier was present during the Younger Dryas (YD), and we estimate YD equilibrium-line altitude (ELA) lowering. Further, the Holocene was a period with large changes in the Hakluytvatnet catchment, and the onset of the Neoglacial (ca. 5 ka) marks the start of modern-day conditions in the catchment. The Neoglacial is characterized by fluctuations in the minerogenic input to the lake as well as internal productivity, and we suggest that these fluctuations are driven by atmospherically forced precipitation changes as well as sea ice extent modulating the amount of moisture that can reach Hakluytvatnet.

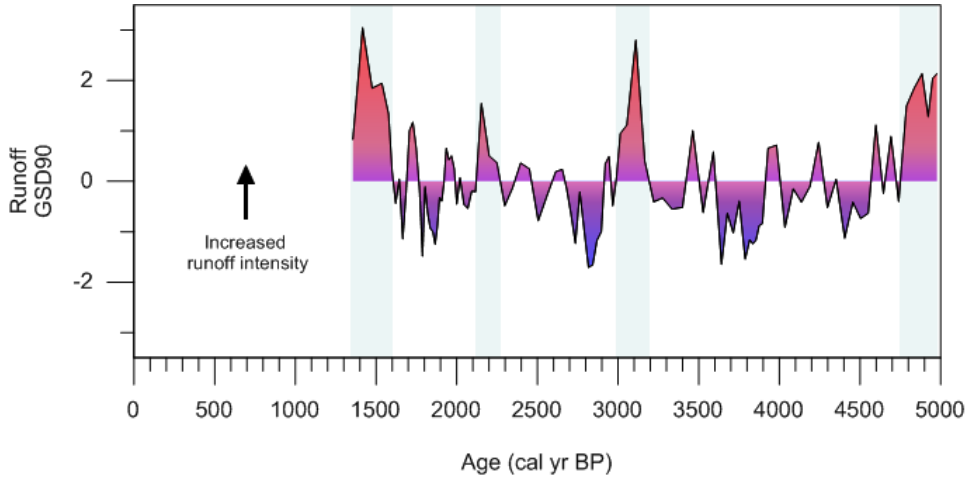


Figure 6: Reconstructed runoff from lake Hakluyvatnet (Paper II) from ~5000-1300 cal yr BP. The runoff record reflects precipitation-induced detrital sediment in-wash to Hakluyvatnet, and is based on standardized and detrended 90 percentile grain-size distribution (GSD90). Grey vertical bars denote periods with relatively large runoff.

Paper III – Storminess reconstruction (Arctic Norway)

A novel record of storminess in Arctic Norway is reconstructed from aeolian sediment input into the coastal lake Måvatnet, Andøya island. The study site is situated at the extreme west coast of Arctic Norway; a sensitive location for changes in North Atlantic westerly winds. We have combined sediment trap monitoring with a multi-proxy lake sediment study for detecting the aeolian member deposited in the lake. The high-resolution record reveals an abrupt increase in storminess synchronously with the onset of the Little Ice Age (LIA), ca. 600 cal yr BP, coeval with increased winter precipitation in western Norway and a strengthening of the persistent low-pressure west of Iceland (Icelandic Low) that exerts a strong effect on North Atlantic storm tracks. Further, the timing of the LIA onset along the coast of Norway appears to be linked to the dynamics of the large-scale atmospheric circulation systems in the North Atlantic, and we propose that the position of the Intertropical Convergence Zone (ITCZ) holds the key to explaining LIA precipitation patterns along the coast of Norway, reflected in the strength and position of the westerlies.

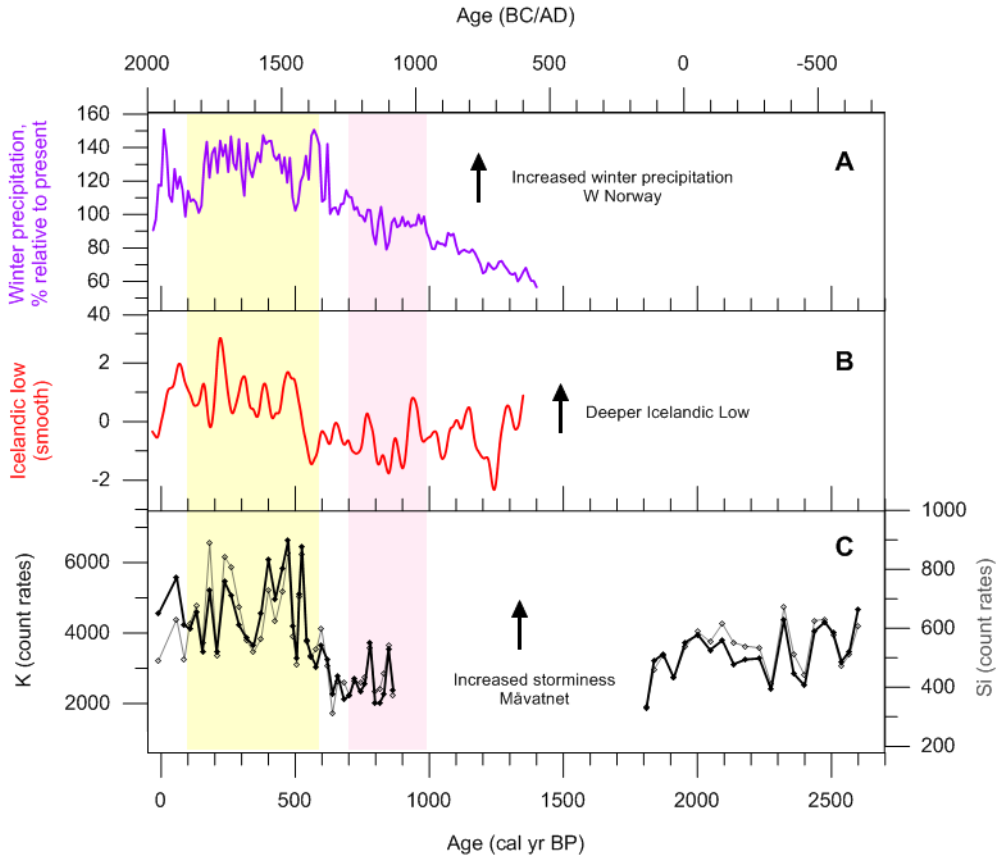


Figure 7: A) Reconstructed winter precipitation, western Norway (Paper I), B) Reconstructed strength of the Icelandic Low (Meeker and Mayewski, 2002), and C) Måvatnet storminess record (Paper III). The LIA (600-100 cal yr BP) highlighted in yellow vertical bar; Medieval Climate Anomaly (MCA) (1000-700 cal yr BP) in pink.

Synthesis and future perspectives

This thesis has focused on using lake sediment archives for reconstruction of past variability in North Atlantic atmospheric circulation as reflected in wind and precipitation changes. A large toolbox is applied to separate between distinct catchment processes affecting lake sedimentation, and inferences on climatically-forced sedimentation are drawn. A thorough assessment of site selection and preliminary bathymetric investigations combined with geomorphological mapping is recommended, as understanding catchment processes affecting lake sediment accumulation is vital for palaeoclimatic interpretations.

Because changes in naturally-occurring climate modes such as the NAO impact weather and climate over large parts of the globe (Hurrell and Deser, 2010), it is important to reconstruct past fluctuations to assess potential influence on future climate. As winter precipitation along the western coast of Norway is strongly related to the North Atlantic westerlies (Nordli et al., 2005), the ELA variations at Ålfotbreen (Paper I) have most likely been influenced by the spatial and temporal variability of the wintertime westerlies in the past. The wintertime westerlies over southern Norway are closely linked with the NAO (e.g. Nordli et al., 2005), and it is therefore possible that our record of past winter precipitation also contains a signal related to past variations in the NAO. If new data sets of similar resolution become available from other sites along the Norwegian coast in the future, it will be possible to reconstruct spatiotemporal patterns of winter precipitation, which may help to elucidate past changes in atmospheric circulation patterns (e.g. the NAO) and the strength and position of the wintertime westerlies over Norway. In particular, the coastal area of Norway is situated in an area sensitive to changes in the NAO and is suggested especially important by Lehner et al. (2012) (Fig. 8). The results from papers I and III suggest that the strength of the westerlies (i.e., the main source for winter precipitation and strong winds) increased during the LIA (Fig. 7), coeval with a strengthened Icelandic Low (Meeker and Mayewski, 2002). Thus, there seems to be a potential in these records to reflect changes in atmospheric circulation driven by changes in the pressure gradient.

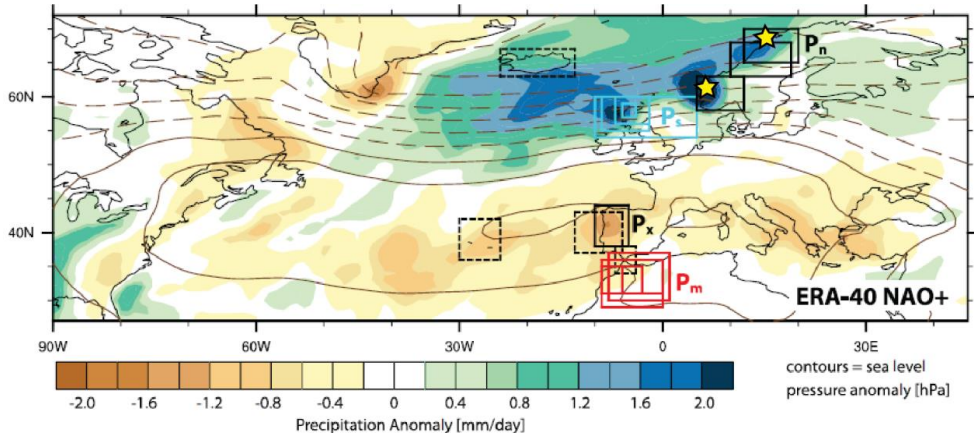


Figure 8: This figure from Lehner et al. (2012) highlights the sensitivity of the study sites from papers I and III (yellow asterisks) to the NAO.

Further, an interesting find from Paper I is that we originally wanted to test if a reconstruction of winter precipitation would co-vary with ELA variations. As is visible in Figure 5, we therefore suggest that when reconstructing winter precipitation at Ålfotbreen there is no need to go via the ‘Liestøl equation’ and we further tentatively propose that modern mass-balance measurements coupled with ELA reconstructions of Ålfotbreen reflect past winter precipitation variability. This assumption could further be explored at similar sites along the coast of Norway.

An intriguing future study proposed as an extension of this thesis is investigating the proposed south-north time-transgressive nature of the LIA in Scandinavia (Paper I). This would acquire new high-resolution glacier reconstructions as well as winter precipitation and storminess reconstructions to capture the full atmospheric effect. Including high-resolution tree-ring records might further help to decipher a potential seasonal signal in the storminess record, as most tree-ring records transfer a summer signal (Briffa et al., 1990). As the storm tracks are projected to shift poleward in near-future climate (Zhang et al., 2004; Yin, 2005), accompanying surface wind stress and precipitation (mostly during NH winter rather than summer) will further act to modulate the normally dry Arctic climate at e.g. Svalbard. At the time of writing, I

am awaiting core material from the last 1300 years from Hakluytvatnet to be analysed for grain-size distribution which will further allow a full late-Holocene south-north transect of the three lake studies and might reveal the timing of the LIA at Hakluytvatnet. Further, a comprehensive study of the timing of the LIA in a global context is proposed, incorporating records from marine and terrestrial sites to investigate the potential link with the position of the Intertropical Convergence Zone as suggested in Paper III. A compilation of the three late-Holocene records reflecting atmospheric circulation variability along the coast of Norway and Svalbard is intended.

References

- Augustsson A., Gaillard M.-J., Peltola P., Mazier F., Bergbäck B. and Saarinen T. (2013) Effects of land use and climate change on erosion intensity and sediment geochemistry at Lake Lehmilampi, Finland. *The Holocene* 23: 1247-1259.
- Bakke J. (2004) Late Weichselian and Holocene glacier fluctuations along a south-north coastal transect in Norway. *Dr. scient. Thesis, University of Bergen*.
- Bakke J., Dahl S. O., Paasche Ø., Løvlie R. and Nesje A. (2005a) Glacier fluctuations, equilibrium-line altitudes and palaeoclimate in Lyngen, northern Norway, during the Lateglacial and Holocene. *The Holocene* 15: 518-540.
- Bakke J., Dahl S. O., Paasche Ø., Riis Simonsen J., Kvisvik B., Bakke K. and Nesje A. (2010) A complete record of Holocene glacier variability at Austre Okstindbreen, northern Norway: an integrated approach. *Quaternary Science Reviews* 29: 1246-1262.
- Bakke J., Lie Ø., Dahl S. O., Nesje A. and Bjune A. E. (2008) Strength and spatial patterns of the Holocene wintertime westerlies in the NE Atlantic region. *Global and Planetary Change* 60: 28-41.
- Bakke J., Nesje A. and Dahl S. O. (2005b) Utilizing physical sediment variability in glacier-fed lakes for continuous glacier reconstructions during the Holocene, northern Folgefonna, western Norway. *The Holocene* 15: 161-176.
- Bakke J., Trachsel M., Kvisvik B. C., Nesje A. and Lyså A. (2013) Numerical analyses of a multi-proxy data set from a distal glacier-fed lake, Sørsendalsvatn, western Norway. *Quaternary Science Reviews* 73: 182-195.
- Ballantyne C. K. (2002) Paraglacial geomorphology. *Quaternary Science Reviews* 21: 1935-2017.
- Berger A. and Loutre M.-F. (1991) Insolation values for the climate of the last 10 million years. *Quaternary Science Reviews* 10: 297-317.
- Berntsson A., Jansson K. N., Kylander M. E., De Vleeschouwer F. and Bertrand S. (2015) Late Holocene high precipitation events recorded in lake sediments and catchment geomorphology, Lake Vuoksjävrätje, NW Sweden. *Boreas* 44: 676-692.
- Bianchi G. G. and McCave I. N. (1999) Holocene periodicity in North Atlantic climate and deep-ocean flow south of Iceland. *Nature* 397: 515-517.

- Bjune A. E., Bakke J., Nesje A. and Birks H. J. B. (2005) Holocene mean July temperature and winter precipitation in western Norway inferred from palynological and glaciological lake-sediment proxies. *The Holocene* 15: 177-189.
- Björck S. and Clemmensen L. B. (2004) Aeolian sediment in raised bog deposits, Halland, SW Sweden: a new proxy record of Holocene winter storminess variation in southern Scandinavia? *The Holocene* 14: 677-688.
- Bradley R. S. (2000) Past global changes and their significance for the future. *Quaternary Science Reviews* 19: 391-402.
- Bradley R. S. and Jones P. D. (1993) 'Little Ice Age' summer temperature variations: their nature and relevance to recent global warming trends. *The Holocene* 3: 367-376.
- Brady N. C. and Weil R. R. (1996) *The nature and properties of soils*: Prentice-Hall Inc.
- Briffa K. R., Bartholin T. S., Eckstein D., Jones P. D., Karlén W., Schweingruber F. H. and Zetterberg P. (1990) A 1,400-year tree-ring record of summer temperatures in Fennoscandia.
- Croudace I. W., Rindby A. and Rothwell R. G. (2006) ITRAX: description and evaluation of a new multi-function X-ray core scanner. *Special Publication - Geological Society Of London* 267: 51.
- Croudace I. W. and Rothwell R. G. (2015) *Micro-XRF Studies of Sediment Cores: Applications of a non-destructive tool for the environmental sciences*: Springer.
- Dahl S. O., Bakke J., Lie Ø. and Nesje A. (2003) Reconstruction of former glacier equilibrium-line altitudes based on proglacial sites: an evaluation of approaches and selection of sites. *Quaternary Science Reviews* 22: 275-287.
- Dahl S. O. and Nesje A. (1992) Paleoclimatic implications based on equilibrium-line altitude depressions of reconstructed Younger Dryas and Holocene cirque glaciers in inner Nordfjord, western Norway. *Palaeogeography, Palaeoclimatology, Palaeoecology* 94: 87-97.
- Dahl S. O. and Nesje A. (1994) Holocene glacier fluctuations at Hardangerjøkulen, central-southern Norway: a high-resolution composite chronology from lacustrine and terrestrial deposits. *The Holocene* 4: 269-277.
- Dahl S. O. and Nesje A. (1996) A new approach to calculating Holocene winter precipitation by combining glacier equilibrium-line altitudes and pine-tree limits: a case study from Hardangerjøkulen, central southern Norway. *The Holocene* 6: 381-398.

-
- Davies S. J., Lamb H. F. and Roberts S. J. (2015) Micro-XRF Core Scanning in Palaeolimnology: Recent Developments. *Micro-XRF Studies of Sediment Cores*. Springer, 189-226.
- de Jong R., Björck S., Björckman L. and Clemmensen L. B. (2006) Storminess variation during the last 6500 years as reconstructed from an ombrotrophic peat bog in Halland, southwest Sweden. *Journal of Quaternary Science* 21: 905.
- de Jong R., Hammarlund D. and Nesje A. (2009) Late Holocene effective precipitation variations in the maritime regions of south-west Scandinavia. *Quaternary Science Reviews* 28: 54-64.
- de Jong R., Schoning K. and Björck S. (2007) Increased aeolian activity during humidity shifts as recorded in a raised bog in south-west Sweden during the past 1700 years. *Climate of the Past* 3: 411-422.
- Dean W. E. (1974) Determination of carbonate and organic matter in calcareous sediments and sedimentary rocks by loss on ignition: comparison with other methods. *Journal of Sedimentary Research* 44.
- Dietze E., Hartmann K., Diekmann B., IJmker J., Lehmkuhl F., Opitz S., Stauch G., Wünnemann B. and Borchers A. (2012) An end-member algorithm for deciphering modern detrital processes from lake sediments of Lake Donggi Cona, NE Tibetan Plateau, China. *Sedimentary Geology* 243: 169-180.
- Fleitmann D., Mudelsee M., Burns S. J., Bradley R. S., Kramers J. and Matter A. (2008) Evidence for a widespread climatic anomaly at around 9.2 ka before present. *Paleoceanography* 23.
- Grove J. M. (2001) The initiation of the "Little Ice Age" in regions round the North Atlantic. *The Iceberg in the Mist: Northern Research in pursuit of a "Little Ice Age"*. Springer, 53-82.
- Haug G. H., Hughen K. A., Sigman D. M., Peterson L. C. and Röhl U. (2001) Southward migration of the intertropical convergence zone through the Holocene. *Science* 293: 1304-1308.
- Heiri O., Lotter A. F. and Lemcke G. (2001) Loss on ignition as a method for estimating organic and carbonate content in sediments: reproducibility and comparability of results. *Journal of Paleolimnology* 25: 101-110.
- Hurrell J. W. (1995) Decadal trends in the North Atlantic Oscillation: regional temperatures and precipitation. *Science* 269: 676.

- Hurrell J. W. and Deser C. (2010) North Atlantic climate variability: the role of the North Atlantic Oscillation. *Journal of Marine Systems* 79: 231-244.
- IPCC. (2013) Climate Change 2013: The Physical Science Basis. Contribution of Working Group I to the Fifth Assessment Report of the Intergovernmental Panel on Climate Change. In: Stocker T, Qin D, Plattner G, et al. (eds). Cambridge Univ Press, Cambridge, United Kingdom and New York, NY, USA, 1555.
- Jansson P., Rosqvist G. and Schneider T. (2005) Glacier fluctuations, suspended sediment flux and glacio-lacustrine sediments. *Geografiska Annaler: Series A, Physical Geography* 87: 37-50.
- Karlén W. (1976) Lacustrine sediments and tree-limit variations as indicators of Holocene climatic fluctuations in Lappland, northern Sweden. *Geografiska Annaler. Series A. Physical Geography*: 1-34.
- Karlén W. (1981) Lacustrine Sediment Studies. A Technique to Obtain a Continuous Record of Holocene Glacier Variations. *Geografiska Annaler. Series A. Physical Geography*: 273-281.
- Karlén W. and Matthews J. A. (1992) Reconstructing Holocene glacier variations from glacial lake sediments: studies from Nordvestlandet and Jostedalbreen-Jotunheimen, southern Norway. *Geografiska Annaler. Series A. Physical Geography*: 327-348.
- Kjøllmoen B. (2011) Glaciological investigations in Norway in 2010. *NVE Report 2 2010*.
- Kleiven H. K. F., Kissel C., Laj C., Ninnemann U. S., Richter T. O. and Cortijo E. (2008) Reduced North Atlantic deep water coeval with the glacial Lake Agassiz freshwater outburst. *Science* 319: 60-64.
- Lamb H. H. (1979) Climatic variation and changes in the wind and ocean circulation: the Little Ice Age in the northeast Atlantic. *Quaternary Research* 11: 1-20.
- Lancaster N. (2002) Flux of eolian sediment in the McMurdo Dry Valleys, Antarctica: a preliminary assessment. *Arctic, Antarctic, and Alpine Research*: 318-323.
- Leemann A. and Niessen F. (1994) Holocene glacial activity and climatic variations in the Swiss Alps: reconstructing a continuous record from proglacial lake sediments. *The Holocene* 4: 259-268.
- Lehner F., Raible C. C. and Stocker T. F. (2012) Testing the robustness of a precipitation proxy-based North Atlantic Oscillation reconstruction. *Quaternary Science Reviews* 45: 85-94.

-
- Lie Ø., Dahl S. O., Nesje A., Matthews J. A. and Sandvold S. (2004) Holocene fluctuations of a polythermal glacier in high-alpine eastern Jotunheimen, central-southern Norway. *Quaternary Science Reviews* 23: 1925-1945.
- Mann M. E., Zhang Z., Rutherford S., Bradley R. S., Hughes M. K., Shindell D., Ammann C., Faluvegi G. and Ni F. (2009) Global signatures and dynamical origins of the Little Ice Age and Medieval Climate Anomaly. *Science* 326: 1256-1260.
- Marshall J., Kushnir Y., Battisti D., Chang P., Czaja A., Dickson R., Hurrell J., McCartney M., Saravanan R. and Visbeck M. (2001) North Atlantic climate variability: phenomena, impacts and mechanisms. *International Journal of Climatology* 21: 1863-1898.
- Matthews J. A. and Briffa K. R. (2005) The 'Little Ice Age': Re-evaluation of an evolving concept. *Geografiska Annaler: Series A, Physical Geography* 87: 17-36.
- Matthews J. A., Dahl S. O., Nesje A., Berrisford M. S. and Andersson C. (2000) Holocene glacier variations in central Jotunheimen, southern Norway based on distal glaciolacustrine sediment cores. *Quaternary Science Reviews* 19: 1625-1647.
- Mayewski P. A., Rohling E. E., Curt Stager J., Karlen W., Maasch K. A., David Meeker L., Meyerson E. A., Gasse F., van Kreveld S. and Holmgren K. (2004) Holocene climate variability. *Quaternary Research* 62: 243-255.
- Meeker L. D. and Mayewski P. A. (2002) A 1400-year high-resolution record of atmospheric circulation over the North Atlantic and Asia. *The Holocene* 12: 257-266.
- Meyer H., Opel T., Laepple T., Dereviagin A. Y., Hoffmann K. and Werner M. (2015) Long-term winter warming trend in the Siberian Arctic during the mid- to late Holocene. *Nature Geoscience* 8: 122-125.
- Nesje A. (1992) A piston corer for lacustrine and marine sediments. *Arctic and Alpine Research*: 257-259.
- Nesje A. (2009) Latest Pleistocene and Holocene alpine glacier fluctuations in Scandinavia. *Quaternary Science Reviews* 28: 2119-2136.
- Nesje A., Bakke J., Dahl S. O., Lie Ø. and Bøe A.-G. (2007) A continuous, high-resolution 8500-yr snow-avalanche record from western Norway. *The Holocene* 17: 269-277.
- Nesje A. and Dahl S. O. (2003) The 'Little Ice Age'—only temperature? *The Holocene* 13: 139-145.
- Nesje A., Dahl S. O. and Løvlie R. (1995) Late Holocene glaciers and avalanche activity in the Ålfotbreen area, western Norway: evidence from a lacustrine sedimentary record. *Nor. Geol. Tidsskr* 75: 120-126.

-
- Nesje A., Kvamme M., Rye N. and Løvlie R. (1991) Holocene glacial and climate history of the Jostedalsgreen region, western Norway; evidence from lake sediments and terrestrial deposits. *Quaternary Science Reviews* 10: 87-114.
- Nesje A. and Matthews J. A. (2012) The Briksdalsbre Event: A winter precipitation-induced decadal-scale glacial advance in southern Norway in the ad 1990s and its implications. *The Holocene* 22: 249-261.
- Nesje A., Matthews J. A., Dahl S. O., Berrisford M. S. and Andersson C. (2001) Holocene glacier fluctuations of Flatebreen and winter-precipitation changes in the Jostedalsgreen region, western Norway, based on glaciolacustrine sediment records. *The Holocene* 11: 267-280.
- Nesje A., Olaf Dahl S., Andersson C. and Matthews J. A. (2000) The lacustrine sedimentary sequence in Syngneskardvatnet, western Norway: a continuous, high-resolution record of the Jostedalsgreen ice cap during the Holocene. *Quaternary Science Reviews* 19: 1047-1065.
- Nordli Ø., Lie Ø., Nesje A. and Benestad R. E. (2005) Glacier Mass Balance in Southern Norway Modelled by Circulation Indices and Spring-Summer Temperatures ad 1781–2000. *Geografiska Annaler: Series A, Physical Geography* 87: 431-445.
- Osborn G., Menounos B., Koch J., Clague J. J. and Vallis V. (2007) Multi-proxy record of Holocene glacial history of the Spearhead and Fitzsimmons ranges, southern Coast Mountains, British Columbia. *Quaternary Science Reviews* 26: 479-493.
- Pinto J. G. and Raible C. C. (2012) Past and recent changes in the North Atlantic oscillation. *Wiley Interdisciplinary Reviews: Climate Change* 3: 79-90.
- Rasmussen S. O., Andersen K. K., Svensson A., Steffensen J. P., Vinther B. M., Clausen H. B., Siggaard-Andersen M. L., Johnsen S. J., Larsen L. B. and Dahl-Jensen D. (2006) A new Greenland ice core chronology for the last glacial termination. *Journal of Geophysical Research: Atmospheres (1984–2012)* 111.
- Renssen H., Seppä H., Heiri O., Roche D., Goosse H. and Fichetef T. (2009) The spatial and temporal complexity of the Holocene thermal maximum. *Nature Geoscience* 2: 411-414.
- Risebrobakken B., Jansen E., Andersson C., Mjelde E. and Hevrøy K. (2003) A high-resolution study of Holocene paleoclimatic and paleoceanographic changes in the Nordic Seas. *Paleoceanography* 18.
- Rogers J. and McHugh M. (2002) On the separability of the North Atlantic oscillation and Arctic oscillation. *Climate Dynamics* 19: 599-608.

-
- Rosqvist G., Jonsson C., Yam R., Karlén W. and Shemesh A. (2004) Diatom oxygen isotopes in pro-glacial lake sediments from northern Sweden: a 5000 year record of atmospheric circulation. *Quaternary Science Reviews* 23: 851-859.
- Rubensdotter L. and Rosqvist G. (2009) Influence of geomorphological setting, fluvial-, glaciofluvial-and mass-movement processes on sedimentation in alpine lakes. *The Holocene* 19: 665-678.
- Røthe T. O., Bakke J., Vasskog K., Gjerde M., D'Andrea W. J. and Bradley R. S. (2015) Arctic Holocene glacier fluctuations reconstructed from lake sediments at Mitrahålvøya, Spitsbergen. *Quaternary Science Reviews* 109: 111-125.
- Schillereff D. N., Chiverrell R. C., Macdonald N. and Hooke J. M. (2014) Flood stratigraphies in lake sediments: A review. *Earth-science reviews* 135: 17-37.
- Schillereff D. N., Chiverrell R. C., Macdonald N. and Hooke J. M. (2015) Hydrological thresholds and basin control over paleoflood records in lakes. *Geology*.
- Shakesby R. A., Smith J. G., Matthews J. A., Winkler S., Dresser P. Q., Bakke J., Dahl S. O., Lie Ø. and Nesje A. (2007) Reconstruction of Holocene glacier history from distal sources: glaciofluvial stream-bank mires and a glaciolacustrine sediment core near Sota Sæter, Breheimen, southern Norway. *The Holocene* 17: 729-745.
- Sissons J. B. (1979) Palaeoclimatic inferences from former glaciers in Scotland and the Lake District. *Nature* 278: 518-521.
- Sletten K., Blikra L. H., Ballantyne C., Nesje A. and Dahl S. O. (2003) Holocene debris flows recognized in a lacustrine sedimentary succession: sedimentology, chronostratigraphy and cause of triggering. *The Holocene* 13: 907-920.
- Snowball I., Sandgren P. and Petterson G. (1999) The mineral magnetic properties of an annually laminated Holocene lake-sediment sequence in northern Sweden. *The Holocene* 9: 353-362.
- Solomina O. N., Bradley R. S., Hodgson D. A., Ivy-Ochs S., Jomelli V., Mackintosh A. N., Nesje A., Owen L. A., Wanner H. and Wiles G. C. (2015) Holocene glacier fluctuations. *Quaternary Science Reviews* 111: 9-34.
- Støren E. N., Dahl S. O., Nesje A. and Paasche Ø. (2010) Identifying the sedimentary imprint of high-frequency Holocene river floods in lake sediments: development and application of a new method. *Quaternary Science Reviews* 29: 3021-3033.
- Støren E. N., Kolstad E. W. and Paasche Ø. (2012) Linking past flood frequencies in Norway to regional atmospheric circulation anomalies. *Journal of Quaternary Science* 27: 71-80.

- Støren E. N. and Paasche Ø. (2014) Scandinavian floods: From past observations to future trends. *Global and Planetary Change* 113: 34-43.
- Thompson R., Battarbee R. W., O'Sullivan P. E. and Oldfield F. (1975) Magnetic susceptibility of lake sediments. *Limnology and Oceanography* 20: 687-698.
- Vasskog K., Nesje A., Støren E. N., Waldmann N., Chapron E. and Ariztegui D. (2011) A Holocene record of snow-avalanche and flood activity reconstructed from a lacustrine sedimentary sequence in Oldevatnet, western Norway. *The Holocene* 21: 597-614.
- Vasskog K., Paasche Ø., Nesje A., Boyle J. F. and Birks H. J. B. (2012) A new approach for reconstructing glacier variability based on lake sediments recording input from more than one glacier. *Quaternary Research* 77: 192-204.
- Vinther B. M., Clausen H. B., Johnsen S. J., Rasmussen S. O., Andersen K. K., Buchardt S. L., Dahl-Jensen D., Seierstad I. K., Siggaard-Andersen M. L. and Steffensen J. P. (2006) A synchronized dating of three Greenland ice cores throughout the Holocene. *Journal of Geophysical Research: Atmospheres (1984–2012)* 111.
- Wanner H., Beer J., Buetikofer J., Crowley T. J., Cubasch U., Flueckiger J., Goosse H., Grosjean M., Joos F. and Kaplan J. O. (2008) Mid-to Late Holocene climate change: an overview. *Quaternary Science Reviews* 27: 1791-1828.
- Wanner H., Brönnimann S., Casty C., Gyalistras D., Luterbacher J., Schmutz C., Stephenson D. B. and Xoplaki E. (2001) North Atlantic Oscillation—concepts and studies. *Surveys in geophysics* 22: 321-381.
- Wittmeier H. E., Bakke J., Vasskog K. and Trachsel M. (2015) Reconstructing Holocene glacier activity at Langfjordjøkelen, Arctic Norway, using multi-proxy fingerprinting of distal glacier-fed lake sediments. *Quaternary Science Reviews* 114: 78-99.
- Yin J. H. (2005) A consistent poleward shift of the storm tracks in simulations of 21st century climate. *Geophysical research letters* 32.
- Zhang X., Walsh J. E., Zhang J., Bhatt U. S. and Ikeda M. (2004) Climatology and interannual variability of Arctic cyclone activity: 1948-2002. *Journal of Climate* 17: 2300-2317.

Paper I

Gjerde, M., Bakke, J., Vasskog, K., Nesje, A., Hormes, A. 2016. Holocene glacier variability and Neoglacial hydroclimate at Ålfotbreen, western Norway. *Quaternary Science Reviews*, 133. pp 28-47. doi:10.1016/j.quascirev.2015.12.004



Contents lists available at ScienceDirect

Quaternary Science Reviews

journal homepage: www.elsevier.com/locate/quascirev

Holocene glacier variability and Neoglacial hydroclimate at Ålftobreen, western Norway

Marthe Gjerde^{a, c, *}, Jostein Bakke^a, Kristian Vasskog^{a, b}, Atle Nesje^{a, b}, Anne Hormes^{c, d}^a Department of Earth Science and Bjerknæs Centre for Climate Research, University of Bergen, Allégaten 41, NO-5007, Bergen, Norway^b Uni Research Climate AS, Allégaten 55, NO-5007, Bergen, Norway^c Department of Arctic Geology, The University Centre in Svalbard, NO-9171, Longyearbyen, Norway^d Department of Earth Sciences, University of Gothenburg, SE-405 30, Gothenburg, Sweden

ARTICLE INFO

Article history:

Received 29 May 2015

Received in revised form

26 November 2015

Accepted 8 December 2015

Available online 21 December 2015

Keywords:

Glacier
Lake sediments
Holocene
Neoglacial
Winter precipitation
Hydroclimate
ELA
Western Norway
Ålftobreen

ABSTRACT

Glaciers and small ice caps respond rapidly to climate perturbations (mainly winter precipitation, and summer temperature), and the mass-balance of glaciers located in western Norway is governed mainly by winter precipitation (Pw). Records of past Pw can offer important insight into long-term changes in atmospheric circulation, but few proxies are able to accurately capture winter climate variations in Scandinavia. Reconstructions of equilibrium-line-altitude (ELA) variations from glaciers that are sensitive to changes in Pw therefore provide a unique opportunity to quantify past winter climate in this region. Here we present a new, Holocene glacier activity reconstruction for the maritime ice cap Ålftobreen in western Norway, based on investigations of distal glacier-fed lake sediments and modern mass balance measurements (1963–2010). Several lake sediment cores have been subject to a suite of laboratory analyses, including measurements of physical parameters such as dry bulk density (DBD) and loss-on-ignition (LOI), geochemistry (XRF), surface magnetic susceptibility (MS), and grain size distribution, to identify glacial sedimentation in the lake. Both radiocarbon (AMS ¹⁴C) and ²¹⁰Pb dating were applied to establish age-depth relationships in the sediment cores. A novel approach was used to calibrate the sedimentary record against a simple ELA model, which allowed reconstruction of continuous ELA changes for Ålftobreen during the Neoglacial (when Ålftobreen was present, i.e. the last ~1400 years). Furthermore, the resulting ELA variations were combined with an independent summer temperature record to calculate Neoglacial Pw using the 'Liestøl equation'. The resulting Pw record is of higher resolution than previous reconstructions from glaciers in Norway and shows the potential of glacier records to provide high-resolution data reflecting past variations in hydroclimate. Complete deglaciation of the Ålftobreen occurred ~9700 cal yr BP, and the ice cap was subsequently absent or very small until a short-lived glacier event is seen in the lake sediments ~8200 cal yr BP. The ice cap was most likely completely melted until a new glacier event occurred around ~5300 cal yr BP, coeval with the onset of the Neoglacial at several other glaciers in southwestern Norway. Ålftobreen was thereafter absent (or very small) until the onset of the Neoglacial period ~1400 cal yr BP. The 'Little Ice Age' (LIA) ~650–50 cal yr BP was the largest glacier advance of Ålftobreen since deglaciation, with a maximum extent at ~400–200 cal yr BP, when the ELA was lowered approximately 200 m relative to today. The late onset of the Neoglacial at Ålftobreen is suggested to be a result of its low altitude relative to the regional ELA. A synthesis of Neoglacial ELA fluctuations along the coast of Norway indicates a time-transgressive trend in the maximum extent of the LIA, which apparently seems to have occurred progressively later as we move northwards. We suggest that this trend is likely due to regional winter precipitation differences along the coast of Norway.

© 2015 The Authors. Published by Elsevier Ltd. This is an open access article under the CC BY-NC-ND license (<http://creativecommons.org/licenses/by-nc-nd/4.0/>).

1. Introduction

In order to create robust projections of future climate change, it is of great importance to understand past natural climate variability, as this may help to discern the relative importance of

* Corresponding author. Department of Earth Science, University of Bergen, Allégaten 41, NO-5007, Bergen, Norway.

E-mail addresses: Marthe.gjerde@uib.no (M. Gjerde), Jostein.bakke@uib.no (J. Bakke), Kristian.vasskog@uib.no (K. Vasskog), Atle.nesje@uib.no (A. Nesje), Anne.hormes@gvc.gu.se (A. Hormes).

natural and anthropogenic forcing on the climate system (Masson-Delmotte et al., 2013). Glaciers and ice caps are excellent climate indicators, as they respond to changes in temperature and precipitation; and thus, records of past glacier fluctuations can give information about past climate variability (Oerlemans, 2005). Presently, the annual mass-balance of small plateau glaciers located at the coast of south-western Norway is controlled mainly by winter accumulation, and mass-balance measurements from this area are therefore useful tools for exploring past variations in winter precipitation (Marzeion and Nesje, 2012). Glacier mass-balance data are, however, generally scarce; in some cases discontinuous; and extend only a few decades back in time. In order to expand records of glacier variability and associated winter precipitation beyond the instrumental record we therefore utilize natural archives, such as continuous sedimentary records from distal glacier-fed lakes.

Distal glacier-fed lakes act as traps for glacially eroded sediments that are transported by glacial meltwater streams down-valley, and by quantifying the influx of glacial sediment to these lakes it is possible to reconstruct continuous changes in upstream glacial erosion and hence glacier size through time. A large number of distal glacier-fed lakes have been investigated throughout Scandinavia, together providing an extensive overview of past glacier variability in this region (Karlén, 1976, 1981; Nesje et al., 1991; Dahl and Nesje, 1992; Karlén and Matthews, 1992; Dahl and Nesje, 1994; Matthews et al., 2000; Nesje et al., 2000b, 2001; Lie et al., 2004; Rosqvist et al., 2004; Bakke et al., 2005; Shakesby et al., 2007; Bakke et al., 2010; Vasskog et al., 2012; Bakke et al., 2013; Røthe et al., 2015; Wittmeier et al., 2015).

Some of these records present only relative changes in glacial input to the lakes, but in cases where dated moraine ridges are available to reconstruct the glacier extent at specific points in time, lake records can be calibrated to produce continuous reconstructions of changes in equilibrium-line altitude (ELA) (e.g. Nesje et al., 2001; Dahl et al., 2003; Bakke et al., 2010; Røthe et al., 2015). If an independent record of summer temperature is available, estimates of past winter precipitation can be extracted from continuous ELA reconstructions (e.g. Dahl and Nesje, 1996; Bjune et al., 2005) through the so-called 'Liestøl equation' described by O. Liestøl in Sissons (1979); a mathematical expression based on the empirical relationship between annual precipitation and summer temperature at the ELA of ten Norwegian glaciers.

Ålfotbreen is the westernmost ice cap in Norway, and the extreme maritime nature of this plateau glacier makes it a particularly interesting target for high-resolution reconstructions of past glacier fluctuations. From CE1963–2010, changes in the annual mass balance of Ålfotbreen have been mainly governed by the amount of winter accumulation ($R^2 = 0.71$) (data from: Kjølmoen, 2011), but the relative importance of winter accumulation vs. summer ablation might be different when longer timescales are considered (Trachsel and Nesje, 2015). Long-term ELA reconstructions are therefore valuable tools for evaluating long-term natural variability of past winter climate. Here we present (1) a relative glacier fluctuation reconstruction of the Ålfotbreen ice cap during the Holocene; (2) a high-resolution reconstruction of Neoglacial ELA variations; (3) a constraint on the timing of the 'Little Ice Age' (LIA) maximum; and (4) reconstructed Neoglacial winter precipitation for the study area. Finally, we discuss the climatic implications of our findings in relation to other palaeoclimatic records in the North Atlantic region, including glacier records and winter precipitation reconstructions from other parts of Scandinavia, as well as possible forcing mechanisms that could explain the observed glacier variability.

2. Study area

2.1. Glacier, climate and bedrock

The Ålfotbreen plateau glacier (here defined as encompassing the two separate ice caps 'Ålfotbreen' and 'Blåbreen' with surrounding ice patches) covers an area of 15.5 km² (Andreassen et al., 2012), where the majority of the glaciated area is constrained to a limited altitude interval near the maximum elevation (Kjølmoen, 2011; Andreassen et al., 2012). The glacier covers ~2.5 km² (~6%) of the total catchment area (41.5 km²) of the downstream glacier-fed lake Grøndalsvatnet (see Section 2.2 below). Ålfotbreen ('Å' in Fig. 1C) and Blåbreen ('B' in Fig. 1C) are separated by a steep cliff in the area's tilted sedimentary Devonian bedrock (Bryhni and Lutro, 2000). Because of the distinct steps in the landscape, along with the narrow hypsometry of Ålfotbreen (altitude range <600 m), the ice cap does not feature very prominent outlet glaciers. Two adjacent north-facing outlet glaciers named Ålfotbreen (4.0 km²; not to be confused with the ice cap itself) and Hansebreen (2.8 km²) have been subject to mass-balance studies since CE1963 and CE1986, respectively (Kjølmoen, 2011). During recent years the annual ELA has been raised above the highest elevation of the ice cap (>1382 m a.s.l.) several times (Kjølmoen, 2011). See Fig. 1 for an overview of the study area, and Fig. 2 for an overview of the narrow hypsometry of the two outlet glaciers mentioned above. From here on, the term 'Ålfotbreen' includes both outlet glaciers mentioned above, the two ice caps Blåbreen and Ålfotbreen as well as the surrounding ice patches, unless stated otherwise.

Relative to area, Ålfotbreen has the largest annual mass turnover of the monitored glaciers in Norway, with the highest recorded values for both winter accumulation and summer ablation (Kjølmoen, 2011). For Ålfotbreen, winter accumulation is considered more important in determining its net mass balance than summer ablation (Nesje, 2005), and a large gain in mass between CE1989–95 was mainly caused by high winter balance (Andreassen et al., 2005). Despite the large mass turnover, Ålfotbreen is ranked as the most vulnerable glacier in Norway, mainly due to its narrow hypsometric distribution above the steady-state ELA (~200 m, Fig. 2), and it might therefore be one of the first glaciers to disappear completely in a warmer future climate (Nesje et al., 2008; Andreassen et al., 2012). Inferences about past extent and fluctuations of Ålfotbreen have previously been published by Nesje et al. (1995) and Sønstegeard et al. (1999); however, neither of these studies obtained a complete Holocene glacial history. Nesje et al. (1995) focused on the late-Holocene glacier history and avalanche activity, whereas Sønstegeard et al. (1999) were targeting the deglaciation history of the area. As an isolated ice cap from the main Scandinavian ice sheet during the Younger Dryas (YD), Ålfotbreen obtained its maximum YD extent just before the deposition of the Vedde Ash Bed (Sønstegeard et al., 1999). The further history of deglaciation and Holocene glacier variations has so far been poorly constrained for Ålfotbreen (Nesje, 2009).

The present climate of the study area is maritime with a mean CE1961–1990 summer temperature (Ts; 1 May–30 September) of 12.12 °C (climate station 58070 Sandane, ca. 30 km east of Ålfotbreen; 51 m a.s.l.). Mean CE1961–1990 winter precipitation (Pw; 1 October – 30 April) at the 57680 Eikefjord climate station (ca. 20 km south-southwest of Ålfotbreen; 30 m a.s.l.) is 1677 mm (eKlima.no); and snow accumulations of up to 8–10 m during winter are not unusual at the top of Ålfotbreen (Andreassen et al., 2012).

2.2. Catchment lakes and geomorphological setting

Lake Grøndalsvatnet (~0.27 km²; N 61°41', E05°34') is located

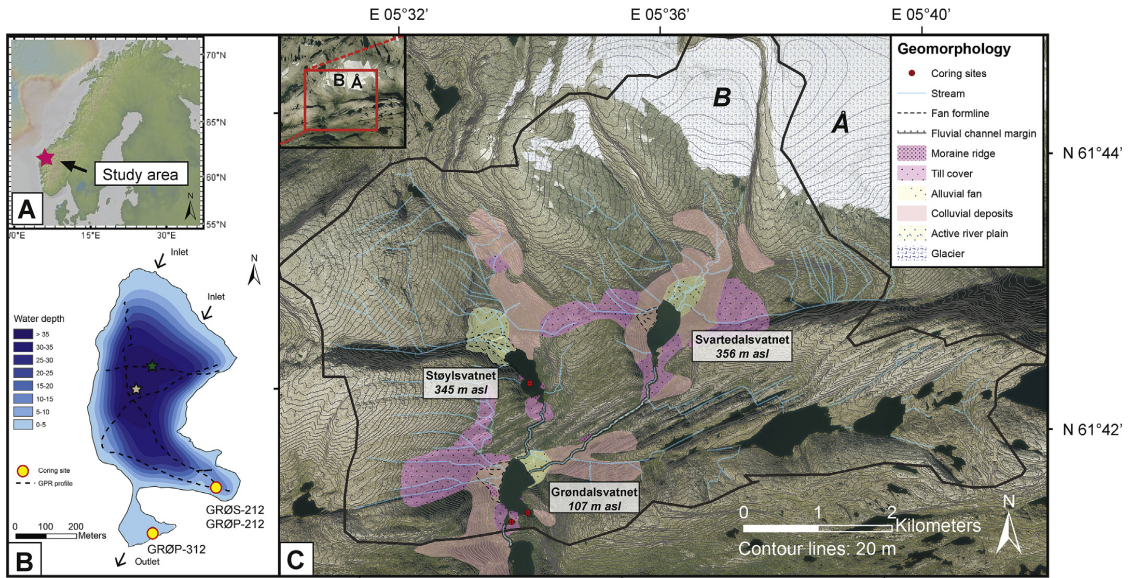


Fig. 1. Overview of the study area. A) Study site location in Scandinavia; B) Bathymetrical map of Grøndalsvatnet, showing coring sites and GPR profiles (water depth in m). Green asterisk marks coring location from Neuje et al. (1995). Grey asterisk marks coring location for GRØP-112 (not analysed, see Section 4.1); C) Geomorphological map of the catchment area with coring sites marked in red; black solid line outlines the catchment limit. Upper left shows the area surrounding the ice cap. (For interpretation of the references to colour in this figure legend, the reader is referred to the web version of this article.)

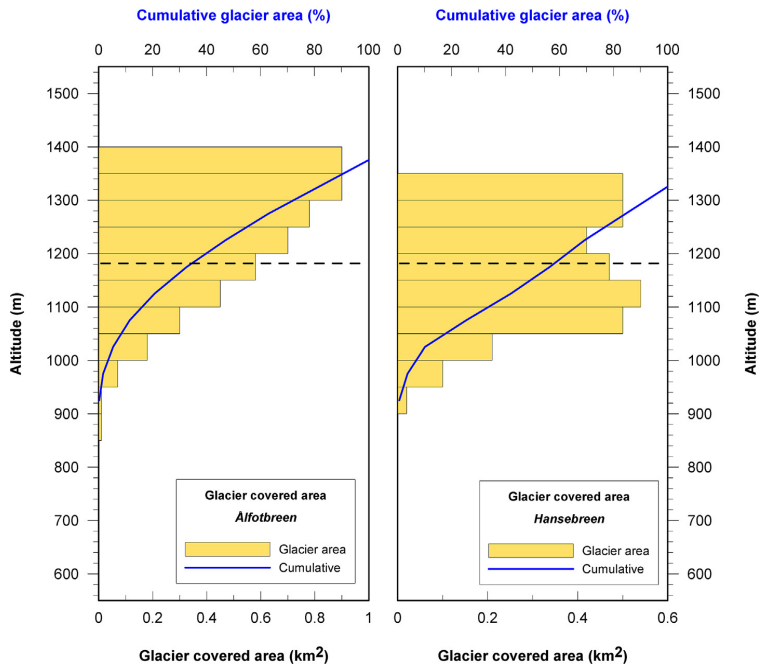


Fig. 2. Hypsometry of two outlet glaciers from Älfotbreen ice cap: Älfotbreen and Hansebreen. Stippled line represents calculated steady-state ELA (~1180 m a.s.l.) for Älfotbreen (for the monitoring period CE1963-2010).

south of Älfotbreen, at an elevation of 107 m a.s.l. Deep glacial troughs and steep cliffs characterize the surrounding catchment topography. The catchment is dominated by exposed bedrock, with unconsolidated sedimentary deposits being limited mainly to the large inlet delta in the northern end of the lake, a distinct colluvial fan along its western shore, and a moraine ridge close to the outlet (Fig. 1). Vegetation cover is relatively dense across most of the colluvial fan, the moraine ridge, and the remaining till cover, up to an altitude of about 500–600 m a.s.l., whereas the inlet delta is covered by farmland. The main inlet is a river transporting meltwater from Älfotbreen into the lake across the delta, although the meltwater needs to pass through the upstream lake Svartedalsvatnet (356 m a.s.l.) before reaching Grøndalsvatnet. This setting allows only relatively fine-grained glacial sediments to continue downstream to Grøndalsvatnet. Lake Støylsvatnet (–0.18 km²; N 61°42', E05°34') is also situated upstream from Grøndalsvatnet at an elevation of 345 m a.s.l., but this lake is part of a different catchment area and the lake is not fed by glacial meltwater from Älfotbreen at present. A small river presently drains from Støylsvatnet into Grøndalsvatnet across the western end of the inlet delta. Apart from this, only three smaller creeks drain into the lake, all of which are orders of magnitude smaller than the main inlet. Støylsvatnet has probably received glacial meltwater from Älfotbreen in the past when the ice cap covered a larger area, and Støylsvatnet was therefore targeted as a potential 'threshold lake' (e.g. Dahl et al., 2003; Briner et al., 2010) to constrain the timing of particularly large glacier advances; e.g. during the 'Little Ice Age' (LIA). A soft sediment map for Grøndalsvatnet is shown in Supplementary Fig. S1, and a bathymetrical map of Støylsvatnet in Supplementary Fig. S2.

3. Methods

A combination of geomorphological field mapping, studies of aerial photographs and available online data on superficial deposits from the Geological Survey of Norway (ngu.no) and the Norwegian Mapping Authority (norgeskart.no) form the basis for the data presented in the geomorphological map of the area (Fig. 1). The reconstruction of Holocene glacier fluctuations at Älfotbreen is based on a range of different laboratory analyses (see below) performed on the sediment cores obtained from the distal glacier-fed lake Grøndalsvatnet and the 'threshold lake' Støylsvatnet. The term 'threshold lake' is adapted from Briner et al. (2010) as a lake where the catchment area has been partly covered by advancing ice during certain periods, so that the non-glacial lake undergoes a transformation to a glacier-fed lake (without the lake basin being overridden by ice). As a result, the lake sediment fill consist of organic-rich sediments during periods where ice extent is relatively small (e.g. before the LIA), and minerogenic-rich sediments during periods of relatively large ice extent (e.g. during the LIA) (Briner et al., 2010). A robust chronology has been established for the cores through AMS radiocarbon (¹⁴C) dating of terrestrial macrofossils in combination with lead (²¹⁰Pb) ages obtained on the most recent sediments.

3.1. Geophysical survey and lake sediment coring

Prior to lake coring, combined echo sounding and ground penetrating radar (GPR) surveys of Lake Grøndalsvatnet were conducted in May 2012 to determine suitable coring sites. GPR profiles were collected using a RAMAC GPR from Malå with a 25 MHz RTA antenna in order to map the soft sediment thickness, whereas the bathymetry was measured with an echo sounder (Fig. 1 and S1). Three cores; GRØP-112 (239 cm); GRØP-212 (243 cm); and GRØP-312 (212.5 cm), were retrieved from a raft

using a modified piston corer with a 110 mm diameter core tube (Nesje, 1992). The uppermost ~10 cm of GRØP-312 were lost during coring. In order to recover the sediment-water interface, two short HTH (Renberg-type) gravity cores, GRØS-112 and GRØS-212, were collected adjacent to the GRØP-112 and GRØP-212 coring sites, respectively. In order to avoid disturbances from colluvial activity, mass-movement on the delta front, and any possible long-term effects of delta progradation, the main cores (GRØP-212/GRØS-212) were retrieved in a backwater area close to the lake outlet (Fig. 1).

In June 2014, the threshold lake Støylsvatnet was cored to investigate recent glacier fluctuations in the area using ²¹⁰Pb dates for age estimation. Prior to coring, an echo sounder combined with the 'Dr Depth' software was used to record the bathymetry of the lake (Fig. S2). Two short cores; STØS-114 (30 cm) and STØS-214 (32 cm), were both collected using a UWITEC gravity coring device.

3.2. Laboratory analyses

The sediment cores were split lengthwise in the laboratory and one half of each core was stored for reference. Core surfaces were then carefully cleaned and photographed. Lithofacies and sedimentological structures and textures were described in detail before scanning and sub-sampling was initiated.

Geochemical data and radiographic images were obtained using an ITRAX x-ray fluorescence (XRF) Scanner (Croudace et al., 2006) in EARTHLAB, Department of Earth Science, University of Bergen. A molybdenum (Mo) x-ray tube was used for radiographic measurements, whereas XRF analyses were performed applying a chromium (Cr) tube, with a down-core resolution of 500 µm. Power settings of 30 kV and 35 mA were used with a 10 s counting time. Down-core variations in surface magnetic susceptibility (MS) were measured on the split cores at 0.2 cm resolution using a Bartington MS2E point sensor.

Standard procedures for estimating weight loss-on-ignition (LOI, %), dry bulk density (DBD, g/cm³) and water content (WC, %) were followed (Dean, 1974; Heiri et al., 2001), and the cores were sampled for this purpose every 0.5 cm (GRØP-212; *n* = 486, GRØP-312; *n* = 425, GRØS-212; *n* = 59, STØS-214; *n* = 64) using a syringe for fixed volume extraction (1 cm³). The samples were weighed and dried overnight at 105 °C before being weighed again for DBD and WC. Following subsequent ignition at 550 °C for one hour, the samples were cooled in a desiccator and reweighed for LOI.

Samples from minerogenic sections of GRØP-212 (*n* = 38) were analysed for grain-size distribution. 6–8 g samples (wet weight) were extracted and stirred for two days in a 5% H₂O₂ aqueous solution in order to remove possible organic bindings between grains. The samples were then stirred in a 0.05% Calgon (sodium hexametaphosphate) solution overnight. Finally, the material <63 µm was analysed using a Micromeritics Sedigraph 5100 and Mastertech 5.1 auto sampler. Each sample was analysed several times (five or six) and all of the runs were averaged in order to obtain the final grain-size distribution. The grain-size data were processed using the Gradistat v.8.0 software (Blott and Pye, 2001).

3.3. Chronology

A total of *n* = 20 samples of wet sediments with an average weight of 8 g were extracted every cm from the top 20 cm of GRØS-212. The samples were freeze-dried and submitted for ²¹⁰Pb dating (as well as measuring of ²²⁶Ra, ¹³⁷Cs and ²⁴¹Am by direct gamma assay) at the Environmental Radioactivity Research Centre, University of Liverpool. The same procedure of freeze-drying was

followed for the upper 12 cm of STØS-214, but here the sampling was done every 0.5 cm ($n = 24$). ^{210}Pb ages obtained for GRØS-212 and STØS-214 are shown in Supplementary Tables S1 and S2, respectively.

A total of $n = 20$ terrestrial macrofossil samples (e.g. leaves, twigs, fruits, and seeds) were extracted from GRØP-212 and GRØP-312 and submitted for accelerator mass spectrometry (AMS) radiocarbon dating at the Poznan Radiocarbon Laboratory in Poland (Table 1). 1-cm sediment slices were extracted at selected depths and wet-sieved, after which plant macrofossils were handpicked and identified using a stereo microscope. Macrofossils were dried overnight at 50 °C and placed in sterilized glass vials before submission to AMS dating. At the radiocarbon laboratory, macrofossils were chemically prepared with acid-alkali-acid in a three-step treatment (<http://www.radiocarbon.pl/>).

Age-depth models were constructed using the 'clam' source code from Blaauw (2010), applied in the open-source statistical software 'R' (R Development Core Team, 2012). Radiocarbon ages are reported in calibrated radiocarbon years before present (cal yr BP; BP = 1950) and Common Era (CE). Several samples contained less than 1 mg of carbon (Poz-54061; Poz-54062; Poz-54066; Poz-54068; Poz-54070; Poz-54074; see Table 1) and a number of these were not included for modelling of the age-depth relationship (see Section 4.4).

3.4. Principal Component Analysis

The multivariate sedimentary data sets from GRØP-212 and GRØP-312 were explored using Principal Component Analysis (PCA) in order to detect patterns of shared variability between the measured proxies (e.g. Syms, 2008). Because PCA assumes linearity between the analysed variables (e.g. Bakke et al., 2013), the relationship between all variables in the dataset were examined individually using biplots and regression analysis to see whether any data transformation was needed before running the PCA. A logarithmic relationship was found between LOI and the other data, and LOI was therefore Log-transformed before analysis. The entire dataset was then standardized before running the PCA in the software Canoco for Windows (v. 4.5) (Leps and Šmilauer, 2003).

In total, 11 variables were included in the PCA from both cores

GRØP-212 and GRØP-312. In addition to the physical proxies DBD, LogLOI, and MS, geochemical elements that are commonly sensitive to changes in detrital input (Si, Ti, K, and Ca; e.g. Bakke et al. (2010)), redox processes (Fe and Mn; e.g. Naeher et al. (2013)), and grain-size (Rb and Sr; e.g. Vasskog et al. (2012)) were added into the analysis.

3.5. Instrumental meteorological data and mass-balance modelling

In order to reconstruct continuous ELA changes from distal glacier-fed lake sediments, the sediment parameters need to be calibrated against periods when the ELA is known or can be inferred. This calibration is commonly obtained using moraine ridges of known age (Dahl et al., 2003; Bakke et al., 2010), but this approach cannot be applied here as there are no observed distinct late-Holocene/LIA moraine ridges around Ålfotbreen. However, ELA measurements are available for Ålfotbreen (the outlet glacier) between CE1963 and CE2010 (Kjøllmoen, 2011), and this record can be extended by modelling the ELA using instrumental meteorological data. Nordli et al. (2005) applied a stepwise multiple regression and found that a combination of two atmospheric indices; the wintertime westerly geostrophic wind component (uw) and the summertime southerly shear vorticity ($\xi_v s$), was able to predict the ELA at Ålfotbreen with relatively high precision (Pearson's correlation coefficient, $r = 0.72$). These indices can be calculated from mean sea-level pressure (MSLP) data that are available back to CE1781 for northern Europe (Jones et al., 1999). However, some of the summertime MSLP data used in calculation of the shear vorticity index are not considered to be robust beyond CE1850 (Jones et al., 1999), and this index does not seem to capture long-term trends in summer temperature very well. However, over decadal timescales, summer temperatures along the west coast of Norway are strongly correlated with North Atlantic sea surface temperatures ($r = 0.88$) (Supplementary Fig. S3), and we therefore tested a reconstruction of the Atlantic Multidecadal Oscillation (AMO) (Mann et al., 2009) as an alternative predictor of summer ablation in our ELA model, and this resulted in a better fit ($r = 0.77$, $R^2 = 0.59$) with measured ELA than the model from Nordli et al. (2005). Thus, the ELA model employed here uses wintertime geostrophic wind (uw) (Nordli et al., 2005) and AMO temperature anomalies (Mann et al., 2009) as predictors, and is expressed as:

Table 1
Radiocarbon dates obtained for GRØP-212 and GRØP-312. Calibrated ages obtained using 'clam' (Blaauw, 2010). Samples marked* were rejected for the age-depth modelling in 'clam'.

Core	Lab.no	Depth (cm)	Material	^{14}C age	± 2 sigma (cal yr BP)	$\delta^{13}\text{C}$ (‰)	Remark
GRØP-212	Poz-54060	10–11	Terrestrial plant remains	90 \pm 35 BP	15–268*	–26.6	
GRØP-212	Poz-54061	13–14	Terrestrial plant remains	105 \pm 30 BP	14–268*	–29.2	TOC, 0.7mgC
GRØP-212	Poz-54062	25–26	Terrestrial plant remains	115.12 \pm 0.42 pMC	(–43)–8*	–32.4	TOC, 0.4mgC
GRØP-212	Poz-54063	30–31	Terrestrial plant remains	540 \pm 30 BP	514–633	–28.1	
GRØP-212	Poz-54064	45–46	Terrestrial plant remains	1840 \pm 30 BP	1709–1864*	–23.6	
GRØP-212	Poz-54066	50–51	Terrestrial plant remains	1580 \pm 40 BP	1389–1551	–32.7	0.3mgC
GRØP-212	Poz-54067	80–81	Terrestrial plant remains	2540 \pm 40 BP	2491–2751	–25.3	
GRØP-212	Poz-54068	110–111	Terrestrial plant remains	2600 \pm 40 BP	2512–2786*	–33.2	TOC, 0.4mgC
GRØP-212	Poz-61506	114–115	Terrestrial plant remains	3925 \pm 35 BP	4245–4498	–25.8	
GRØP-212	Poz-54070	132–133	Terrestrial plant remains	>0 BP			Too small
GRØP-212	Poz-54071	150–151	Terrestrial plant remains	5910 \pm 40 BP	6654–6845	–24.7	
GRØP-212	Poz-61505	180–181	Terrestrial plant remains	7740 \pm 40 BP	8433–8590	–28.7	
GRØP-212	Poz-54072	185–186	Terrestrial plant remains	8030 \pm 50 BP	8663–9030*	–30.2	
GRØP-212	Poz-54073	230–231	Terrestrial plant remains	8720 \pm 50 BP	9550–9887	–29.8	
GRØP-312	Poz-54074	10–11	Terrestrial plant remains	55 \pm 35 BP	(–5)–259*	–28.3	0.8mgC
GRØP-312	Poz-54075	30–31	Terrestrial plant remains	345 \pm 30 BP	314–483	–24.3	
GRØP-312	Poz-54076	35–36	Terrestrial plant remains	460 \pm 30 BP	485–537	–26.2	
GRØP-312	Poz-54077	47–48	Terrestrial plant remains	845 \pm 35 BP	686–899	–25.4	
GRØP-312	Poz-54078	88–89	Terrestrial plant remains	1570 \pm 30 BP	1397–1533	–29.9	
GRØP-312	Poz-54080	156–157	Terrestrial plant remains	2295 \pm 30 BP	2183–2354	–24.8	

$$\begin{aligned} \text{ELA} &= (-29 * uw) + (226 * \text{AMO}) + 1360 (\text{m a.s.l.}) \left(R^2 \right. \\ &= 0.59, p < 0.003 \left. \right) \end{aligned} \quad (1)$$

3.6. Quantifying winter precipitation

We use the approach presented by Dahl and Nesje (1996) for reconstructing winter precipitation (Pw), which is based on the close empirical relationship between mean ablation-season (1 May to 30 September) temperature (Ts) and Pw at the ELA of Norwegian glaciers; i.e. the 'Liestøl equation' (Sissons, 1979; Sutherland, 1984; Ballantyne, 1989). This relationship is expressed by the regression equation:

$$\text{Pw} = 0.915 e^{0.339T_s} \left(R^2 = 0.989, p < 0.0001 \right) \quad (2)$$

where Pw is meters of water equivalents and Ts is the mean ablation season (summer) temperature at the ELA in °C. This implies that if the mean summer temperature at the ELA is measured/reconstructed, the mean winter precipitation can be calculated. Using an environmental lapse rate of 0.65 °C/100 m as in Sutherland (1984) and Oerlemans (1992), this gives a mean summer temperature (Ts) of 4.77 °C at the present steady-state ELA of Ålfotbreen at 1182 m a.s.l. (obtained through linear regression of net mass balance against measured ELAs for the period CE1963–2010, c.f. Fig. 2). Using Eq. (2), we find that the Pw required to balance summer ablation at the steady-state ELA is ~4.61 m. This procedure can be used to reconstruct past Pw at the ELA by combining a continuous ELA reconstruction with an independent temperature record (e.g. Dahl and Nesje, 1996; Bjune et al., 2005). Finally, winter precipitation can be calculated for a fixed altitude (e.g. sea level) by accounting for fluctuations in the ELA using the observed exponential increase in Pw with altitude of 8%/100 m in southern Norway (Haakensen, 1989).

4. Results

4.1. Lithostratigraphy

Core GRØP-112 (N61.68948 E5.56832; water depth: 39 m) was retrieved from the middle part of the Grøndalsvatnet basin, corresponding to the approximate location of the core studied by Nesje et al. (1995) (Fig. 1). Like Nesje et al. we found that the lacustrine stratigraphy at this site is dominated by rapidly deposited layers (e.g. avalanche-, flood- or debris-flow deposits); most likely introduced to the basin from a large alluvial fan west of the lake; and the core was therefore not considered for further analyses. Cores GRØP-212 (N61.68665 E5.57280; water depth: 12 m) and GRØP-312 (N61.68543 E5.56881; water depth: 5 m) were collected from the south-eastern parts of the lake, where the risk of disturbances from floods and colluvial events was considered to be lower and the distance to the main inlet is larger. The description of lithostratigraphy (below) refers to GRØP-212, because a hiatus in GRØP-312 indicates that this core is missing a large part of the lower sediments (i.e. lithostratigraphic units B; C; D; and parts of unit E; see below). The lithostratigraphic division of the core into nine units, A–I, is based on visual logging. A correlation was made between all cores based on XRF Ti count rates (Fig. 3), as this parameter distinguishes well the different sedimentary units.

Unit A (206–243 cm) consists of grey clayey- and silty-, highly-minerogenic sediments. The unit is massive and comprises varying

grain sizes ranging from clay to fine sand. Thin (<0.5 cm) horizons with visible plant remains are relatively frequent, and a prominent horizon was sampled for radiocarbon dating (Poz-54073). DBD values are generally very high; decreasing upwards in the unit from 1.47 to 0.47 g/cm³ and averaging at 0.98 g/cm³. The opposite trend is observed for LOI, which increases from values around 5% in the lower part up to more than 9% in the topmost part of unit A, reflecting an increase in organic content.

Unit B (187–206 cm) consists of very dark greyish brown silty gyttja with lighter-coloured laminations that gradually becomes weaker upwards. DBD is relatively stable (around 0.5 g/cm³), whereas LOI shows greater variability and an increasing trend (from ~7 to ~12%). An erosional contact marks the transition to unit C.

Unit C (178–187 cm) consists of greyish brown, chaotic, clayey- and silty minerogenic sediments in the lower part, and contains angular clasts up to ~0.5 cm diameter. The lower section of the unit (181–187 cm) is massive and can be distinguished both visually and in X-ray images (cf. Fig. 4). From 180 to 181 cm the sediments consist of laminated greyish-brown, silty gyttja, and from 178 to 180 cm it is characterized by a very dark brown, highly organic horizon rich in terrestrial plant remains. Unit C has a distinct development from highly minerogenic in the lower part (DBD = ~1.0 g/cm³; LOI = ~4%) to highly organic in the upper part (DBD = ~0.4 g/cm³; LOI = ~22%). The lower section of the unit (181–187 cm) is interpreted to have been deposited rapidly. The erosional contact at the base, the stirred appearance of the sediments, and the angular morphology of the grains suggest that this may be an avalanche deposit. The upper section of the unit, 178–180 cm, is interpreted to represent a flood event delivering organic detritus from the catchment area to the lake.

Unit D (172–178 cm) consists of very dark, greyish-brown silty gyttja with lighter-coloured laminations. The unit is characterised by a peak in all parameters except LOI, which decreases to a minimum of ~8% in this unit. X-ray images show that the sediments are relatively dense, which is also reflected in relatively high DBD values (~0.5–0.7 g/cm³). The percentage of fine silt shows a distinct peak, rising from ~20 to 40% before decreasing again towards the top of the unit.

Unit E (40.5–172 cm) consists of very dark brown to olive brown gyttja with lighter-coloured laminations. The section from 120 to 130 cm has a lighter colour with more frequent laminations, and X-ray imagery shows that the sediments in that section are relatively dense compared to the sediments above and below. DBD values remain low and stable throughout the unit; with values averaging ~0.4 g/cm³. LOI shows greater variability than DBD throughout unit E, fluctuating between ~12 and 21%, with the trend gently increasing. A dark brown horizon consisting mainly of plant remains is observed from 43.5 to 46 cm depth, and this section is interpreted to represent a flood event.

Unit F (27–40.5 cm) consists of dark, greyish-brown silty gyttja, and is largely a transitional unit from organic sediments at the base to more minerogenic sediments in the top. DBD increases from ~0.4 to a maximum of ~0.6 g/cm³ through the unit, reflecting an increasing density that can also be seen in the radiographic images, while LOI decreases from ~13 to ~6%. Lighter-coloured laminations also increase in frequency upwards.

Unit G (22–27 cm) consists of olive brown silty gyttja that is slightly more organic than the underlying unit. DBD drops to an average of ~0.5 g/cm³ and LOI increases to an average of ~9%.

Unit H (6–22 cm) consists of greyish brown, slightly organic, clayey silt. Several distinct peaks in DBD of up to ~1.0 g/cm³ can be seen, and together with a colour change of the sediment this indicates a shift in the depositional environment. LOI shows an opposite pattern of DBD, with values averaging at 5%. A dark,

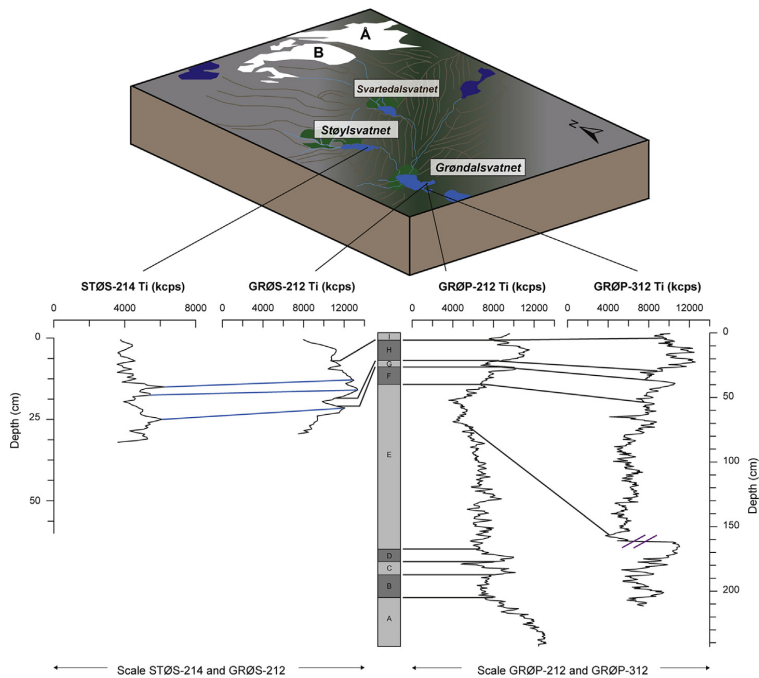


Fig. 3. Schematic 3D profile of the catchment area for Støylsvatnet and Grøndalsvatnet with visual correlation of the cores based on XRF Ti count rates (kcps) in combination with ^{210}Pb and ^{14}C ages and visual structures. Blue lines mark the correlation between Ti peaks in STØS-214 and GRØS-212. Note hiatus in GRØP-312 marked in purple (158 cm depth). (For interpretation of the references to colour in this figure legend, the reader is referred to the web version of this article.)

organic-rich horizon with LOI up to ~9% is seen from 8 to 10.5 cm, which consists predominantly of plant remains. This is interpreted to represent a layer of instantaneous deposition, most likely a flood event.

Unit I (0–6 cm) consists of very dark, greyish-brown silty gyttja. DBD lowers to an average value of -0.5 g/cm^3 , and LOI increases to ~7% on average.

In previous studies (e.g. Nesje et al., 2007; Vasskog et al., 2011), river flood deposits have been characterised by their brown colour, high-organic content, and large amount of terrestrial plant macrofossils, whereas horizons containing clasts >1 mm are interpreted as snow-avalanche deposits. Based on these criteria, the specific horizons ≥ 1 cm that have been interpreted as layers representing flood events and avalanche deposits (i.e. 'instantaneous' deposition, see Fig. 4) were omitted from the age-depth relationship modelling and further discussion of the results.

4.2. Magnetic susceptibility

In general, MS values in GRØP-212, GRØP-312, GRØS-212 and STØS-214 are quite low; on average 9; 8; 13 and 3 ($\text{Si } 10^{-5}$), respectively. Because the bedrock in the catchment area consists of sandstones and conglomerates it contains a large proportion of the diamagnetic mineral quartz (SiO_2), which will return a net negative magnetic moment when subjected to a magnetic field (Sandgren and Snowball, 2001). This might explain the relatively low surface MS signal in the cores; but nevertheless, the main trends in MS seem to co-vary with the other indicators of detrital input (e.g. DBD and XRF Ti count rates, see Fig. 4A and B).

4.3. Geochemistry

Most of the geochemical elements included in this study show similar trends to that of Ti. Notable exceptions are the redox-sensitive elements Fe and Mn, which reflect a different pattern of variability than the other geochemical proxies in unit E of GRØP-212. On the other hand, Fe co-varies with the other geochemical proxies in GRØP-312, whereas Mn differs strongly throughout most of that core (see Section 4.5 for a closer description). See Fig. 4 for a compilation of selected physical and geochemical variables from cores GRØP-212 and GRØP-312, where event layers are highlighted in brown.

4.4. Age-depth relationships

Chronologies have been established for both piston cores from Grøndalsvatnet (GRØP-212 and GRØP-312) based on AMS radiocarbon ages and ^{210}Pb ages transferred from GRØS-212 through visual correlation based on the measured physical and geochemical proxies (see Table 1 for radiocarbon ages; Table S1 for ^{210}Pb ages). Age-depth relationships produced in 'clam' (v. 2.2; Blaauw (2010)), using the IntCal13 calibration curve from Reimer et al. (2013), are shown for cores GRØP-212 and GRØP-312 in Fig. 5A and B, respectively. Ages are not extrapolated beyond the lowermost dated depths (GRØP-212: 230.5 cm; GRØP-312: 156.5 cm). Outliers that showed inverted or future ages were omitted from the age-depth relationships and are shown in red in the figures. In Fig. 5C, the ^{210}Pb age profile for GRØS-212 is shown with a dark grey shading marking a ± 8.5 year uncertainty, which is added here because ^{137}Cs peaks indicates that up to ~1 cm of the uppermost

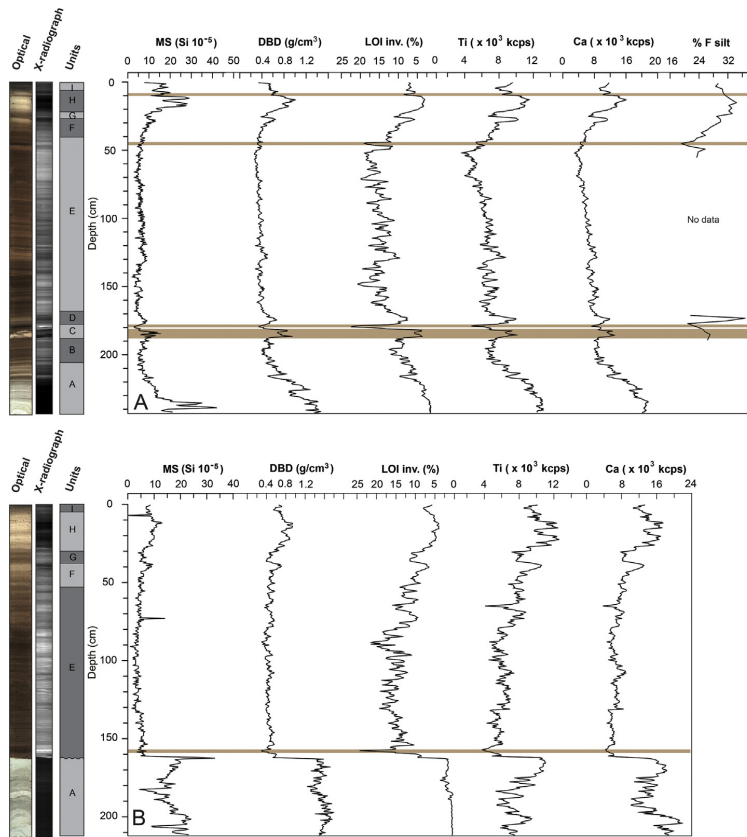


Fig. 4. Selected sediment variables from A) GRØP-212; and B) GRØP-312. Line-scan images, radiographic images and lithostratigraphy are shown to the left. Event layers are marked in brown. All data smoothed to 0.5 cm except grain size data from GRØP-212 (2-cm resolution). (For interpretation of the references to colour in this figure legend, the reader is referred to the web version of this article.)

sediment may have been lost during coring (1 cm = -17 years), while the additional light grey shading marks the regular laboratory uncertainty of the ^{210}Pb measurements. An independent age-depth relationship was also constructed for STØS-214 using ^{210}Pb (Fig. S4, see Table S2 for ^{210}Pb ages). A composite age-model for GRØS-212 was constructed, where ages below the ^{210}Pb dates were obtained by tuning the GRØS-212 Ti record against the radiocarbon dated GRØP-212 (Fig. 5D). This age-depth relationship is the one used for calibrating the lake sediment data against the ELA-model and in the reconstructions of Neoglacial ELA and winter precipitation (see Sections 4.7 And 4.8).

4.5. Principal Component Analysis

For both GRØP-212 and GRØP-312 the PCA returned only one significant Principal Component (PC) axis that explains 88 and 83%, respectively, of the total variance in the datasets (Supplementary Table S3). In both cores the first PC axis captures well the variability of LogLOI, DBD, MS, Ti, K, Ca, Si, Rb, and Sr (Fig. 6). These variables are all strongly correlated, with LOI being inversely correlated to the others. Fe and Mn show a somewhat different pattern of variability than the other geochemical proxies in GRØP-

212, and this difference is captured by the second PC axis (Table S3). While the second PC axis is not significant in this analysis, this does not necessarily mean that the PCA2 signal is not related to an underlying causal process. It does, however, indicate that this signal is much weaker than the main pattern of variability in the dataset (represented by PC axis 1), and that Fe and Mn are also strongly affected by this main signal as reflected in their relatively high scores along PC axis 1 (Table S3). In GRØP-312, which covers a shorter time period than GRØP-212 (c.f. Section 4.4), Fe has a very similar variability to that of all the other geochemical proxies, whereas Mn differs strongly with most of its variability captured by PC axis 2. Down-core PCA1 scores for GRØP-212 and GRØP-312 are shown compared to standardized values of all analysed variables in Fig. 6.

4.6. Grain-size analyses

Grain-size analyses were performed for selected intervals of GRØP-212 based on time periods of specific interest (and minerogenic content), which included the Neoglacial period and the '8.2 ka BP Event'/Finse Event. Additionally, the high organic content in unit E makes it less suitable for grain-size analyses, as this makes it more

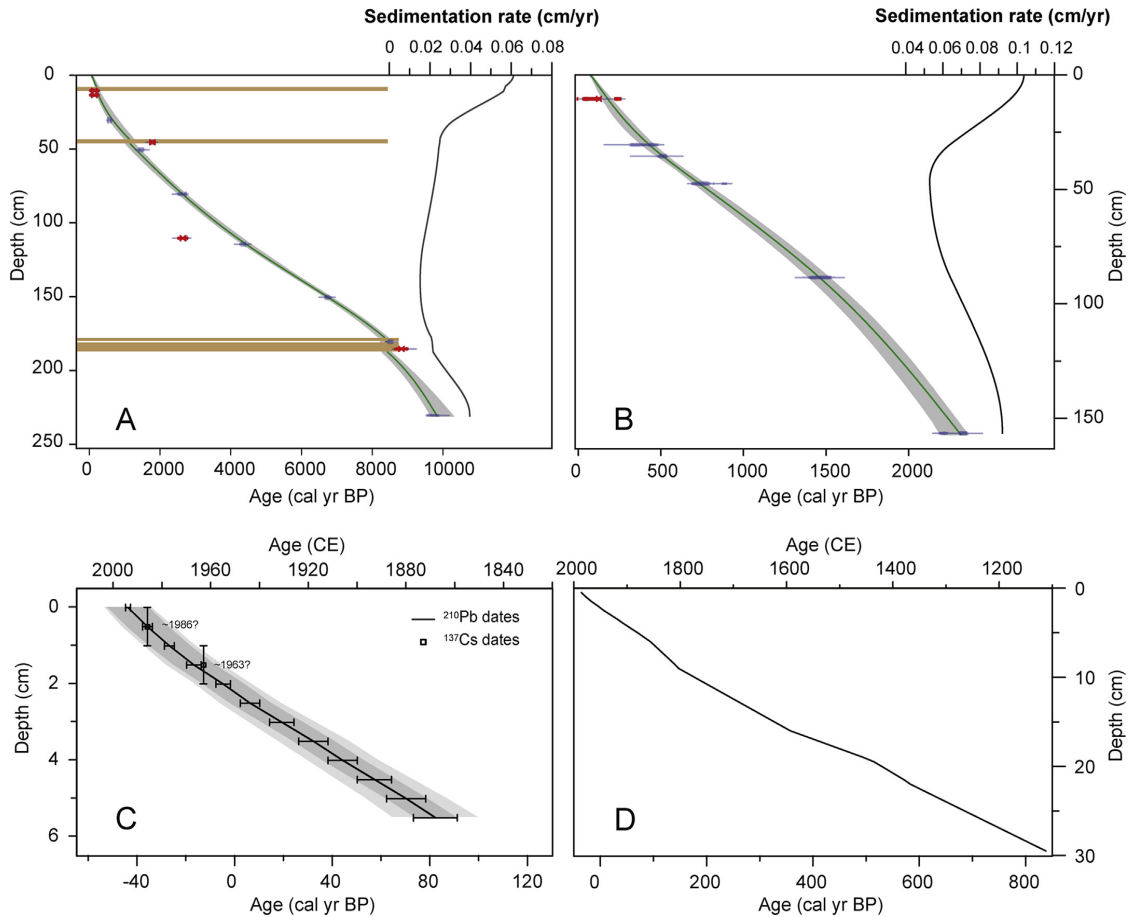


Fig. 5. A) Age-depth relationship and sedimentation rate for GRØP-212. Green line is the best estimate smooth spline model age; grey shading marks the 95% (2σ) confidence interval. Blue shaded areas show probability density functions of the calibrated radiocarbon dates. Red shaded areas mark inferred outliers. Horizontal brown layers mark event layer depths. B) Age-depth relationship and sedimentation rate for GRØP-312 (same colour coding as for A). Note the large difference in sedimentation rate compared with GRØP-212. C) ^{210}Pb age profile for GRØS-212. D) Composite age-depth relationship for GRØS-212, based on ^{210}Pb ages and ^{137}Cs ages from GRØS-212, with the lowermost part tuned to the ^{14}C -based GRØP-212 age-depth relationship. (For interpretation of the references to colour in this figure legend, the reader is referred to the web version of this article.)

challenging to remove all organic material during pre-treatment. Grain-size variations can indicate changes in the amount of glacially eroded rock flour washed into the lake, and in particular, silt fractions can indicate abrasive glacier activity of temperate glaciers (Matthews and Karlén, 1992; Matthews et al., 2000; Nesje et al., 2001; Lie et al., 2004). Of the different grain-size classes, fine silt was found to have the highest co-variance with other indicators of detrital input in GRØP-212 (Fig. 4A).

4.7. Calibration of lake record against instrumental data and equilibrium-line altitude reconstructions

We determined the onset of the local Neoglacial based on variations along PC axis 1 in core GRØP-212 where the trend turns towards increased glacial input at 1400 cal yr BP, and reflects maximum Neoglacial expansion during the LIA (CE1300–1900). In order to reconstruct ELA variations from the lake sediment record, it needs to be calibrated against periods of known or inferred ELA

variations. Because moraines are lacking around Ålftobreen, we applied an ELA model driven by AMO temperature anomalies (Mann et al., 2009) and an index of wintertime westerly geostrophic winds (Nordli et al., 2005) (c.f. Section 3.5). The ELA model could be extended to CE1781 using these data and applied to calibrate the dated lake sediment record covering the same period. In order to get as high temporal resolution as possible, it was desirable to use the ITRAX XRF data for this purpose, and from the PCA it is evident that the elements Ti, Si, K, and Ca all reflect detrital input to the lake, and during the Neoglacial this is inferred to have been driven mainly by glacier activity. Because Ti is insensitive to redox processes (e.g. Croudace et al., 2006) and has previously been shown as a good indicator of glacier erosion (Bakke et al., 2009; Wittmeier et al., 2015), we have used Ti count rates as a glacier proxy, and for the purpose of calibration against modelled ELA, we used the most robustly dated Ti record from GRØS-212. It is expected that the glacier signal captured in the sediments of a distal glacier-fed lake will appear smoothed and lagging behind changes

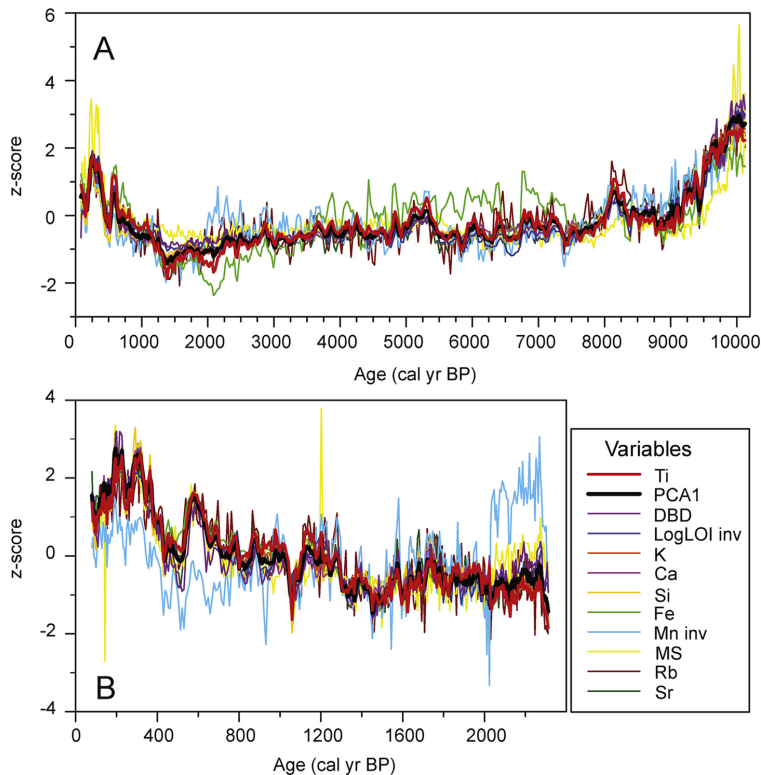


Fig. 6. A) Standardized sediment variables and PCA1 scores for GRØP-212. B) Standardized sediment variables and PCA1 scores for GRØP-312. A) and B); LOI is log-transformed and inverted. Note how Fe and Mn deviate from the general pattern of variability during certain time periods, and the different age scales between A and B.

in the upstream glacier's ELA due to the response time of the glacier itself and dynamics of the downstream sedimentary system. We performed an autocorrelation between modelled ELA changes and the lake Ti record using Analyseries (Paillard et al., 1996), and obtained the best fit when a lag of 14 years is introduced in the lake record. This lag is within the ^{210}Pb dating uncertainty (Fig. 5C) before ~CE1930, whereas in the most recent part of the Ti record an actual lag (i.e. outside the ^{210}Pb uncertainty range) of up to 4.5 years is required to obtain the maximum fit with the ELA model (Fig. 7). A simple linear regression model was constructed between modelled ELA changes and the Ti record from the GRØS-212 core (Fig. 7). Below the lowermost ^{210}Pb -date in GRØS-212 we tuned the age-model to the ^{14}C -dated GRØP-212 using the Ti record, and thus extended the ELA reconstruction to the base of GRØS-212 (Fig. 5D). Beyond this point we applied the same regression model to Ti counts from GRØP-212, although this makes the ELA reconstruction less reliable for this interval because the variability in Ti-counts is slightly different in GRØP-212 than in GRØS-212.

4.8. Winter precipitation reconstructions

In order to reconstruct winter precipitation from our reconstructed ELA record, an independent record of summer temperature is needed (c.f. Liestøl in: Sissons, 1979). For this purpose we have calibrated the AMO reconstruction from Mann et al. (2009) against the instrumental summer temperature record in Bergen

(using linear regression; $R^2 = 0.78$) and adjusted it for the slight difference in summer temperature ($0.15\text{ }^\circ\text{C}$, based on the CE1961–1990 normal period) between Bergen and Sandane (located 30 km east of Ålfotbreen) (Fig. S3). This gives a reconstruction of representative summer temperature for Sandane (Fig. 8A), which can be used to calculate corresponding temperatures at the changing elevation of the reconstructed ELA of Ålfotbreen (Fig. 8B) using a lapse rate of $0.65\text{ }^\circ\text{C}/100\text{ m}$. Based on the 'Liestøl equation' (eq. (2)), we can then reconstruct winter precipitation (Pw) at the ELA for the entire interval covered by the ELA reconstruction, and finally, the Pw can be adjusted from the variable ELA to a fixed altitude, in this case sea level, using a precipitation reduction of 8%/100 m (c.f. Section 3.6). The reconstructed Pw at sea level is shown in percentage of the modern value (1.7 m water equivalents) in Fig. 8C. Note that both our ELA reconstruction and the temperature record based on the Mann et al. (2009) AMO reconstruction were resampled to a common temporal resolution of 10 years before being used in reconstruction of Pw. While the original AMO reconstruction is available in annual resolution, it does include proxy records that are not annually resolved and the authors of that study state that variability below decadal scales may not necessarily reflect a meaningful climate signal (Mann et al., 2009). Similarly, we assume that due to the response time of the glacier and downstream sedimentary system, the Ti record from Grøndalsvatnet is probably not able to resolve glacier fluctuations below decadal scales.

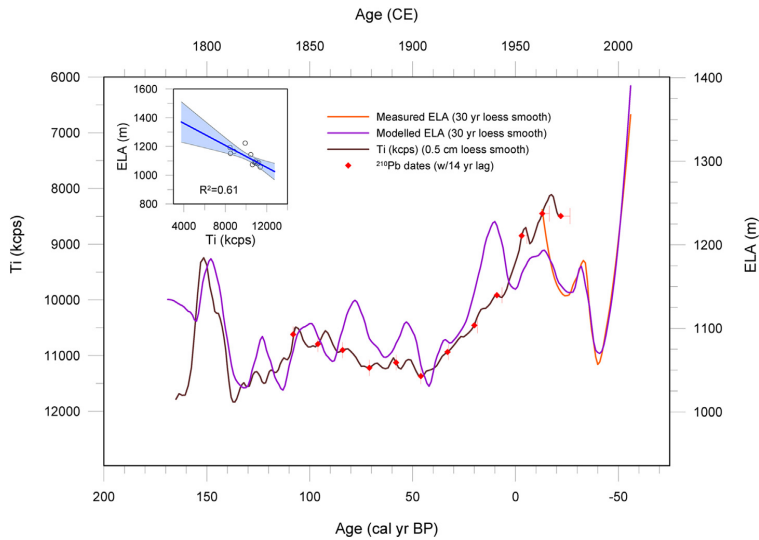


Fig. 7. Measured (orange) and modelled (purple) ELA of Ålfotbreen plotted against variations in Ti count rates from the GRØS-212 core (brown). Ti is plotted with a 14-year lag, which gave the best fit against the ELA model. Red points represent ^{210}Pb -dated levels in the core with error bars showing the minimum lag needed to obtain the optimal fit after accounting for uncertainties in the ^{210}Pb dating. A linear regression between Ti counts and modelled ELA is shown in the inset figure with 95% confidence bands shaded blue. This regression model was used to reconstruct ELA changes further back in time (Figs. 8 and 10) using the Ti record from GRØS-212 and GRØP-212 (see Section 4.7 for details). (For interpretation of the references to colour in this figure legend, the reader is referred to the web version of this article.)

The central estimates of our reconstructed winter precipitation (Fig. 8C) vary between approximately 55% and 150% of present-day values. Note that the width of the 95% and 68% confidence bands vary between 15% and 115%, and 7%–60%, respectively (see Section 5.3 for discussion of uncertainties). This range of variability in decadal-scale precipitation over the last ~1400 years does not seem unlikely; as a comparison the 10-year average precipitation in Bergen increased from 85% to 125% of the CE1961–1990 mean in the period between CE1960 and CE1995 (data: Norwegian Meteorological Institute; klima.met.no).

5. Discussion

The main objective of this study has been to reconstruct Holocene glacier fluctuations and convert sediment parameters into a quantitative ELA reconstruction that could be further used to calculate past winter precipitation at the Ålfotbreen ice cap. In the following discussion we first assess the utilization of lake sediments for this purpose, and the methodologies applied are evaluated. Second, the results are discussed; first in a broad, Holocene climatic context; and thereafter in the context of Neoglacial ELA variations and winter precipitation. Finally, the results are discussed and compared with relevant climate records from the North Atlantic region, and implications regarding climatic forcing of the Ålfotbreen record are assessed.

5.1. Interpretation and application of lake sediments

While lake sediments are valuable palaeoclimatic archives, it is important to be aware of potential sources of error when interpreting these records in a climatic context (Nesje et al., 2004). Instantaneously deposited layers are important to exclude from age-depth modelling, as they might produce erroneous ages and perturb the accumulation rates that result from the age-depth

relationship (Rubensdotter and Rosqvist, 2009). As discussed in Section 4.1, we omitted all identified event layers before age-depth relationships were established. Additionally, another possible source of error when studying lake sediments; and in particular proglacial lake sediments, is reworking of older glacial sediments (Ballantyne, 2002; Carrivick and Tweed, 2013). However, for small catchments this 'paraglacial' effect will be most significant for a relatively short time period after deglaciation. Provenance studies also indicate that magnetic and geochemical properties of older glacial deposits change over time due to weathering and soil formation (e.g. Vasskog et al., 2012; Wittmeier et al., 2015). Due to the resistant, acidic bedrock in the area (sandstones/conglomerates) superficial deposits are scarce and covered by vegetation in the few places where it is found (mainly the inlet delta and the colluvial fan), meaning that there is generally very little unconsolidated material of non-glacial origin available for erosion in the catchment of Grøndalsvatnet. Input of glacial sediments should therefore, due to the highly effective nature of glacial erosion, be able to dominate the minerogenic sedimentation budget in Grøndalsvatnet when Ålfotbreen is present. Human activities could possibly cause a bias in minerogenic sedimentation, e.g. due to forest clearance and establishment of farmland (e.g. Augustsson et al., 2013). Such effects are difficult to quantify, however, and here we attempt to take such potential biases into account by including a wide confidence range in our final results, as discussed further in Sections 5.2.2 and 5.2.3.

The high correspondence between most of the geochemical elements and the common indicators of detrital input; LogLOI (inverse), MS, and DBD; indicates that the main signal recorded by PC axis 1 in the cores from Grøndalsvatnet reflects the balance between minerogenic and organic content (and water content) in the sediment. This balance is mainly controlled by detrital input from the catchment on one side, and a combination of input of organic detritus from the catchment and organic productivity

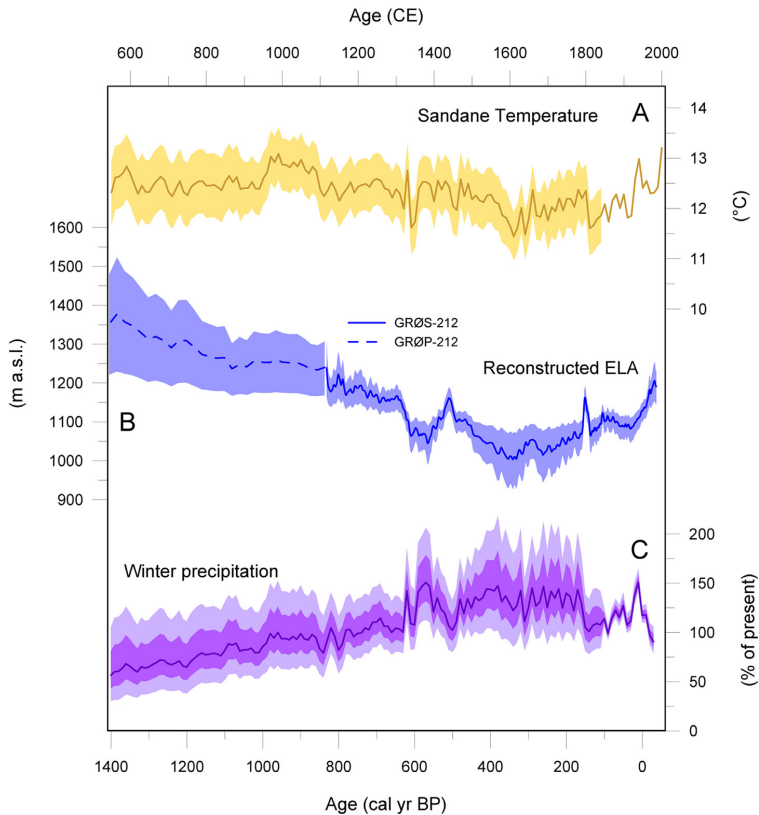


Fig. 8. A) Reconstructed Sandane Ts at sea level, adjusted from the regression between Bergen temperatures and the AMO; B) Reconstructed ELA for Ålfotbreen; C) Reconstructed winter precipitation adjusted to sea level. All plots shaded with 95% confidence bands (until start of instrumental period). Winter precipitation is also shown with 68% confidence band.

within the lake itself on the other. These factors may vary independently over time due to e.g. changes in climate and vegetation (input of organic detritus), lake trophic state (internal organic production), or sediment availability (detrital input). The only elements showing signals significantly different from the one captured by PCA1 are Fe and Mn, and this may be explained by their susceptibility to redox processes, both in the catchment or within the lake (Davison, 1993; Naeher et al., 2013). Because of the sparse sedimentary cover in the catchment area, we argue that when the Ålfotbreen ice cap is present, it will probably provide a significant part of the minerogenic input to Grøndalsvatnet through glacial erosion and downstream transport of the resulting glacial flour. Fe and Mn has a higher co-variability with the other parameters from 10,000–7500 cal yr BP and after 1400 cal yr BP in GRØP-212 (Fig. 6). A possible interpretation of this pattern is that increased input of minerogenic material from the glacier will also overprint the effect of redox processes on the deposition of Fe and Mn when the glacier is present.

In all, we conclude that the PCA1 signal reflects detrital input to Grøndalsvatnet, and may thus also give an indication of when the Ålfotbreen glacier has been present in the catchment (Fig. 6). Following deglaciation (~10,100–~9700 cal yr BP) we observe distinct phases of increased PCA1 values centred around 8200 cal yr BP and 5300 cal yr BP, in addition to the period from ~1400 cal yr BP

(CE550) until present. The distinct reversal of the PCA1 trend at ~1400 cal yr BP is interpreted as the onset of the Neoglacial period in the study area, after which the glacier has most likely existed continuously until the present. It is not possible to determine for certain from our data whether the glacier was completely melted away during the periods of reduced minerogenic input or just strongly reduced in size (see Section 5.2.1). Furthermore, from relative variations in the sedimentary signal within the Neoglacial, we conclude that the LIA lasted from ~650 cal yr BP (CE1300) until ~50 cal yr BP (CE1900) at Ålfotbreen, with a pronounced glacial maximum between ~400 and 200 cal yr BP (CE1550–1750).

From the age-depth relationships (Fig. 5), and correlation between the cores (Fig. 3), it is apparent that GRØP-212 and GRØP-312 have quite large differences (one order of magnitude) in sediment accumulation rates. The main sedimentary signal recorded by the two cores are very similar over the past ~2300 years (Fig. 6); however, the lower-resolution data from the GRØP-212 coring site was preferred for the further analysis because it covers a longer continuous time period (without any hiatus), and because the ^{210}Pb dating of the upper part of the record allows calibration against instrumental data at this coring site (Section 4.7). By correlating variations in XRF Ti counts, we found that the lowermost ^{210}Pb date from GRØS-212 corresponds to the very top of GRØP-212, where some sediment was lost during coring. The obtained ^{210}Pb dates

from the Støylsvatnet core (STØS-214) do not cover the LIA, but the near linear sedimentation rate determined for the upper 6.5 cm may be extrapolated with some confidence down to the strong increase in Ti counts at ~12 cm. Below this level the peaks in Ti counts indicate an increased detrital input and thus most probably increased sedimentation rates, and these peaks have been correlated to the Ti record in GRØS-212 and GRØP-212 (Fig. 3). We infer that the small ice patch southwest of Blåbreen that currently drains into Svartedalsvatnet must have expanded into the catchment of Støylsvatnet (Fig. 1) at the time represented by these Ti-peaks, and conclude that it was probably retreating from its maximum LIA position at 12 cm depth in the STØS-214 core, which corresponds to approximately CE1720 (Supplementary Fig. S4B).

5.2. Holocene glacier fluctuations at Ålfotbreen

5.2.1. Glacier fluctuations in the early to mid-Holocene

Fig. 9 shows the reconstructed relative Holocene glacier variations of Ålfotbreen, as represented by the PCA1 record from core GRØP-212, compared with relevant proxy records from the North

Atlantic region.

The timing of deglaciation for Ålfotbreen is concurrent with the end of the 'Erdalen Event II' (e.g. Nesje et al., 2008; Nesje, 2009); a period with glacier advance at Jostedalbreen, interpreted as a response to colder temperatures around 9700 cal yr BP (Dahl et al., 2002). Weakening laminations upwards in Unit B might reflect a decreasing influx of glacially-eroded sediments, or reworking of paraglacial sediments following this glacier event. If the deglaciation of Ålfotbreen occurred after the 'Erdalen Event II', this shows a regional consistency and coeval glacier retreat in the region encompassing Ålfotbreen and Jostedalbreen ice caps. Centred around 8200 cal yr BP, there is a marked increase in minerogenic input (Fig. 9E); synchronous with the timing of the '8.2 ka BP Event' recorded in ice cores from Greenland (Fig. 9A) (Rasmussen et al., 2006; Vinther et al., 2006), known as the 'Finse event' in Norway (Nesje and Dahl, 1991; Dahl and Nesje, 1994; Nesje et al., 2008; Nesje, 2009), and a cooling seen in reconstructed July temperature at the nearby Kråkenes site (Fig. 9D; Sylvia M. Peglar and H.J.B. Birks unpublished data). Hormes et al. (2009) found

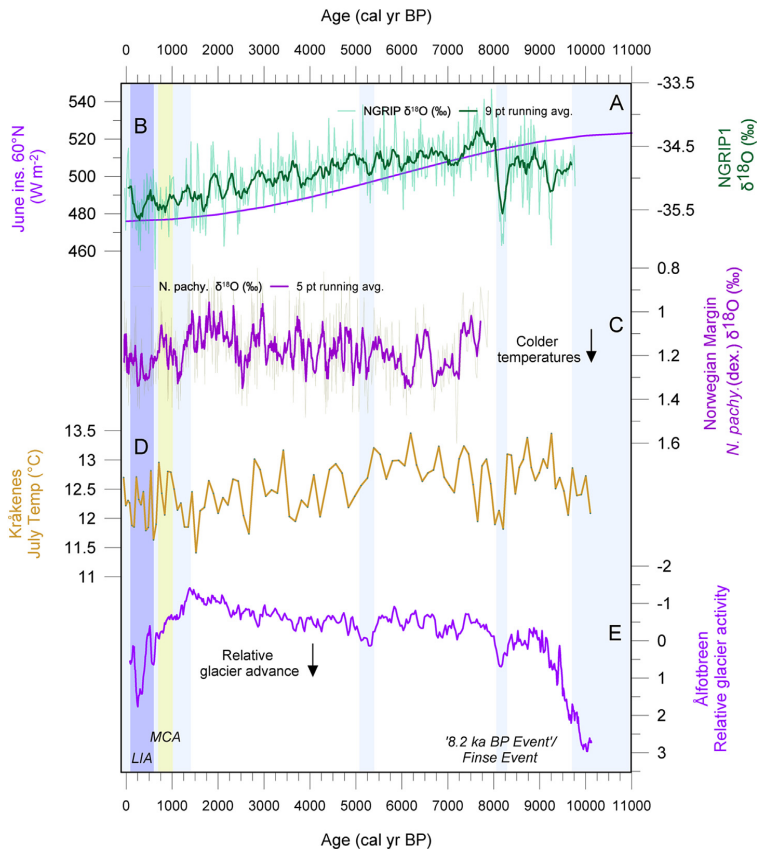


Fig. 9. Comparison of reconstructed Holocene glacial activity of E) Ålfotbreen (PCA1; this study) with oxygen isotope records from A) NGRIP (Rasmussen et al., 2006; Vinther et al., 2006); B) June insolation curve for 60°N (Berger and Loutre, 1991); C) Foraminiferal SST oxygen isotope records from the Norwegian Margin (Sejrup et al., 2011); and D) Kråkenes July Temperature (°C) (Sylvia M. Peglar and H.J.B. Birks, unpublished data). Proxy data are plotted according to latitude with increasing latitude upwards. Light blue shaded areas mark times of possible glacier advances that are discussed in Section 5.2.1, including onset of the Neoglacial at Ålfotbreen. Yellow shaded area marks the Medieval Climatic Anomaly (MCA; 1000–700 cal yr BP), and darker blue shaded area marks the LIA (600–100 cal yr BP); definitions of MCA and LIA from IPCC (2013) and Solomina et al. (2015). (For interpretation of the references to colour in this figure legend, the reader is referred to the web version of this article.)

three glacial events recorded in Nedre Hervavatnet in Sognefjell, western Norway, at 9200, 8600 and 8200 cal yr BP superimposed on a long-term glacier retreat between 9700 and 8000 cal yr BP. It seems likely that the increased input of minerogenic material to Grøndalsvatnet around 8200 cal yr BP might reflect an advance of the Ålfotbreen glacier initiated by colder conditions, or possibly the glacier reformed during this period after having been absent for ~1500 years after deglaciation. See [Supplementary Fig. S5](#) for a comparison of the Ålfotbreen record with NGRIP oxygen isotopes and LOI (i.e., inverted glacier activity) records from Norway from 9500 to 6000 cal yr BP.

From ~8200 to ~5400 cal yr BP, the minerogenic input to Grøndalsvatnet fluctuates, but it is not possible to conclude whether this is related to glacier variability or if the glacier had melted away and the observed fluctuations simply reflect variations in the influx of paraglacial or non-glacial detrital material and organic input/internal productivity in the lake. From ~5400 to 5100 cal yr BP, a relatively strong increase in detrital input is recognized in the record ([Fig. 9E](#)), and we suggest that this reflects a period of glacier advance for Ålfotbreen. Following the possible glacier events centred around 8200 and 5300 cal yr BP, the minerogenic content of the core decreases until ~1400 cal yr BP. We suggest that the most likely explanation for the reversal of this trend around 1400 cal yr BP is due to the glacier reforming at the onset of the Neoglacial.

5.2.2. Neoglacial and 'Little Ice Age' variations in equilibrium-line altitude

In [Fig. 10](#) we present the reconstructed high-resolution Neoglacial ELA variations at Ålfotbreen compared with glacier records from Norway and Svalbard, in a south-to-north transect and reconstructed AMO temperature anomalies. Our composite (GRØS-212 and GRØP-212) reconstructed ELA curve suggests that Ålfotbreen could have formed around CE750 (1400 cal yr BP) when the reconstructed ELA is lowered below the top of the present day glacier, and that it may have reached an extent similar to today's around CE1125 (825 cal yr BP) ([Fig. 10E](#)). During the LIA maximum (~CE1550–1750), our reconstruction suggests an ELA lowering of ~200 m relative to the present steady-state ELA at ~1180 m.

Interestingly, we observe that the LIA maximum extent period of the individual ice caps/glaciers seems to occur progressively later as we move northwards along the Norwegian coast (indicated by stippled line in [Fig. 10](#)). Potential climatic implications of this are discussed in [Section 5.4.2](#).

5.3. Past winter precipitation at Ålfotbreen

A proper quantification of the uncertainties in the reconstructed Pw is hard to obtain. For instance, we do not have any quantitative measurement errors for the ITRAX XRF data used in the ELA reconstruction, and there are several potential biases in our record that are hard to quantify, e.g. the effect of forest clearance by humans and changes in land use on the delta plain over the calibration period of our ELA reconstruction, and general changes in input of non-glacial minerogenic material. Instead of a quantitative measure of uncertainty, we therefore present the 95% confidence bands in our ELA reconstruction, as calculated for the linear regression model between Ti counts and modelled ELA ([Fig. 8](#)). [Mann et al. \(2009\)](#) estimated 95% uncertainty intervals for their AMO reconstruction, and we have transferred these directly to our reconstructed Sandane temperature record without adding any additional uncertainty arising from the regression procedure against the instrumental temperatures

([Supplementary Fig. S3](#)). The final Pw reconstruction is therefore presented with a light shaded band showing the maximum and minimum estimates obtained using the 95% uncertainty interval of the temperature reconstruction and the 95% confidence bands of the ELA reconstruction, and a darker shading to indicate the combined 68% confidence bands ([Fig. 8](#)). From CE1860 until present the AMO values are based on instrumental data and for this interval we do not use any uncertainty in temperature. We therefore stress that the final confidence bands shown in [Fig. 8C](#) do not represent quantitative uncertainty estimates, but it gives some impression of how confident we can be in interpreting changes in the final reconstructed Pw at different times. Regarding age uncertainties, the age control of the youngest (younger than ~CE1850) time period is based on ^{210}Pb ages which yield an uncertainty of ~±10 years. Before ~CE1850, the radiocarbon age uncertainties are ranging from ±10–100 years, increasing with age down-core.

5.3.1. Comparing reconstructed winter precipitation at Ålfotbreen with records from ice caps in SW Norway

The extreme maritime setting of Ålfotbreen makes reconstructions of past glacier fluctuations and precipitation from this ice cap interesting with respect to how maritime glaciers will respond to projected future increases in both summer temperature and winter precipitation. Precipitation is projected to increase with global rise in temperatures, but this increase is very unlikely to compensate for the effect of increasing temperatures on glacier mass balance ([IPCC, 2013](#)). Because ~80% of the net mass balance of Ålfotbreen is presently controlled by (accumulation–season) precipitation (Bn/Bw: $R^2 = 0.76$; [Nesje et al. \(2000a\)](#)), it is interesting to investigate if this relationship holds true also for the past. By doing a simple regression analysis, we find that the Sandane summer temperature record (based on AMO temperature anomalies) explains 32% of the variability in our reconstructed ELA record ($R^2 = 0.32$). By default, the reconstructed Pw record will then explain the remaining 68% ($R^2 = 0.68$), as it is a direct function of the summer temperature and ELA (c.f. the 'Liestøl equation'). It should be noted that the AMO is used as a predictor in the ELA model that was used to transform our Ti measurements to ELA. However, because the transformation is simply linear, it will not serve to falsely increase the correlation between reconstructed ELA and the AMO record (i.e. a correlation against uncalibrated Ti counts will give the same result). Doing a similar analysis of measured mass-balance and ELA on Ålfotbreen between CE1963 and 2010 we find that ablation–season mass-balance explains ~40% of variations in the ELA and winter balance explains ~60%. However, the relative importance of winter and summer balance might change over longer timescales ([Trachsel and Nesje, 2015](#)), and we are not able to distinguish any such temporal changes from our reconstruction.

As shown in [Fig. 11A](#), the latest half of our high-resolution dataset of reconstructed Pw (CE550–1980) at Ålfotbreen shows a high degree of similarity with Pw reconstructions at other (maritime) glaciers in SW Norway. The highest degree of covariance is found with the Folgefonna record ([Bakke et al., 2005](#)), which is expected, as this record is also highly influenced by maritime conditions and the strength and position of the westerlies. Due to the higher resolution of our record, it is not possible to correlate decadal-scale Pw fluctuations with the other records, but the main trends are similar from ~CE1300 until present. Before CE1300, there is a large discrepancy in the main trend of our record compared to the other Pw records. Part of this difference may be explained by the fact that precipitation reconstructions based on the 'Liestøl equation' are very sensitive to differences in the temperature records applied, as shown in

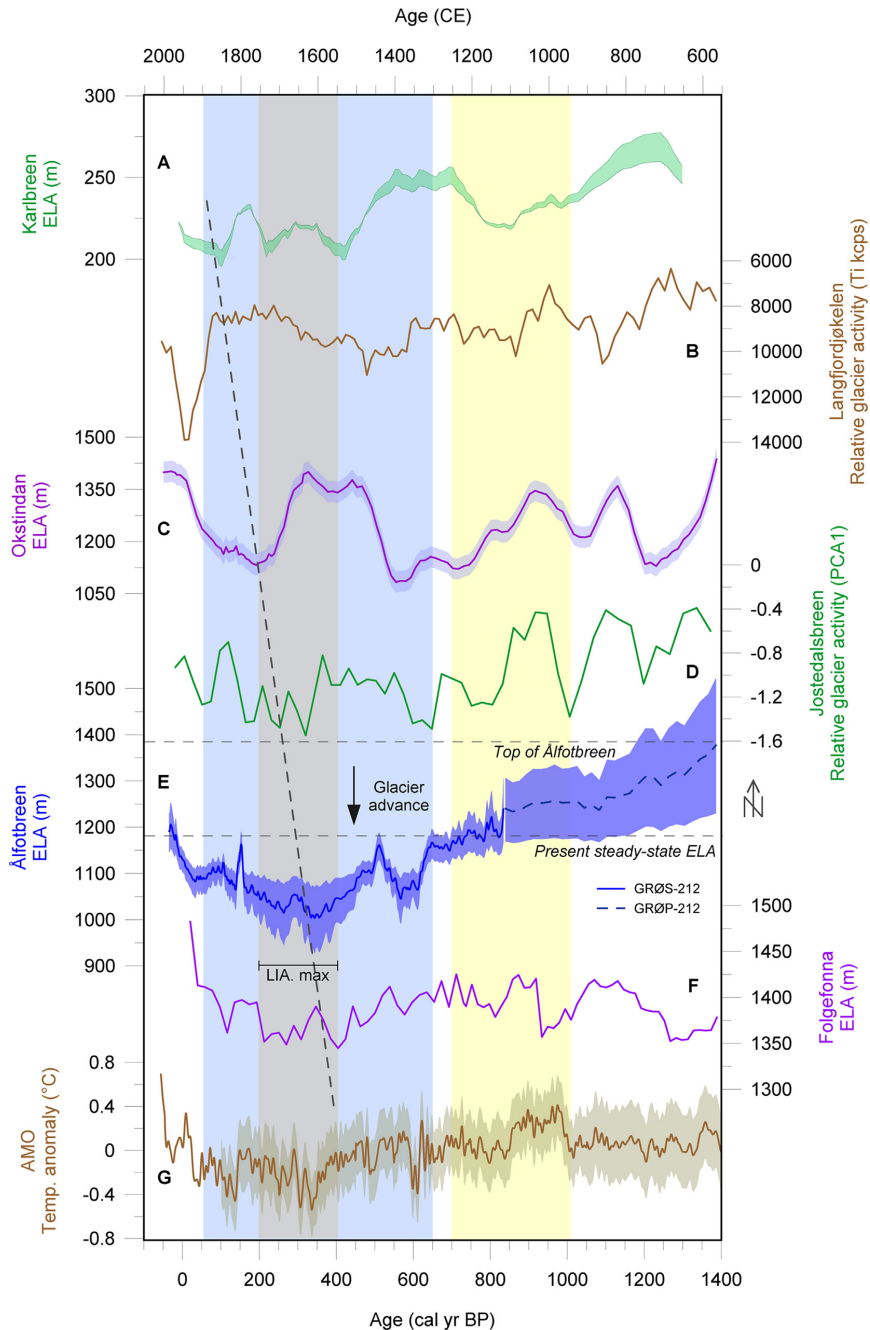


Fig. 10. Neoglacial ELA variations at Ålftobreen (E; this study) compared with A) ELA variations at Karlbreen, NW Svalbard (Rothe et al., 2015); B) Relative glacier activity at Langfjordjøkelen, Arctic Norway (Wittmeier et al., 2015); C) ELA variations at Okstindan, Northern Norway (Bakke et al., 2010); D) Relative glacier activity at Jostedalbreen, Western Norway (Vasskog et al., 2012); F) ELA variations at Folgefonna, SW Norway (Bakke et al., 2005); and G) Reconstructed AMO temperature anomalies (Mann et al., 2009). Ålftobreen ELA variations are shown with 95% confidence bands. Light blue shaded vertical area marks the LIA at Ålftobreen (~650–50 cal yr BP); yellow shaded vertical area marks the MCA (~1000–700 cal yr BP) (following definitions in: IPCC, 2013; Solomina et al., 2015). Light grey shaded vertical area marks the maximum LIA extent at Ålftobreen (~400–200 cal yr BP). In Supplementary Fig. S6 a similar compilation covering the entire Holocene is shown. (For interpretation of the references to colour in this figure legend, the reader is referred to the web version of this article.)

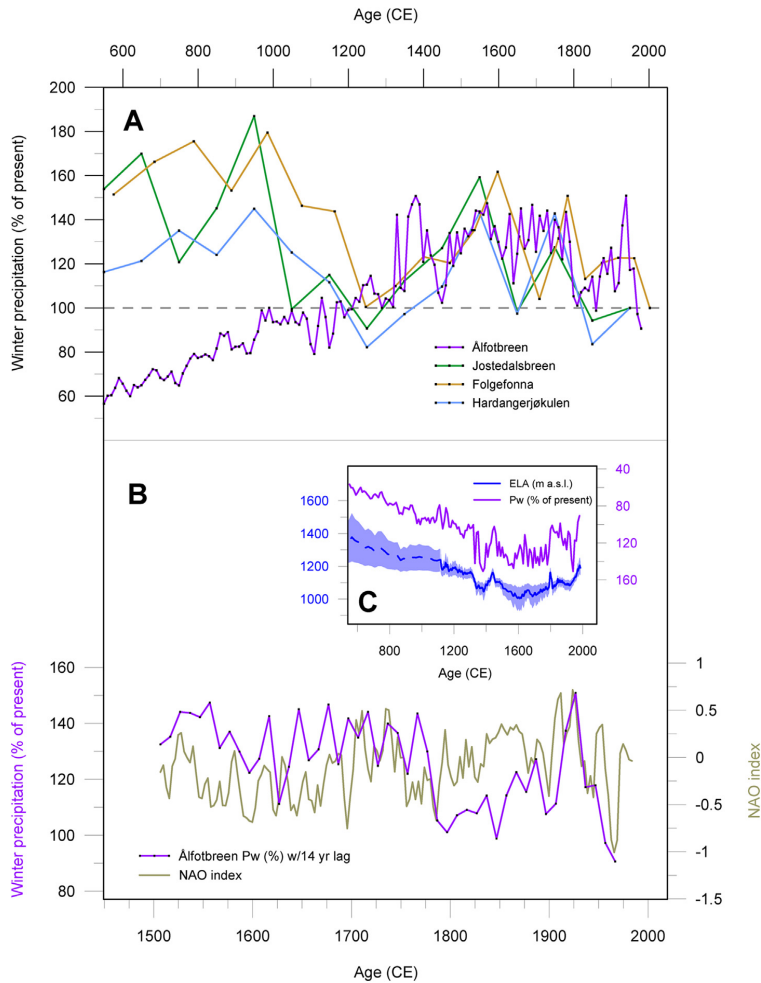


Fig. 11. A) Reconstructed winter precipitation (% of present) from Ålfotbreen compared with reconstructed Pw from Jostedalbreen (Nesje et al., 2001), Folgefonna (Bakke et al., 2005), and Hardangerjøkulen (Dahl and Nesje, 1996). Reference line (stippled) marks present winter precipitation (100%). B) Reconstructed winter precipitation from Ålfotbreen compared with the NAO index from Luterbacher et al. (2001), accounting for a 14-year lag (see Section 4.7). Note change in age scale from A). C) Reconstructed ELA vs. reconstructed Pw (inverted).

Bjune et al. (2005). The pollen record from Vestre Øykjamyrtjørn, which was implemented in the studies from Jostedalbreen, Folgefonna and Hardangerjøkulen, shows remarkably stable temperatures over the last 4000 years (Bjune et al., 2005), where many other Norwegian records reflect a cooling trend similar to the Kråkenes site (Fig. 9D) and reconstructed AMO (Fig. 10G). This might explain some of the discrepancy between the precipitation reconstructions from the other ice caps and Ålfotbreen before CE1300, although it should also be noted that this is the most uncertain part of our reconstruction. Our record indicates Pw values below present levels before ~CE1200, after which they increase rapidly and remain above present values until near present (Fig. 11A). Values above 130% of present Pw are found close to ~CE1350, 1540, between 1650 and 1770, and at ~CE1930. As winter precipitation along the western coast of Norway is

strongly related to the North Atlantic westerlies (Nordli et al., 2005), the ELA variations at Ålfotbreen have most likely been influenced by the spatial and temporal variability of the wintertime westerlies in the past. The wintertime westerlies over southern Norway are closely linked with the NAO (e.g. Nordli et al., 2005), and it is therefore possible that our record of past Pw also contains a signal related to past variations in the NAO (see Section 5.4.2). If new data sets of similar resolution become available from other sites along the Norwegian coast in the future, it will be possible to reconstruct spatiotemporal patterns of winter precipitation, which may help to elucidate past changes in atmospheric circulation patterns (e.g. the NAO) and the strength and position of the wintertime westerlies over Norway. See Supplementary Fig. S7 for mass-balance data from Ålfotbreen compared with the NAO index.

5.4. Climatic implications and comparison with northern hemisphere climate records

5.4.1. Deglaciation and early to mid-Holocene glacier fluctuations at Ålfotbreen

Observed Holocene Northern Hemisphere (NH) glacier trends with small or absent glaciers in the mid-Holocene and onset of the Neoglacial between 6000 and 4000 cal yr BP are commonly attributed to decreasing summer temperatures forced by orbitally-controlled insolation changes (Mayewski et al., 2004; Solomina et al., 2015) (Fig. 9B). The resulting NH summer-season cooling caused a progressive southward shift of the NH summer position of the Intertropical Convergence Zone (ITCZ) during the mid-to late Holocene (Haug et al., 2001; Wanner et al., 2008, 2011). In the case of Ålfotbreen, the relationship between glacier variability and climatic forcing is not straight-forward, and we advocate that different mechanisms might have influenced the ice cap at different times. We propose that the timing of deglaciation at Ålfotbreen was a result of the warmer NH summer temperatures driven by increased summer insolation at that time. We further suggest that our glacier reconstruction record the '8.2 ka BP Event'/Finse Event (Nesje and Dahl, 1991; Dahl and Nesje, 1994, 1996; Nesje et al., 2006); a well-established cooling event in the North Atlantic region which was most likely induced by meltwater pulses (Alley et al., 1997; Alley and Ágústsdóttir, 2005; Nesje et al., 2006; Kobashi et al., 2007; Thomas et al., 2007; Kleiven et al., 2008) and subsequent decline in North Atlantic Deep Water formation (Kleiven et al., 2008). It is unclear if the ice cap melted away completely or if it simply retreated following the glacier advance centred around 8200 cal yr BP, but from ~5400 to 5100 cal yr BP we infer a glacier advance at Ålfotbreen. In the Kråkenes temperature record we also observe the onset of a decreasing temperature trend around this time (Fig. 9D). The timing of this glacier advance at Ålfotbreen corresponds well with periods of glacier advance/onset of the Neoglacial at several other ice caps in Norway; in particular Folgefonna (Bakke et al., 2005) (Suppl. Fig. S6F) and Jostedalbreen [composite record from Nesje et al. (2001) and Vasskog et al. (2012)] (Suppl. Fig. S6D); two ice caps situated relatively close to Ålfotbreen that are likely to be influenced by similar atmospheric and oceanic forcing. We infer that the decreasing NH June insolation acted as the mechanism responsible for this glacier advance in southern Norway and subsequent onset of the Neoglacial at several ice caps.

5.4.2. The Neoglacial and the 'Little Ice Age' at Ålfotbreen

Both the northern parts of Jostedalbreen and the Northern Folgefonna ice cap eventually melted away due to the 1.5–2 °C warmer summer temperatures that prevailed in the early-to mid-Holocene subsequent to the Finse Event (Bjune et al., 2005; Nesje et al., 2008), before reforming at ~6100 cal yr BP (Nesje et al., 2001) and ~5200 cal yr BP (Bakke et al., 2005), respectively. The higher elevation could explain an earlier initiation of the Neoglacial at Jostedalbreen, whereas Northern Folgefonna seems to have reformed more-or-less at the same time as the possible glacier advance at Ålfotbreen between 5100 and 5300 cal yr BP. However, after 5100 cal yr BP the trend reverses at Ålfotbreen, and it may have melted completely until ~1400 cal yr BP (Section 5.2.1), while Jostedalbreen and Folgefonna on the other hand continued to grow throughout this period (Fig. S6). This mid-to late-Holocene reversal at Ålfotbreen is opposite of what we expect as a result from a gradual summer cooling, which should have induced a response more similar to what is seen at both Folgefonna and Jostedalbreen. Contrary to the increasing terrestrial Neoglacial activity in Scandinavia, the mid- and late Holocene was relatively warm in marine records retrieved outside Norway (Risebrobakken et al., 2003;

Sejrup et al., 2011) (Fig. 9C), and this could have served to further reduce the accumulation season length on Ålfotbreen.

Maritime glaciers in Norway are strongly influenced by winter precipitation and the wintertime westerlies (Ballantyne, 1990; Hurrell, 1995; Nesje et al., 2000a; Bakke et al., 2005; Nordli et al., 2005), and Ålfotbreen in particular has shown a very high correlation ($R^2 = 0.51$) between winter mass balance and the leading mode of atmospheric variability in the North Atlantic; the NAO (Nesje et al., 2000a; Nesje, 2009) (Suppl. Fig. S7). Positive NAO-mode years are reflected in the glacier mass-balance of Ålfotbreen as years with a high positive glacier net mass-balance, whereas negative NAO years are associated with atmospheric blocking, forcing the humid air masses to the south or north of SW Norway leading to prevailing colder temperatures and lower winter precipitation on the glaciers in the maritime western Norway. Hence, NAO fluctuations act as a controlling factor governing the amounts of accumulation on glaciers in SW Norway and Holocene glacier records and ELA reconstructions from these glaciers are considered to contain a signal related to past NAO variations (Nesje et al., 2000a). Fig. 11B shows a comparison between reconstructed Pw from Ålfotbreen with the NAO reconstruction from Luterbacher et al. (2001). We observe that there are similar multidecadal trends in our dataset and the reconstructed NAO, although around CE1770–1800 there is a distinct drop in Pw while the NAO values are increasing steadily. Over the last 30 years instrumental NAO measurements are able to explain almost 80% of the variability in the wintertime westerlies over southern Norway; however, this relationship has not been constant over time. Between CE1840 and present there are several 30-year intervals where the NAO explains less than 35% of observed changes in the westerlies index (Suppl. Fig. S8), and we cannot rule out that this relationship has been even weaker in periods beyond the instrumental record. The opposite trends in the reconstructed Ålfotbreen Pw and the NAO around CE1770–1800 (Fig. 11B) could therefore indicate a weaker link between the NAO and wintertime westerlies over Norway in this period. Another possible explanation is that the distinct decrease in North Atlantic Ocean temperatures indicated by the AMO at this time could have served to reduce the moisture availability, thereby reducing winter accumulation on Ålfotbreen. This potential influence of ocean temperatures on winter precipitation is, however, exceedingly difficult to disentangle from the opposite effect that a colder ocean would have on glacier mass-balance through reduced ablation during summer.

During the Medieval Climatic Anomaly (MCA) from 1000 to 700 cal yr BP (CE950–1250) (Solomina et al., 2015), the climate in the North Atlantic region was relatively warm (e.g. Mann et al., 2009). The ELA of Ålfotbreen shows a steady lowering from the start of our record at CE550 before stabilizing at a level close to its present elevation during most of the MCA (Fig. 10). This implies that reconstructed Pw increases over the same interval, and it is during the MCA that our central estimate of Pw first reaches present-day levels and above (Fig. 11B).

The 'Little Ice Age' was a period of glacier advance across the world, but the mechanisms driving these advances are presently not fully understood (Broecker, 2000; Nesje and Dahl, 2003; Solomina et al., 2015). One of the key issues addressed is defining the exact timing of the LIA, which may vary significantly from site to site depending on the types of proxy records used (e.g. glaciers, temperature, or precipitation) and different climatic settings. The LIA at Ålfotbreen shows a pattern similar to other glacier records from Norway and Svalbard (Fig. 10) with an onset ~650 cal yr BP (CE1300), lasting until ~50 cal yr BP (CE1900). The LIA maximum extent of Ålfotbreen occurred between ~400 and 200 cal yr BP (CE1550–1750). In Fig. 10E, our reconstruction shows an ELA lowering of ~200 m during the LIA relative to the present

steady-state ELA at ~1180 m. This order of magnitude is similar to what we find for e.g. Okstindan in Arctic Norway (Bakke et al., 2010), which showed an ELA lowering of 250 m during the LIA (Fig. 10C).

An interesting time-transgressive trend in the LIA maximum can be observed in Fig. 10: The timing of the LIA maximum tends to occur progressively later as we move northwards (see stippled line). Because temperatures during the LIA are regionally consistent for the area of interest (Mann et al., 2009) we suggest that winter precipitation might be the most important factor controlling the timing of the LIA maximum for the glaciers in this south-north transect. We acknowledge that the compiled glacier reconstructions have significant uncertainties in age control, but the overall difference in timing from north to south is larger than what can be explained by age uncertainty alone. We therefore suggest that the observed progressively later maximum glacier advances are likely forced by regional differences in winter precipitation. From observations we know that regional changes in precipitation in the North Atlantic are strongly linked to the NAO, but there are still large uncertainties in how the NAO has behaved in the past (Lehner et al., 2012; Pinto and Raible, 2012). Proxy reconstructions of the NAO often show widely conflicting results prior to the instrumental record, with some reconstructions suggesting a change to a generally more positive NAO mode during the LIA (e.g. Meeker and Mayewski, 2002), while others indicate the opposite (e.g. Trouet et al., 2009). One challenge in this respect is to distinguish between the effects of strength versus frequency of North Atlantic cyclones on long-term trends in the reconstructed NAO (e.g. Trouet et al., 2012). From the connection between winter mass balance on Ålfotbreen and the NAO, our reconstruction seems to favour a change towards a generally more positive NAO situation during the LIA, but the question of cyclone frequency versus intensity remains. New high-resolution precipitation reconstructions along the coast of Norway might add to our knowledge of past changes in the NAO (Lehner et al., 2012), and reveal whether the time-transgressive northward migration of the LIA glacier maximum is related to this atmospheric circulation feature.

5.5. What does the future hold for Ålfotbreen?

Ålfotbreen might become one of the first glaciers in Norway to melt completely if the present warming trend continues without being compensated for by increased accumulation-season precipitation (Nesje et al., 2008; Andreassen et al., 2012). According to an energy-balance modelling study, Ålfotbreen is predicted to respond with an ELA rise of 135 m and a mass balance change of -1.11 m water equivalents (m.w.e.) per year as a response to a 1 °C increase in temperature (Oerlemans, 1992). Temperature projections for the future exceed 1.5 °C of warming (relative to CE1850-1900) by the end of the 21st century (IPCC, 2013), which is similar in magnitude to peak warming during the Holocene Thermal Maximum (Seppä and Birks, 2001; Davis et al., 2003; Renssen et al., 2009). As our record shows that Ålfotbreen was most likely melted away during this period (from 8200 to ~5400 cal yr BP) we infer that Ålfotbreen might melt away completely within the end of the 21st century. If a positive NAO mode were to prevail along with cooler summer temperatures for several years, this could lead to an expansion of the Ålfotbreen ice cap; however, the current warming trend is expected to continue, and the future variability of the NAO is not possible to predict. If the ice cap should melt away completely within the end of the 21st century, as our current best knowledge seems to suggest, this will be the first time in more than 1400 years that the Ålfotbreen mountain plateau becomes entirely ice-free.

6. Conclusions

In a future warmer climate, Ålfotbreen is one of the most vulnerable glaciers in Norway and the ice cap might disappear completely within few decades due to its narrow hypsometry and low altitude. Here we have presented and assessed novel data on past variations of Ålfotbreen, including periods where the glacier might have been totally melted away. We have focused in particular on the Neoglacial period with high-resolution reconstructions of ELA variations and winter precipitation covering the last ~1400 years. Our results can be summarized as follows:

- (1) Ålfotbreen retreated/melted away between ca. 10,100–9700 cal yr BP, following deglaciation. The ice cap reformed and/or experienced a glacier advance during the '8.2 ka BP Event'/Finse event (centred ~8200 cal yr BP). Thereafter, the ice cap probably melted away completely until a possible new glacier advance is recorded from ca. 5400–5100 cal yr BP. The timing of this advance is approximately synchronous with other glacier advances in western Norway at the Jostedalbreen and Folgefonna ice caps. Following this glacier event, the ice cap probably melted away completely again and did not reform until the onset of the local Neoglacial period at ~1400 cal yr BP. The LIA is determined to have lasted from ~650 cal yr BP (CE1300) until ~50 cal yr BP (CE1900), with the LIA maximum occurring from ~400 to 200 cal yr BP (CE1550-1750). The LIA maximum was probably the largest glacier extent of Ålfotbreen since deglaciation.
- (2) A regional synthesis of Neoglacial glacier variations is presented in a south-north transect, showing an apparent time-transgressive trend of the LIA maximum extents with the onset of the LIA seemingly starting progressively later as we move further north. We suggest that this is likely forced by regional winter precipitation differences along the coast of Norway.
- (3) Our high-resolution precipitation reconstruction, based on independent Ts and ELA reconstructions, correlates well with other Pw reconstructions from SW Norway after CE1300. Before this (between CE550-1300) the records diverge, possibly due to differences in the summer temperature records used when reconstructing Pw through the 'Liestøl equation'. Our novel approach of calculating ELA and winter precipitation could be applied at other sites where lack of (dated) moraines complicates the accurate timing and extent of past glacier advances, although this requires instrumental measurements of ELA.

Acknowledgements

This research was supported by the Centre for Climate Dynamics at the Bjerknes Centre for Climate Research and the SHIFTS project funded by the Norwegian Research Council (210004). Gunhild Rosqvist is thanked for helpful comments on earlier drafts of the manuscript. We thank landowner Leidulv Solvang for permission to core Lake Grøndalsvatnet and for providing boats used during fieldwork, and Bjørn André Skjæret for invaluable help with coring. Anne Bjune helped identify terrestrial plant remains for AMS radiocarbon dating. Permission to core Støylsvatnet was granted from Alf Erik Røyrvik and the Norwegian Environment Agency. Magnetic measurements were carried out at the Palaeomagnetic Laboratory at the University of Bergen (under administration of the late Prof. Reidar Løvlie). Radiocarbon dating was carried out at the Poznan Radiocarbon Laboratory under supervision of Tomasz Goslar. Peter Appleby supervised the ²¹⁰Pb dating at the

Environmental Radioactivity Research Centre, University of Liverpool. The authors would like to thank an anonymous reviewer for valuable feedback that served to improve the manuscript.

Ålfotbreen ELA and Pw reconstruction dataset is to be deposited in the NOAA data repository.

Appendix A. Supplementary data

Supplementary data related to this article can be found at <http://dx.doi.org/10.1016/j.quascirev.2015.12.004>.

References

- Alley, R.B., Ágústsdóttir, A.M., 2005. The 8k event: cause and consequences of a major Holocene abrupt climate change. *Quat. Sci. Rev.* 24, 1123–1149.
- Alley, R.B., Mayewski, P.A., Sowers, T., Stuiver, M., Taylor, K.C., Clark, P.U., 1997. Holocene climatic instability: a prominent, widespread event 8200 yr ago. *Geology* 25, 483–486.
- Andreasen, L., Winsvold, S., Paul, F., Hausberg, J., 2012. Inventory of Norwegian Glaciers. NVE, Oslo.
- Andreasen, L.M., Elvehøy, H., Kjollmoen, B., Engeset, R.V., Haakensen, N., 2005. Glacier mass-balance and length variation in Norway. *Ann. Glaciol.* 42, 317–325.
- Augustsson, A., Gaillard, M.-J., Peltola, P., Mazier, F., Bergbäck, B., Saarinen, T., 2013. Effects of land use and climate change on erosion intensity and sediment geochemistry at Lake Lehmiälampi, Finland. *Holocene*, 0959683613484615.
- Bakke, J., Dahl, S.O., Paasche, Ø., Riis Simonsen, J., Kvisvik, B., Bakke, K., Nesje, A., 2010. A complete record of Holocene glacier variability at Austrre Okstindbreen, northern Norway: an integrated approach. *Quat. Sci. Rev.* 29, 1246–1262.
- Bakke, J., Lie, Ø., Heegaard, E., Dokken, T., Haug, G.H., Birks, H.H., Dulski, P., Nilsen, T., 2009. Rapid oceanic and atmospheric changes during the younger dryas cold period. *Nat. Geosci.* 2, 202–205.
- Bakke, J., Nesje, A., Dahl, S.O., 2005. Utilizing physical sediment variability in glacier-fed lakes for continuous glacier reconstructions during the Holocene, northern Fjellfonna, western Norway. *The Holocene* 15, 161–176.
- Bakke, J., Trachsel, M., Kvisvik, B.C., Nesje, A., Lyså, A., 2013. Numerical analyses of a multi-proxy data set from a distal glacier-fed lake, Sørsendalsvatn, western Norway. *Quat. Sci. Rev.* 73, 182–195.
- Ballantyne, C.K., 1989. The Loch Lomond Readvance on the Isle of Skye, Scotland: glacier reconstruction and palaeoclimatic implications. *J. Quat. Sci.* 4, 95–108.
- Ballantyne, C.K., 1990. The Holocene glacial history of Lyngshalvøya, northern Norway: chronology and climatic implications. *Boreas* 19, 93–117.
- Ballantyne, C.K., 2002. Paraglacial geomorphology. *Quat. Sci. Rev.* 21, 1935–2017.
- Berger, A., Loutre, M.-F., 1991. Insolation values for the climate of the last 10 million years. *Quat. Sci. Rev.* 10, 297–317.
- Bjune, A.E., Bakke, J., Nesje, A., Birks, H.J.B., 2005. Holocene mean July temperature and winter precipitation in western Norway inferred from palynological and glaciological lake-sediment proxies. *The Holocene* 15, 177–189.
- Blaauw, M., 2010. Methods and code for 'classical' age-modelling of radiocarbon sequences. *Quat. Geochronol.* 5, 512–518.
- Blott, S.J., Pye, K., 2001. GRADISTAT: a grain size distribution and statistics package for the analysis of unconsolidated sediments. *Earth Surf. Process. Landforms* 26, 1237–1248.
- Briner, J., Stewart, H., Young, N., Philipps, W., Losee, S., 2010. Using proglacial-threshold lakes to constrain fluctuations of the Jakobshavn Isbræ ice margin, western Greenland, during the Holocene. *Quat. Sci. Rev.* 29, 3861–3874.
- Broecker, W.S., 2000. Was a change in thermohaline circulation responsible for the Little Ice Age? *Proc. Natl. Acad. Sci.* 97, 1339–1342.
- Bryhni, I., Lutro, O., 2000. Berggrunnskart Naustdal 1218 III, M: 1:50,000. NGU, Carrivick J.L., Tweed, F.S., 2013. Proglacial lakes: character, behaviour and geological importance. *Quat. Sci. Rev.* 78, 34–52.
- Croudace, I.W., Rindby, A., Rothwell, R.G., 2006. ITRAX: description and evaluation of a new multi-function X-ray core scanner. *Special Publ. Geol. Soc. Lond.* 267, 51.
- Dahl, S.O., Bakke, J., Lie, Ø., Nesje, A., 2003. Reconstruction of former glacier equilibrium-line altitudes based on proglacial sites: an evaluation of approaches and selection of sites. *Quat. Sci. Rev.* 22, 275–287.
- Dahl, S.O., Nesje, A., 1992. Paleoclimatic implications based on equilibrium-line altitude depressions of reconstructed younger dryas and Holocene cirque glaciers in inner Nordfjord, western Norway. *Palaeoogeogr. Palaoclimatol. Palaeoecol.* 94, 87–97.
- Dahl, S.O., Nesje, A., 1994. Holocene glacier fluctuations at Hardangerjøkulen, central-southern Norway: a high-resolution composite chronology from lacustrine and terrestrial deposits. *The Holocene* 4, 269–277.
- Dahl, S.O., Nesje, A., 1996. A new approach to calculating Holocene winter precipitation by combining glacier equilibrium-line altitudes and pine-tree limits: a case study from Hardangerjøkulen, central southern Norway. *The Holocene* 6, 381–398.
- Dahl, S.O., Nesje, A., Lie, Ø., Fjordheim, K., Matthews, J.A., 2002. Timing, equilibrium-line altitudes and climatic implications of two early-Holocene glacier readvances during the Erdalen Event at Jostedalbreen, western Norway. *The Holocene* 12, 17–25.
- Davis, B., Brewer, S., Stevenson, A., Guiot, J., 2003. The temperature of Europe during the Holocene reconstructed from pollen data. *Quat. Sci. Rev.* 22, 1701–1716.
- Davison, W., 1993. Iron and manganese in lakes. *Earth Sci. Rev.* 34, 119–163.
- Dean, W.E., 1974. Determination of carbonate and organic matter in calcareous sediments and sedimentary rocks by loss on ignition: comparison with other methods. *J. Sediment. Res.* 44.
- Haakensen, N., 1989. Akkumulasjon på breene i Norge vinteren 1988–89. *Været* 13, 91–94.
- Haug, G.H., Hughen, K.A., Sigman, D.M., Peterson, L.C., Röhl, U., 2001. Southward migration of the intertropical convergence zone through the Holocene. *Science* 293, 1304–1308.
- Heiri, O., Lotter, A.F., Lemcke, G., 2001. Loss on ignition as a method for estimating organic and carbonate content in sediments: reproducibility and comparability of results. *J. Paleolimnol.* 25, 101–110.
- Hormes, A., Blaauw, M., Dahl, S.O., Nesje, A., Possnert, G., 2009. Radiocarbon wiggle-match dating of proglacial lake sediments—Implications for the 8.2 ka event. *Quat. Geochronol.* 4, 267–277.
- Hurrell, J.W., 1995. Decadal trends in the North Atlantic oscillation: regional temperatures and precipitation. *Science* 269, 676.
- IPCC, 2013. In: Stocker, T., Qin, D., Plattner, G., Tignor, M., Allen, S., Boschung, J., Nauels, A., Xia, Y., Bex, V., Midgley, P. (Eds.), *Climate Change 2013: the Physical Science Basis. Contribution of Working Group I to the Fifth Assessment Report of the Intergovernmental Panel on Climate Change*. Cambridge Univ Press, Cambridge, United Kingdom and New York, NY, USA.
- Jones, P., Davies, T., Lister, D., Slonosky, V., Jonsson, T., Bärring, L., Jönsson, P., Maheras, P., Kolyva-Machera, F., Barriendos, M., 1999. Monthly mean pressure reconstructions for Europe for the 1780–1995 period. *Int. J. Climatol.* 19, 347–364.
- Karlén, W., 1976. Lacustrine sediments and tree-limit variations as indicators of Holocene climatic fluctuations in Lappland, northern Sweden. *Geogr. Ann. Ser. A. Phys. Geogr.* 1–34.
- Karlén, W., 1981. Lacustrine sediment studies. A technique to obtain a continuous record of holocene glacier variations. *Geogr. Ann. Ser. A. Phys. Geogr.* 273–281.
- Karlén, W., Matthews, J.A., 1992. Reconstructing Holocene glacier variations from glacial lake sediments: studies from Nordvestlandet and Jostedalbreen-Jotunheimen, southern Norway. *Geogr. Ann. Ser. A. Phys. Geogr.* 327–348.
- Kjollmoen, B., 2011. *Glaciological Investigations in Norway in 2010*. NVE Report 2 2010.
- Kleiven, H.K.F., Kissel, C., Laj, C., Ninemann, U.S., Richter, T.O., Cortijo, E., 2008. Reduced North Atlantic deep water coeval with the glacial Lake Agassiz freshwater outburst. *Science* 319, 60–64.
- Kobashi, T., Severinghaus, J.P., Brook, E.J., Barnola, J.-M., Grachev, A.M., 2002. Precise timing and characterization of abrupt climate change 8200 years ago from air trapped in polar ice. *Quat. Sci. Rev.* 26, 1212–1222.
- Lehner, F., Raible, C.C., Stocker, T.F., 2012. Testing the robustness of a precipitation proxy-based North Atlantic oscillation reconstruction. *Quat. Sci. Rev.* 45, 85–94.
- Leps, J., Smilauer, P., 2003. *Multivariate Analysis of Ecological Data Using CANOCO*. Cambridge University Press, Cambridge.
- Lie, Ø., Dahl, S.O., Nesje, A., Matthews, J.A., Sandvold, S., 2004. Holocene fluctuations of a polythermal glacier in high-alpine eastern Jotunheimen, central-southern Norway. *Quat. Sci. Rev.* 23, 1925–1945.
- Luterbacher, J., Xoplaki, E., Dietrich, D., Jones, P., Davies, T., Portis, D., Gonzalez-Rouco, J., Von Storch, H., Gyalistras, D., Casty, C., 2001. Extending North Atlantic oscillation reconstructions back to 1500. *Atmos. Sci. Lett.* 2, 114–124.
- Mann, M.E., Zhang, Z., Rutherford, S., Bradley, R.S., Hughes, M.K., Shindell, D., Ammann, C., Faluvegi, G., Ni, F., 2009. Global signatures and dynamical origins of the Little Ice Age and medieval climate anomaly. *Science* 326, 1256–1260.
- Marzeion, B., Nesje, A., 2012. Spatial patterns of North Atlantic oscillation influence on mass balance variability of European glaciers. *Cryosphere Discuss.* 6, 1–35.
- Masson-Delmotte, V., Schulz, M., Abe-Ouchi, A., Beer, J., Ganopolski, A., Rouco, J.G., Jansen, E., Lambeck, K., Luterbacher, J., Naish, T., 2013. Information from paleoclimatic archives. In: Stocker, T., Qin, D., Plattner, G., Tignor, M., Allen, S., Boschung, J., Nauels, A., Xia, Y., Bex, V., Midgley, P. (Eds.), *Climate Change 2013: the Physical Science Basis. Contribution of Working Group I to the Fifth Assessment Report of the Intergovernmental Panel on Climate Change*. Cambridge Univ Press, Cambridge, United Kingdom and New York, NY, USA, pp. 383–464.
- Matthews, J.A., Karlén, W., 1992. Asynchronous neoglaciation and Holocene climatic change reconstructed from Norwegian glaciolacustrine sedimentary sequences. *Geology* 20, 991.
- Matthews, J.A., Olaf Dahl, S., Nesje, A., Berrisford, M.S., Andersson, C., 2000. Holocene glacier variations in central Jotunheimen, southern Norway based on distal glaciolacustrine sediment cores. *Quat. Sci. Rev.* 19, 1625–1647.
- Mayewski, P.A., Rohling, E.E., Curt Stager, J., Karlen, W., Maasch, K.A., David Meeker, L., Meyerson, E.A., Gasse, F., van Kreveld, S., Holmgren, K., 2004. Holocene climate variability. *Quat. Res.* 62, 243–255.
- Meeker, L.D., Mayewski, P.A., 2002. A 1400-year high-resolution record of atmospheric circulation over the north Atlantic and Asia. *The Holocene* 12, 257–266.
- Naeher, S., Gilli, A., North, R.P., Hamann, Y., Schubert, C.J., 2013. Tracing bottom water oxygenation with sedimentary Mn/Fe ratios in Lake Zurich, Switzerland. *Chem. Geol.* 352, 125–133.
- Nesje, A., 1992. A piston core for lacustrine and marine sediments. *Arct. Alp. Res.* 257–259.
- Nesje, A., 2005. Brikdsalsbreen in western Norway: AD 1900–2004 frontal

- fluctuations as a combined effect of variations in winter precipitation and summer temperature. *The Holocene* 15, 1245–1252.
- Nesje, A., 2009. Latest Pleistocene and Holocene alpine glacier fluctuations in Scandinavia. *Quat. Sci. Rev.* 28, 2119–2136.
- Nesje, A., Bakke, J., Dahl, S.O., Lie, Ø., Bøe, A.-G., 2007. A continuous, high-resolution 8500-yr snow-avalanche record from western Norway. *The Holocene* 17, 269–277.
- Nesje, A., Bakke, J., Dahl, S.O., Lie, Ø., Matthews, J.A., 2008. Norwegian mountain glaciers in the past, present and future. *Glob. Planet. Change* 60, 10–27.
- Nesje, A., Bjune, A.E., Bakke, J., Dahl, S.O., Lie, Ø., Birks, H.J.B., 2006. Holocene palaeoclimate reconstructions at Vannalsvatnet, western Norway, with particular reference to the 8200 cal. yr BP event. *The Holocene* 16, 717–729.
- Nesje, A., Dahl, S.O., 1991. Holocene glacier variations of Blåisen, Hardangerjøkulen, central southern Norway. *Quat. Res.* 35, 25–40.
- Nesje, A., Dahl, S.O., 2003. The 'Little Ice Age'—only temperature? *The Holocene* 13, 139–145.
- Nesje, A., Dahl, S.O., Bakke, J., 2004. Were abrupt lateglacial and early-Holocene climatic changes in northwest Europe linked to freshwater outbursts to the north Atlantic and Arctic oceans? *The Holocene* 14, 299–310.
- Nesje, A., Dahl, S.O., Løvlie, R., 1995. Late Holocene glaciers and avalanche activity in the Alftobreen area, western Norway: evidence from a lacustrine sedimentary record. *Nor. Geol. Tidsskr.* 75, 120–126.
- Nesje, A., Kvamme, M., Rye, N., Løvlie, R., 1991. Holocene glacial and climate history of the Jostedalbreen region, western Norway; evidence from lake sediments and terrestrial deposits. *Quat. Sci. Rev.* 10, 87–114.
- Nesje, A., Lie, Ø., Dahl, S.O., 2000a. Is the North Atlantic oscillation reflected in Scandinavian glacier mass balance records? *J. Quat. Sci.* 15, 587–601.
- Nesje, A., Matthews, J.A., Dahl, S.O., Berrisford, M.S., Andersson, C., 2001. Holocene glacier fluctuations of Flatebreen and winter-precipitation changes in the Jostedalbreen region, western Norway, based on glaciolacustrine sediment records. *The Holocene* 11, 267–280.
- Nesje, A., Olaf Dahl, S., Andersson, C., Matthews, J.A., 2000b. The lacustrine sedimentary sequence in Synneskardvatnet, western Norway: a continuous, high-resolution record of the Jostedalbreen ice cap during the Holocene. *Quat. Sci. Rev.* 19, 1047–1065.
- Nordli, Ø., Lie, Ø., Nesje, A., Benestad, R.E., 2005. Glacier mass balance in southern Norway modelled by circulation indices and Spring-Summer temperatures ad 1781–2000. *Geogr. Ann. Ser. A Phys. Geogr.* 87, 431–445.
- Oerlemans, J., 1992. Climate sensitivity of glaciers in southern Norway: application of an energy-balance model to Nigardsbreen, Hellstugubreen and Alftobreen. *J. Glaciol.* 38, 223–232.
- Oerlemans, J., 2005. Extracting a climate signal from 169 glacier records. *Science* 308, 675–677.
- Paillard, D., Labeyrie, L., Yiou, P., 1996. Macintosh program performs time-series analysis. *Eos Trans. Am. Geophys. Union* 77, 379–379.
- Pinto, J.G., Raible, C.C., 2012. Past and recent changes in the North Atlantic oscillation. *Wiley Interdiscip. Rev. Clim. Change* 3, 79–90.
- R Development Core Team, 2012. R: a Language and Environment for Statistical Computing. R Foundation for Statistical Computing, R Foundation for Statistical Computing, Vienna, Austria.
- Rasmussen, S.O., Andersen, K.K., Svensson, A., Steffensen, J.P., Vinther, B.M., Clausen, H.B., Siggaard-Andersen, M.L., Johnsen, S.J., Larsen, L.B., Dahl-Jensen, D., 2006. A new Greenland ice core chronology for the last glacial termination. *J. Geophys. Res. Atmos.* (1984–2012) 111.
- Reimer, P.J., Bard, E., Bayliss, A., Beck, J.W., Blackwell, P.G., Ramsey, C.B., Buck, C.E., Cheng, H., Edwards, R.L., Friedrich, M., 2013. IntCal13 and Marine13 radiocarbon age calibration curves 0–50,000 years cal BP. *Radiocarbon* 55, 1869–1887.
- Renssen, H., Seppä, H., Heiri, O., Roche, D., Goosse, H., Fichetef, T., 2009. The spatial and temporal complexity of the Holocene thermal maximum. *Nat. Geosci.* 2, 411–414.
- Risebrobakken, B., Jansen, E., Andersson, C., Mjelde, E., Hevrøy, K., 2003. A high-resolution study of Holocene paleoclimatic and paleoceanographic changes in the Nordic Seas. *Paleoceanography* 18.
- Rosqvist, G., Jonsson, C., Yam, R., Karlén, W., Shemesh, A., 2004. Diatom oxygen isotopes in pro-glacial lake sediments from northern Sweden: a 5000 year record of atmospheric circulation. *Quat. Sci. Rev.* 23, 851–859.
- Rubensdotter, L., Rosqvist, G., 2009. Influence of geomorphological setting, fluvial-, glacioluvial- and mass-movement processes on sedimentation in alpine lakes. *The Holocene* 19, 665–678.
- Røthe, T.O., Bakke, J., Vasskog, K., Gjerde, M., D'Andrea, W.J., Bradley, R.S., 2015. Arctic Holocene glacier fluctuations reconstructed from lake sediments at Mitrahallvøya, Spitsbergen. *Quat. Sci. Rev.* 109, 111–125.
- Sandgren, P., Snowball, I., 2001. Application of Mineral Magnetic Techniques to Paleolimnology, Tracking Environmental Change Using Lake Sediments. Springer, pp. 217–237.
- Sejrup, H., Hafliðason, H., Andrews, J., 2011. A Holocene North Atlantic SST record and regional climate variability. *Quat. Sci. Rev.* 30, 3181–3195.
- Seppä, H., Birks, H.J.B., 2001. July mean temperature and annual precipitation trends during the Holocene in the Fennoscandian tree-line area: pollen-based climate reconstructions. *The Holocene* 11, 527–539.
- Shakesby, R.A., Smith, J.G., Matthews, J.A., Winkler, S., Dresser, P.Q., Bakke, J., Dahl, S.O., Lie, Ø., Nesje, A., 2007. Reconstruction of Holocene glacier history from distal sources: glacioluvial stream-bank mires and a glaciolacustrine sediment core near Sota Sæter, Breheimen, southern Norway. *The Holocene* 17, 729–745.
- Sissons, J., 1979. Palaeoclimatic inferences from former glaciers in Scotland and the Lake district. *Nature* 278, 518–521.
- Solomina, O.N., Bradley, R.S., Hodgson, D.A., Ivy-Ochs, S., Jomelli, V., Mackintosh, A.N., Nesje, A., Owen, L.A., Wanner, H., Wiles, G.C., 2015. Holocene glacier fluctuations. *Quat. Sci. Rev.* 111, 9–34.
- Sutherland, D.G., 1984. Modern glacier characteristics as a basis for inferring former climates with particular reference to the Loch Lomond Stadial. *Quat. Sci. Rev.* 3, 291–309.
- Syms, C., 2008. Principal components analysis. In: Jørgensen, S.E., Fath Brian, D. (Eds.), *Encyclopedia of Ecology*. Academic Press, Oxford, pp. 2940–2949.
- Sønstegeard, E., Aa, A.R., Klakegg, O., 1999. Younger dryas glaciation in the Alftobreen area, western Norway; evidence from lake sediments and marginal moraines. *Nor. Geol. Tidsskr.* 79, 33–45.
- Thomas, E.R., Wolff, E.W., Mulvaney, R., Steffensen, J.P., Johnsen, S.J., Arrowsmith, C., White, J.W., Vaughn, B., Popp, T., 2007. The 8.2 ka event from Greenland ice cores. *Quat. Sci. Rev.* 26, 70–81.
- Trachsel, M., Nesje, A., 2015. Modelling annual mass balances of eight Scandinavian glaciers using statistical models. *Cryosphere Discuss* 9, 383–415.
- Trouet, V., Esper, J., Graham, N.E., Baker, A., Scourse, J.D., Frank, D.C., 2009. Persistent positive North Atlantic oscillation mode dominated the medieval climate anomaly. *Science* 324, 78–80.
- Trouet, V., Scourse, J., Raible, C., 2012. North Atlantic storminess and Atlantic meridional overturning circulation during the last millennium: reconciling contradictory proxy records of NAO variability. *Glob. Planet. Change* 84, 48–55.
- Vasskog, K., Nesje, A., Støren, E.N., Waldmann, N., Chapron, E., Ariztegui, D., 2011. A Holocene record of snow-avalanche and flood activity reconstructed from a lacustrine sedimentary sequence in Oldevatnet, western Norway. *The Holocene* 21, 597–614.
- Vasskog, K., Paasche, Ø., Nesje, A., Boyle, J.F., Birks, H.J.B., 2012. A new approach for reconstructing glacier variability based on lake sediments recording input from more than one glacier. *Quat. Res.* 77, 192–204.
- Vinther, B.M., Clausen, H.B., Johnsen, S.J., Rasmussen, S.O., Andersen, K.K., Buchardt, S.L., Dahl-Jensen, D., Seierstad, I.K., Siggaard-Andersen, M.L., Steffensen, J.P., 2006. A synchronized dating of three Greenland ice cores throughout the Holocene. *J. Geophys. Res. Atmos.* (1984–2012) 111.
- Wanner, H., Beer, J., Buettikofer, J., Crowley, T.J., Cubasch, U., Flueckiger, J., Goosse, H., Grosjean, M., Joos, F., Kaplan, J.O., 2008. Mid- to late Holocene climate change: an overview. *Quat. Sci. Rev.* 27, 1791–1828.
- Wanner, H., Solomina, O., Grosjean, M., Ritz, S.P., Jetel, M., 2011. Structure and origin of Holocene cold events. *Quat. Sci. Rev.* 30, 3109–3123.
- Wittmeier, H.E., Bakke, J., Vasskog, K., Trachsel, M., 2015. Reconstructing Holocene glacier activity at Langfjordjøkelen, Arctic Norway, using multi-proxy fingerprinting of distal glacier-fed lake sediments. *Quat. Sci. Rev.* 114, 78–99.

Supplementary material for Ms. Ref. No.: JQSR-D-15-00296: “Holocene glacier variability and Neoglacial hydroclimate at Ålftobreen, western Norway”, by Marthe Gjerde, Jostein Bakke, Kristian Vasskog, Atle Nesje, Anne Hormes

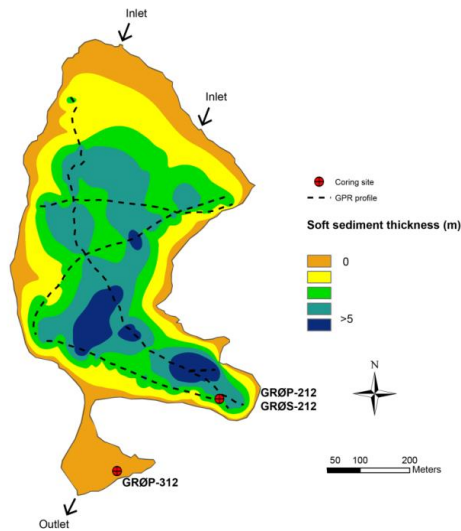


Figure S1: Soft sediment distribution map for Grøndalsvatnet.

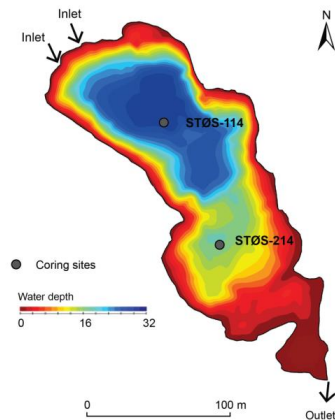


Figure S2: Bathymetrical map and coring sites at Støylsvatnet (produced using Dr Depth Software).

Table S1: Report on the Radiometric Dating of a Lake Sediment Core from Grøndalsvatnet, western Norway (Peter G. Appleby & Gayane T Piliposian, Environmental Radioactivity Research Centre, University of Liverpool). Corrected for ^{137}Cs content, assuming a 1 cm sediment loss from the top of the core (revised March 2015 by Peter G. Appleby & Gayane T Piliposian).

Depth cm	g cm ⁻²	Chronology			Sedimentation Rate		
		Date CE	Age y	±	g cm ⁻² y ⁻¹	cm y ⁻¹	± (%)
0.0	0.0	1994	18	1			
0.5	0.2	1986	26	2	0.030	0.06	6.1
1.0	0.5	1977	35	2	0.030	0.05	6.1
1.5	0.8	1967	45	3	0.030	0.05	6.1
2.0	1.2	1955	57	3	0.030	0.04	6.1
2.5	1.5	1944	68	4	0.030	0.04	6.1
3.0	1.9	1931	81	5	0.030	0.04	6.1
3.5	2.3	1918	94	6	0.030	0.04	6.1
4.0	2.7	1906	106	6	0.030	0.04	6.1
4.5	3.1	1893	119	7	0.030	0.04	6.1
5.0	3.4	1880	132	8	0.030	0.04	6.1
5.5	3.8	1868	144	9	0.030	0.04	6.1
6.0	4.2	1856	156	9	0.030	0.04	6.1

Table S2: Report on the Radiometric Dating of a Lake Sediment Core from Støylsvatnet, western Norway (Peter G. Appleby & Gayane T Piliposian, Environmental Radioactivity Research Centre, University of Liverpool)

Depth cm	g cm ⁻²	Chronology			Sedimentation Rate		
		Date AD	Age y	±	g cm ⁻² y ⁻¹	cm y ⁻¹	± (%)
0.00	0.00	2014	0	0			
0.25	0.11	2008	6	1	0.016	0.04	7.1
0.75	0.32	1995	19	2	0.016	0.04	7.1
1.25	0.53	1982	32	3	0.016	0.04	7.1
1.75	0.76	1967	47	4	0.016	0.03	7.1
2.25	1.02	1951	63	5	0.016	0.03	7.1
2.75	1.26	1937	77	6	0.016	0.04	7.1
3.25	1.48	1923	91	7	0.016	0.04	7.1
3.75	1.69	1910	104	8	0.016	0.04	7.1
4.25	1.88	1899	115	9	0.016	0.04	7.1
5.25	2.27	1875	139	11	0.016	0.04	7.1
6.25	2.65	1852	162	12	0.016	0.04	7.1

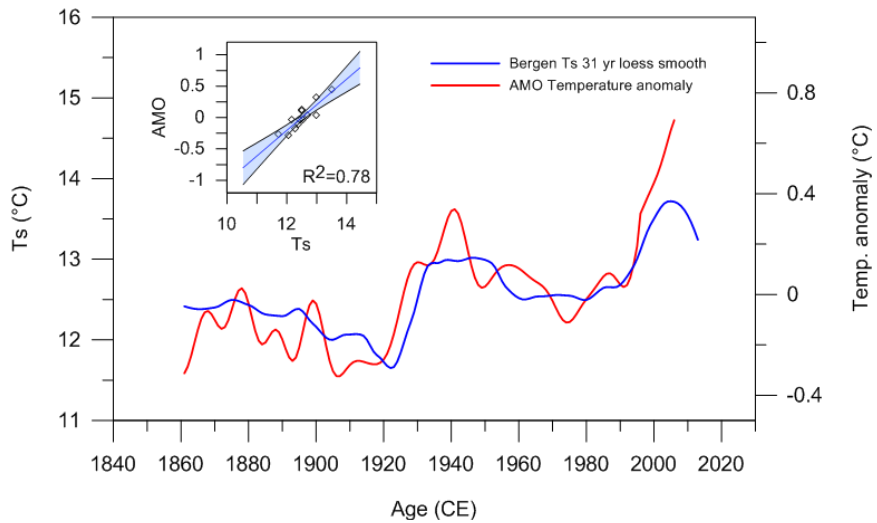


Figure S3: Bergen summer temperature (T_s , 31 yr loess smooth) plotted against AMO temperature anomaly (CE1861-2006). Inset top left: Regression model between Bergen summer temperature and AMO, $R^2=0.78$ (data points every 10 years). Calculated relationship between AMO and the Sandane temperature series:

$$\text{Sandane Summer temp} = (1,92 \cdot \text{AMO}) + 12,5 - 0,15; \quad (S1)$$

where 0,15 is the temperature difference (°C) between Sandane and Bergen.

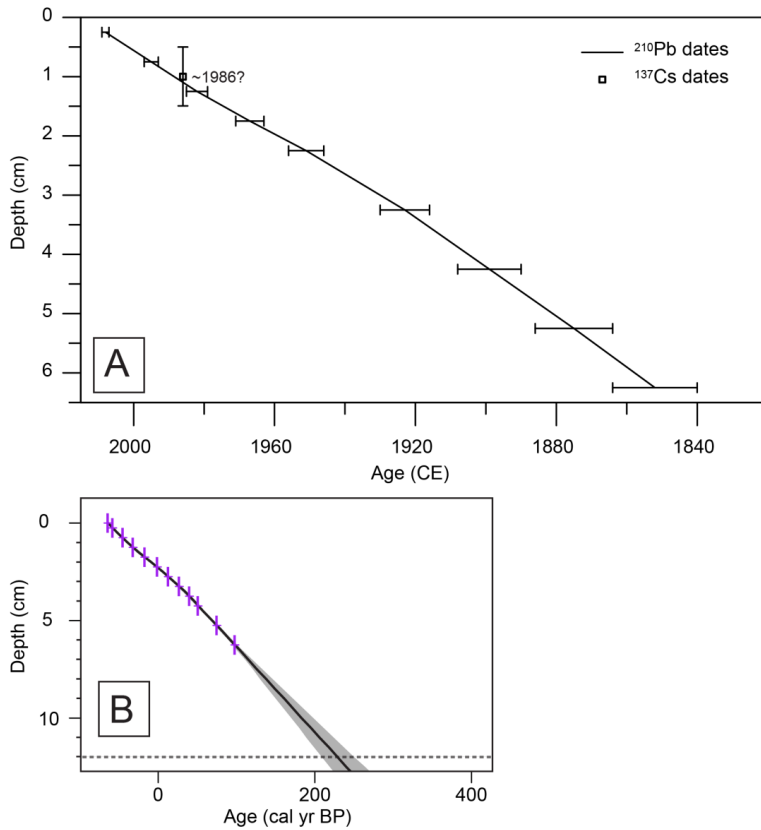


Figure S4: A) ^{210}Pb age profile for STØS-214; B) Age-depth relationship model for STØS-214 made in 'clam', dashed line indicates 12 cm core depth (c.f. section 5.1). Purple marks ^{210}Pb ages, black line is the best estimate smooth spline model age and grey shading marks the 95% (2σ) confidence interval

Table S3: PCA results for GRØP-212 and GRØP-312.

GRØP-212

PC axis	1	2	3	4
Variance explained	88%	4%	4%	1%
DBD	0.97	0.07	0.10	0.03
Log LOI	-0.97	0.01	-0.14	-0.01
MS	0.79	-0.34	0.50	-0.05
Si	0.98	0.10	-0.03	0.06
Ti	0.98	-0.10	-0.10	0.01
Fe	0.82	-0.43	-0.35	0.09
K	0.99	0.01	-0.06	0.01
Ca	0.99	0.03	-0.06	0.01
Mn	-0.90	-0.33	-0.08	-0.17
Rb	0.93	0.13	-0.13	-0.30
Sr	0.97	0.11	-0.03	-0.04

GRØP-312

PC axis	1	2	3	4
Variance explained	83%	10%	3%	2%
DBD	0.94	0.20	-0.08	0.06
Log LOI	-0.97	-0.06	0.07	0.02
MS	0.86	0.25	-0.38	-0.21
Si	0.97	-0.04	0.04	0.15
Ti	0.97	-0.15	0.05	0.05
Fe	0.97	-0.19	-0.01	-0.01
K	0.99	-0.08	0.01	0.07
Ca	0.98	-0.08	-0.02	0.11
Mn	-0.19	-0.96	-0.16	-0.04
Rb	0.89	-0.09	0.30	-0.32
Sr	0.96	-0.04	0.10	0.06

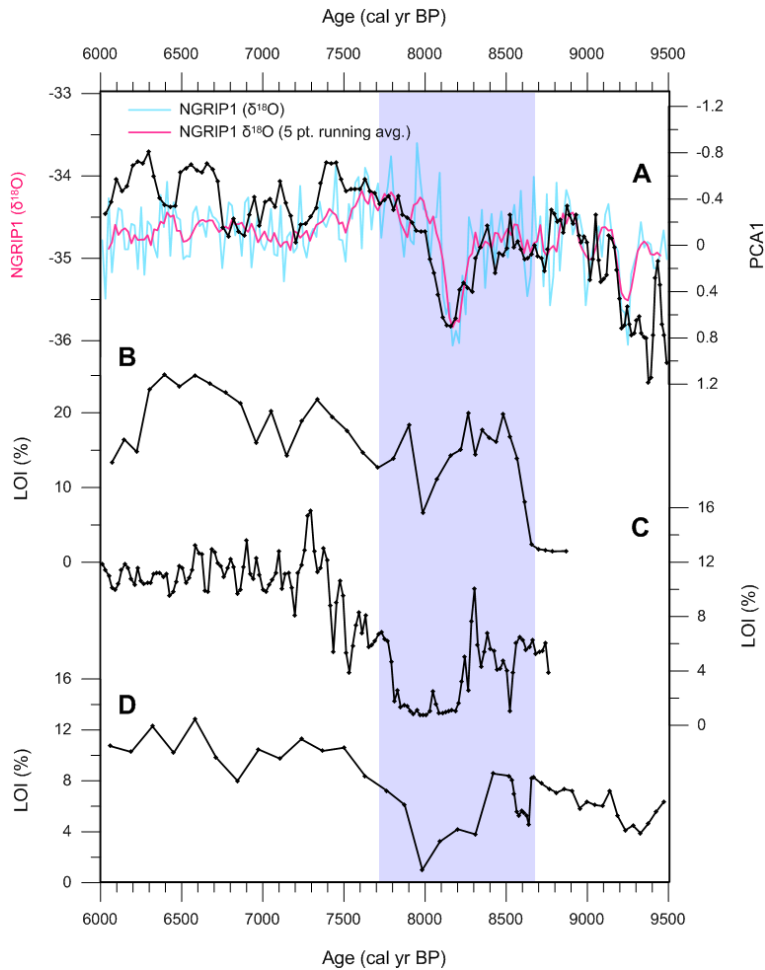


Figure S5: A) Relative glacier activity (PCA1) from GRØP-212 covering the period 6000-9500 cal yr BP and oxygen isotopic record from NGRIP1 ($\delta^{18}\text{O}$, ‰) (Rasmussen et al., 2006; Vinther et al., 2006) plotted against weight loss-on-ignition profiles (%) (=inverted glacier curves) from: B) Vanndalsvatnet, Spørteggbreen (Nesje et al., 2006); C) Dalsvatnet, Smørstabbtindane Massif, Jotunheimen (Matthews et al., 2000); and D) Grønningstølsvatnet, Jostedalsbreen (Nesje and Dahl, 2001). All the lake records apparently record the '8.2 ka BP Event'/Finse Event, with variations in timing of the glacier advances (probably due to slightly different time lags (~30-50 yrs) among the different glaciers in the lake catchments).

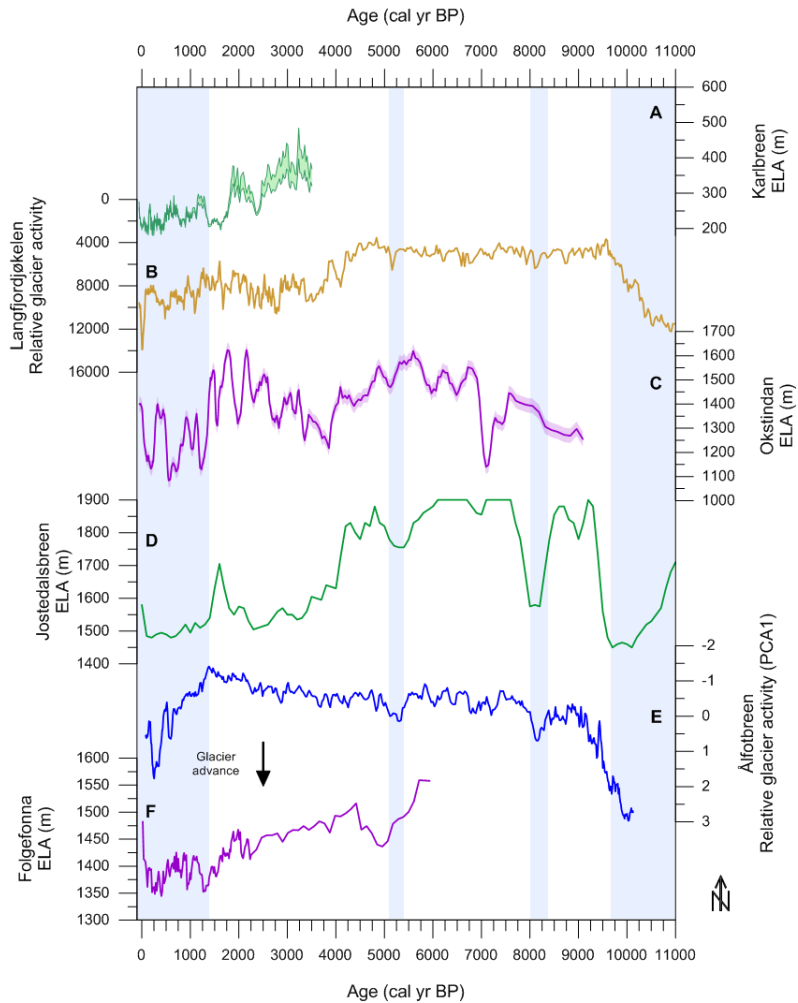


Figure S6: Holocene glacier reconstructions: A: Karlbreven, NW Svalbard (Røthe et al., 2015); B: Langfjordjøkelen, Arctic Norway (Wittmeier et al., 2015); C: Okstindan, N-Norway (Bakke et al., 2010); D: Jostedalsbreen ELA record (based on: Nesje et al., 2001; Vasskog et al., 2012); E: Ålftobreen, W-Norway (this study); F: Folgefonna, SW-Norway (Bakke et al., 2005). Blue shaded areas mark the deglaciation; the '8.2 ka Event'/Finse event; the glacier advance at Ålftobreen ~5400-5100 cal yr BP; and the Neoglacial at Ålftobreen (~1400 cal yr BP - present).

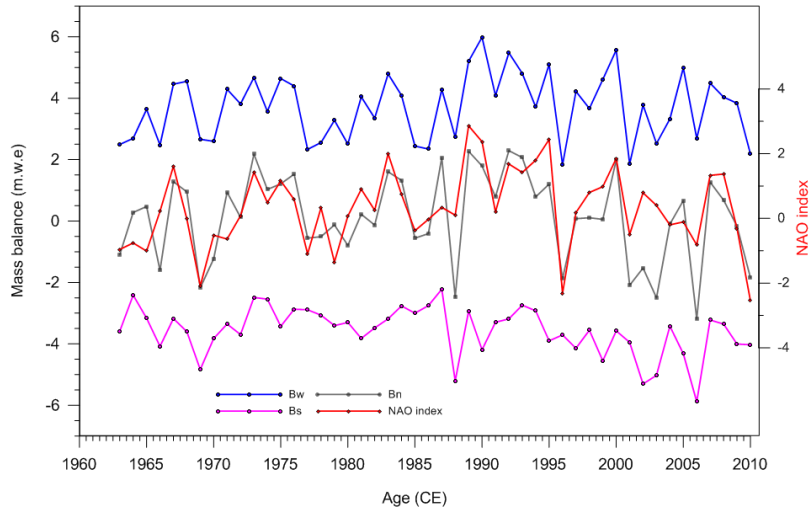


Figure S7: Mass balance measurements from *Ålftobreen* (mass balance data: NVE) (*Bw*=winter balance; *Bs*=summer balance; *Bn*=net mass balance and the NAO index (data: <http://cru.uea.ac.uk/>).

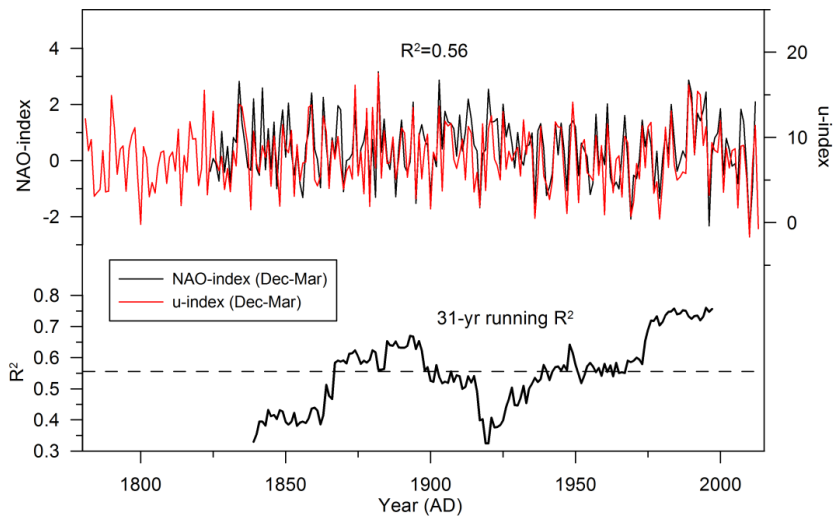


Figure S8: 31-year running coefficient of determination (R^2) between the NAO index and the wintertime westerlies over southern Norway (Allan and Ansell, 2006; Jones et al., 1999).

References

- Allan, R., Ansell, T., 2006. A new globally complete monthly historical gridded mean sea level pressure dataset (HadSLP2): 1850-2004. *Journal of Climate* 19, 5816-5842.
- Bakke, J., Dahl, S.O., Paasche, Ø., Riis Simonsen, J., Kvisvik, B., Bakke, K., Nesje, A., 2010. A complete record of Holocene glacier variability at Austre Okstindbreen, northern Norway: an integrated approach. *Quaternary Science Reviews* 29, 1246-1262.
- Bakke, J., Nesje, A., Dahl, S.O., 2005. Utilizing physical sediment variability in glacier-fed lakes for continuous glacier reconstructions during the Holocene, northern Folgefonna, western Norway. *The Holocene* 15, 161-176.
- Jones, P., Davies, T., Lister, D., Slonosky, V., Jonsson, T., Bärring, L., Jönsson, P., Maheras, P., Kolyva-Machera, F., Barriendos, M., 1999. Monthly mean pressure reconstructions for Europe for the 1780–1995 period. *International Journal of Climatology* 19, 347-364.
- Matthews, J.A., Olaf Dahl, S., Nesje, A., Berrisford, M.S., Andersson, C., 2000. Holocene glacier variations in central Jotunheimen, southern Norway based on distal glaciolacustrine sediment cores. *Quaternary Science Reviews* 19, 1625-1647.
- Nesje, A., Bjune, A.E., Bakke, J., Dahl, S.O., Lie, Ø., Birks, H.J.B., 2006. Holocene palaeoclimate reconstructions at Vanndalsvatnet, western Norway, with particular reference to the 8200 cal. yr BP event. *The Holocene* 16, 717-729.
- Nesje, A., Dahl, S.O., 2001. The Greenland 8200 cal. yr BP event detected in loss-on-ignition profiles in Norwegian lacustrine sediment sequences. *Journal of Quaternary Science* 16, 155-166.
- Nesje, A., Matthews, J.A., Dahl, S.O., Berrisford, M.S., Andersson, C., 2001. Holocene glacier fluctuations of Flatebreen and winter-precipitation changes in the Jostedalbreen region, western Norway, based on glaciolacustrine sediment records. *The Holocene* 11, 267-280.
- Rasmussen, S.O., Andersen, K.K., Svensson, A., Steffensen, J.P., Vinther, B.M., Clausen, H.B., Siggaard-Andersen, M.L., Johnsen, S.J., Larsen, L.B., Dahl-Jensen, D., 2006. A new Greenland ice core chronology for the last glacial termination. *Journal of Geophysical Research: Atmospheres* (1984–2012) 111.
- Røthe, T.O., Bakke, J., Vasskog, K., Gjerde, M., D'Andrea, W.J., Bradley, R.S., 2015. Arctic Holocene glacier fluctuations reconstructed from lake sediments at Mitrahålvøya, Spitsbergen. *Quaternary Science Reviews* 109, 111-125.
- Vasskog, K., Paasche, Ø., Nesje, A., Boyle, J.F., Birks, H.J.B., 2012. A new approach for reconstructing glacier variability based on lake sediments recording input from more than one glacier. *Quaternary Research* 77, 192-204.
- Vinther, B.M., Clausen, H.B., Johnsen, S.J., Rasmussen, S.O., Andersen, K.K., Buchardt, S.L., Dahl-Jensen, D., Seierstad, I.K., Siggaard-Andersen, M.L., Steffensen, J.P., 2006. A

synchronized dating of three Greenland ice cores throughout the Holocene. *Journal of Geophysical Research: Atmospheres* (1984–2012) 111.

Wittmeier, H.E., Bakke, J., Vasskog, K., Trachsel, M., 2015. Reconstructing Holocene glacier activity at Langfjordjøkelen, Arctic Norway, using multi-proxy fingerprinting of distal glacier-fed lake sediments. *Quaternary Science Reviews* 114, 78-99.

Paper II

Gjerde, M., Bakke, J., D'Andrea, W., Balascio, N.S., Bradley, R.S., Vasskog, K., Ólafsdóttir, S., Røthe, T.O., Perren, B., Hormes, A.: Late Glacial and Holocene multi-proxy environmental reconstruction from Lake Hakluytvatnet, Amsterdamøya Island, Svalbard (79.5°N). Submitted to Special Issue: 'Post-glacial/Holocene conditions on Amsterdamøya Island', Quaternary Science Reviews.

Late Glacial and Holocene multi-proxy environmental reconstruction from Lake Hakluytvatnet, Amsterdamøya Island, Svalbard (79.5°N)

Marthe Gjerde^{1,2}, Jostein Bakke¹, William D'Andrea³, Nicholas S. Balascio^{3,4}, Raymond S. Bradley^{1,5}, Kristian Vasskog¹, Sædis Ólafsdóttir¹, Torgeir O. Røthe¹, Bianca B. Perren⁶, Anne Holmes^{2,7}

¹ Department of Earth Science and Bjerknes Centre for Climate Research, University of Bergen, Allégaten 41, 5007 Bergen, Norway

² The University Centre in Svalbard, 9171 Longyearbyen, Norway

³ Lamont-Doherty Earth Observatory of Columbia University, Palisades, NY, USA

⁴ Department of Geology, College of William & Mary, Williamsburg, VA, USA

⁵ Department of Geosciences, University of Massachusetts, Amherst, MA 01003, USA

⁶ British Antarctic Survey, High Cross, Madingley Road, Cambridge, UK CB3 0ET

⁷ Department of Earth Sciences, University of Gothenburg, SE-405 30 Gothenburg, Sweden

Corresponding author: Marthe Gjerde, Department of Earth Science, University of Bergen, Allégaten 41, NO-5007 Bergen, Norway. E-mail: Marthe.gjerde@uib.no. Phone: +47 55 58 81 10.

Keywords: Lake sediments, Runoff, Svalbard, Holocene, Neoglacial, Multi-proxy analyses

ABSTRACT

Robust records of past climatic changes are sparse and poorly resolved in the Arctic due to low organic production that restricts the use of radiocarbon dating and challenging logistics that make data collection difficult. Here, we present a new lake record from lake Hakluytvatnet at Amsterdamøya island (79.5°N), the northwesternmost island on Svalbard. Multi-proxy analyses of lake sediments in combination with geomorphological mapping reveal large environmental shifts that have taken place at Amsterdamøya since the Late Glacial. A robust chronology has been established for the lake sediment core through 28 AMS radiocarbon (^{14}C) ages, and this gives an exceptionally well-constrained age control for a lake at this latitude. The sedimentary archive recorded the last ~13,000 years of climate change, and is the first lake record going back to the Late Glacial at this site. Our findings indicate that a local glacier was present during the Younger Dryas (YD), and we estimate YD equilibrium-line altitude (ELA) lowering. Further, the Holocene was a period with large changes in the Hakluytvatnet catchment, and the onset of the Neoglacial (ca. 5 ka) marks the start of modern-day conditions in the catchment. The Neoglacial is characterized by fluctuations in the minerogenic input to the lake as well as internal productivity, and we suggest that these fluctuations are driven by atmospherically forced precipitation changes as well as sea ice extent modulating the amount of moisture that can reach Hakluytvatnet.

1. INTRODUCTION

Palaeoclimatic reconstructions offer the possibility to extend earth system observations beyond the instrumental time period. Such reconstructions are especially important in the Arctic because the rate of on-going change is unprecedented within Common Era observations. However, our knowledge of the natural climate variability in the Arctic is limited due to the scarcity of data and the relatively short period of observation. Future anthropogenic climate changes will be superimposed on these natural variations, which might result in fundamental changes to internal climate feedback mechanisms, influencing the timing and amplitude of future climate. This leads to a critical emerging question in the scientific community: how will the effects of global warming be manifested in the Arctic? To make meaningful climate projections at the regional scale and to evaluate model simulations of future climate, we need a longer perspective than the short instrumental period provides. Annual precipitation in the Arctic is projected to increase by 20% by the end of the twenty-first century (ACIA, 2004), among the highest globally, and this is a consistent feature among state-of-the-art global climate models (Kattsov et al., 2007). The anticipated climate changes, and especially those related to hydrology, will have a large impact on sources and sinks of greenhouse gases related to the Arctic tundra (Jørgensen et al., 2015), on local societies in the Arctic, and will likely impact lower latitudes through climatic teleconnections (Førland et al., 2009). However, to better anticipate future changes in the Arctic, a significant improvement in our documentation and understanding of the longer-term natural climate variability in this region is required. Due primarily to logistical constraints, the region north of 70°N is heavily under-sampled with respect to Holocene paleoclimate reconstructions.

Svalbard, a high-Arctic Norwegian archipelago (74-81°N, 10-35°E), is situated in a climatically sensitive site in the northern North Atlantic and is well-positioned to record past changes in atmospheric and oceanic circulation patterns of the North Atlantic Arctic. Lake

sediments are excellent archives for recording regional climate change, because lakes trap detrital and organic material from the catchment, as well as organic material produced within the lake. The type of material entering the lake depends on the catchment area surrounding the lake basin (Rubensdotter and Rosqvist, 2009), and this in turn depends on a number of geological, geomorphological and climatic factors. Sedimentary fingerprinting of the various sources contributing to lake sedimentation and their past variations allows for detailed palaeoenvironmental reconstructions.

Here we present new palaeoclimatic data from one of the northernmost lakes in Europe, on Amsterdamøya island, NW Svalbard. We demonstrate that the potential for producing robust chronologies exists even in these remote polar regions, and that by careful selection of sites high-resolution palaeoclimatic reconstruction can be achieved. Here we present: 1) a high precision radiocarbon dated sedimentary lake sequence; 2) reconstructed glacier activity and detrital sedimentation processes from the Late Glacial until the present; and 3) a multi-proxy reconstruction of Neoglacial climate fluctuations at Amsterdamøya based on the runoff and productivity signal recorded in the lake sediments.

2. SETTING

The island of Amsterdamøya (‘øya’=island) (N79°46’, E10°45’) is located at the northwesternmost corner of Svalbard in the North Atlantic Ocean, where the distance from Amsterdamøya to the shelf break is only 8 km. The West Spitsbergen Current (‘WSC’) (Aagaard et al., 1987) is the northernmost limb of the Norwegian Atlantic Current (‘NwAC’), bringing warmer Atlantic waters as an extension of the North Atlantic Current (‘NAC’) to the NW coast of Svalbard (Fig. 1A). Due to this northward transport of warm water and its impact on air masses, the western side of the Svalbard archipelago is dominated by warmer

temperatures, more precipitation and less sea ice than the east coast. On the coast of western Svalbard (Ny-Ålesund and Isfjord Radio) (Fig. 1A) summer temperature (June, July, August) (1961-1990) averages 4°C, and averages range from -12 to -15 °C during the winter months (January, February, March; JFM). Winter (JFM) precipitation on Svalbard ranges from 190-440 mm/year (Førland et al., 2010). The alternating westerlies and the polar-front jet stream modulate the present climate on Svalbard and are influenced by the North Atlantic Oscillation (NAO) and the Arctic Oscillation (AO). During positive AO (AO+) winters, cyclones reach the Barents Sea region thereby bringing more snow to Svalbard; conversely, a negative AO (AO-) leads to a tendency toward NE-E winds, cold temperatures, and lower winter precipitation (e.g Luks et al., 2011).

A metamorphosed basement comprised of migmatites, banded gneisses rich in biotite and late-tectonic granites of Caledonian age form the bedrock in the area. Small outcrops of amphibolite are present on the north side of the catchment, as well as small appearances of marble layers on the north and south side of the catchment area (Hjelle and Ohta, 1974; Ohta et al., 2007). Amsterdamøya island is characterized by gently sloping plateaus >300 m a.s.l. covered by autochthonous block fields. Steep cliffs towards the sea frame the plateaus (Hjelle and Ohta, 1974).

Surface exposure ages on glacial erratics from Amsterdamøya and the neighbouring Danskøya islands (Fig. 1B) indicate that the summits in the area have remained ice-free since >80 ka BP, although the lower grounds remained glaciated until 18-15,000 years ago (Landvik et al., 2003). These more recent ages are further supported by surface exposure ages from Hormes et al. (2013), indicating that the NW sector of Svalbard became deglaciated between 13,600 and 11,700 years ago after a local ice dome covering the NW Svalbard disintegrated. The marine limit (ML) at Amsterdamøya is not constrained, but is probably close to present day sea level (Boulton and Rhodes, 1974; Salvigsen, 1979; Landvik et al.,

1998). There has been little postglacial emergence in the NW part of Svalbard, and neither Amsterdamøya nor Danskøya display clear geomorphological evidence of uplift in relation to sea level since the ice cover disappeared (Boulton and Rhodes, 1974; Salvigsen, 1977; Landvik et al., 1998).

2.1 Lake, catchment, and geomorphological setting

Our study site, lake Hakluytvatnet (79°46'24"N, 10°44'21"E) (12 m a.s.l.) is a small lake with a surface area of ~0.1 km² (Fig. 1A). The catchment area (~2.2 km²) displays steep cliffs incised by two cirque valleys surrounding the flat valley floor. The northwest-facing beach sequence framing the lake forms a terrace towards the sea (Fig. 1C), and consists of well-rounded gravel-and-boulder type beach sediments. Maximum water depth of Hakluytvatnet ('vatnet'=lake) is ~5 m, and the lake is surrounded by 'northern arctic-tundra zone'-type vegetation (Birks et al., 2004). The lake has a pH of 5.9, conductivity values are low and filamentous algae are frequent in the lake and in the lake outflow with extensive submerged moss growth even at 5 m water depth (Birks et al., 2004). Hydrolab field measurements in September 2014 revealed that the lake water had a temperature of 4°C, and that the water was well-mixed by wind and showed no stratification. The geometry of the lake basin is shallow, and it dips gently towards the deepest part where maximum sediment thickness is ~2.5 m (Fig. 1D). At present, there are no glaciers in the catchment; however, two perennial snow patches are present on the plateau in the southern part of the catchment serving as the main source area for the river feeding Hakluytvatnet (Fig. 1C).

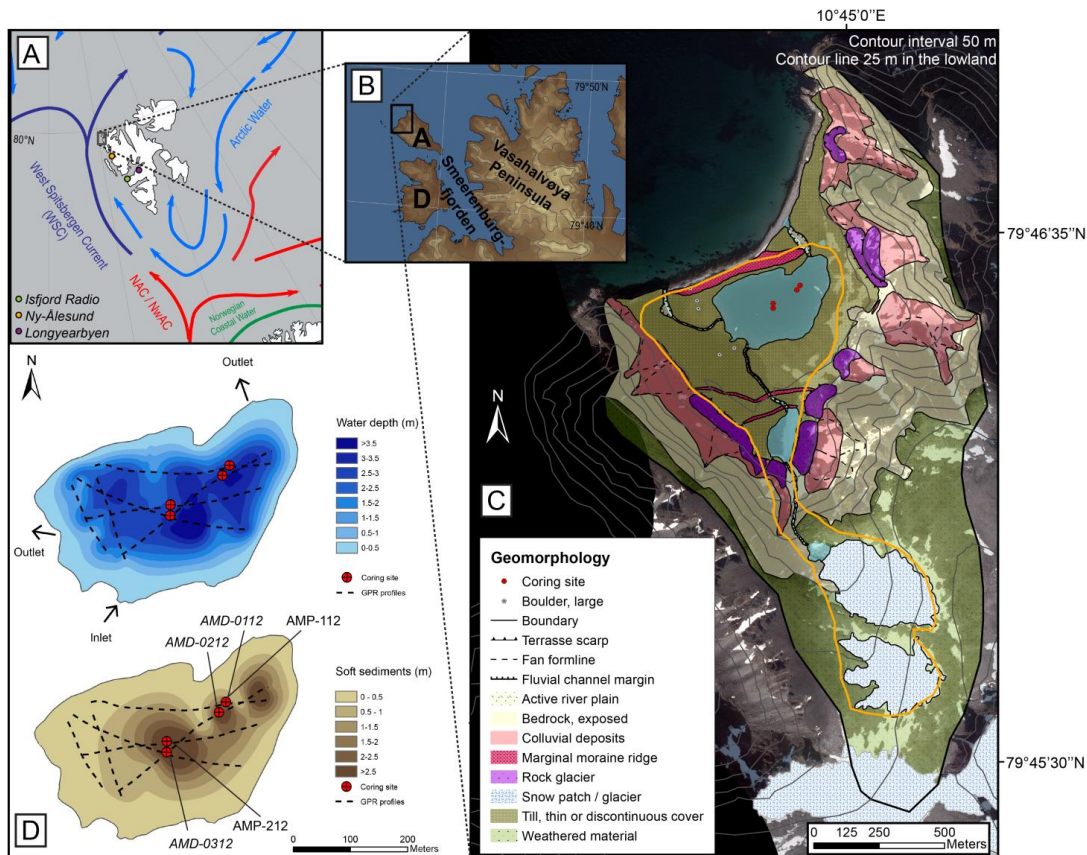


Figure 1: A) Svalbard and surrounding surface currents; B) NW corner of Svalbard (topographic) with place names: A=Amsterdamøya, D=Danskøya; C) Geomorphological map of the study site and catchment area. Orange line denotes inferred former glacier extent (cf. section 4.6; D) Bathymetrical map (top) and soft-sediment thickness (below) with coring sites and GPR profiles. Base maps: Norwegian Polar Institute. Ocean currents data: Institute of Marine Research, Norway.

3. METHODS

The environmental reconstruction in this study is based upon a combination of geomorphological mapping (orthophoto: Norwegian Polar Institute, series S2011_25160), field ground-truthing, lake coring, and multi-proxy laboratory analyses. A firm chronology has been established for the lake sediments from AMS radiocarbon dating.

3.1 Lake coring and laboratory analyses

Prior to lake coring in late summer 2012, Hakluyvatnet was surveyed using a Ground Penetrating Radar (GPR) in order to map the bathymetry and the sediment distribution before determining suitable coring sites. GPR profiles were collected using a RAMAC GPR from Malå with a 50 MHz RTA antenna (Fig. 1D). In total, 5 cores were extracted; 2 piston cores (AMP-112; 170 cm; and AMP-212; 247.5 cm) and 3 gravity cores (AMD-0112; 142 cm; AMD-0212; 42 cm; and AMD-0312; 56 cm) (see Fig. 1D for coring locations). AMD-0212 (core data presented in Balascio et al., this issue) was sampled every 0.5 cm of the top 10 cm while in the field to obtain samples for ^{210}Pb dating. During a second field excursion (late summer 2014), measurements of the lake water properties (using a Hydrolab multiparameter water quality instrument) were made, and more detailed mapping of the catchment area was conducted, including extensive GPR surveying of the beach sequence damming the lake.

The sediment cores AMP-112 and AMP-212 were split lengthwise in the lab and one half of each core were stored for reference. During splitting, both core sections of AMP-212 were disturbed, and this core was therefore not subject to further analyses. Core AMP-112 was carefully cleaned and photographed before lithofacies and sedimentological structures were described based on visual inspection.

For core AMP-112 we measured weight loss-on-ignition (LOI), dry bulk density (DBD) and water content (WC) (Dean, 1974; Heiri et al., 2001) every 0.5 cm ($n = 339$) using a syringe for fixed volume extraction (1 cm^3). This method was applied for the more minerogenic part of the core (below 105 cm depth), whereas for the uppermost 105 cm, where abundant aquatic mosses made it more difficult to apply the syringe (see section 4.2), samples were extracted using a scalpel. The DBD (volume-dependent) measurements for the upper part were therefore considered less accurate. Down-core variations in surface magnetic susceptibility

(MS) were measured on the split cores at 0.2 cm resolution using a Bartington MS2E point sensor.

Geochemical data and radiographic images of AMP-112 were obtained using an ITRAX X-ray fluorescence (XRF) scanner (Croudace et al., 2006) at EARTHLAB, University of Bergen. A molybdenum (Mo) X-ray tube was used for radiographic measurements, whereas XRF analyses were performed applying a chromium (Cr) tube, with a down-core resolution of 500 μm . XRF power settings of 30kV and 40 mA were used with a 10 s counting time. Due to the differences in sediment composition and organic content in the different core sections, we applied normalization using the conservative redox-insensitive element aluminium (Al) (Thomson et al., 2006; Löwemark et al., 2011) as a supplement to the single elemental count rates.

AMP-112 was sampled every cm down-core (from 3-170 cm depth; $n = 167$) for grain size distribution (GSD) analysis (averaged over 5 runs of each sample), using the Mastersizer 3000 from Malvern Instruments Ltd. connected to the Hydroseries wet dispersion unit allowing for laser diffraction measurement of particle sizes (Ryzak and Bieganowski, 2011). Particle absorption index was set to 0.01; particle refractive index to 1.8, and the pump speed was 2400 rpm. 60% ultra-sonication was applied for 60 s before analysis for all samples, and each measurement was set to 25 s counting time (Sperazza et al., 2004; Ryzak and Bieganowski, 2011).

Six samples were chosen for diatom analysis from 97, 108, 130, 150, 158, and 160.5 cm depth in the core to investigate the possible presence of a marine transgressive unit. Diatoms were isolated from the sediments using standard oxidative techniques modified from Renberg (1990) and mounted on glass coverslips using Naphrax mounting medium. At least 300 diatom samples were identified from each slide at 1000x under oil immersion and identified

using predominantly arctic diatom floras (e.g. Antoniadou et al., 2008). Constrained cluster analysis (CONISS, broken stick model) performed in the open-source statistical software 'R' (R Development Core Team, 2012) delineated the significant stratigraphic zones.

3.2 Radiocarbon dating, palaeomagnetic secular variations and age-depth relationship

The surface top 10 cm including the sediment-water interface in core AMD-0212 were extracted in the field for ^{210}Pb dating. Although the resulting analyses were unsuccessful in establishing a lead profile for accurate chronological constraint, they revealed lead activity in the top demonstrating that the sediments on top of AMD-0212 are modern. For radiocarbon dating, a total of 31 plant macrofossil fragment samples were extracted from cores AMD-0212/AMP-112 (3 of the samples did not contain enough carbon to be dated; see Table 1). An age-depth relationship was established using the Bayesian framework calibration software code 'Bacon' (v. 2.2; Blaauw and Christen, 2011), applied into 'R' (v. 3.2.2). Radiocarbon ages are reported in calibrated radiocarbon years before present ('cal yr BP'; BP=1950) according to IntCal13 (Reimer et al., 2013).

We then attempted to further constrain this radiocarbon age-depth relationship by applying a palaeomagnetic method known as palaeomagnetic secular variations (PSV) (e.g. Merrill et al., 1996). As sediment archives can contain continuous information on the fine-scale variations of the geomagnetic field, reconstruction of PSV may serve as an independent stratigraphic tool in various sediment environments (e.g. Stoner and St-Onge, 2007). A PSV-reconstruction was therefore carried out on core AMP-112 among other sediment archives from Svalbard (Ólafsdóttir et al., this issue). This allowed for PSV-based synchronization between AMP-112 and another ^{14}C -dated lacustrine sediment core 'HAP0212' from Lake Hajeren, a glacier-fed lake ca. 60 km south of Amsterdamøya (van der Bilt et al., 2015). Based on the PSV-

correlation, a total of 43 radiocarbon dates from both cores were combined to a single composite age-model where each radiocarbon date was PSV-correlated within the 2σ radiocarbon calibration uncertainty range (with some exceptions, c.f. section 5.1/Ólafsdóttir et al., this issue), resulting in a mutual depth scale and age-depth relationship for further proxy comparison. Additional details on the PSV-synchronization and construction of the composite age model are discussed in Ólafsdóttir et al. (this issue).

Table 1: Radiocarbon ages AMD-0212 and AMP-112. Samples in italics: Could not be dated. $\delta^{13}\text{C}$ values: graphitisation process introduces significant isotopic fractionation. *: Estimate of carbon content (50%) from the sample mass. Calibrated applying IntCal13 curve.

Core	Lab.no.	Depth (cm)	Material	^{14}C age	Error +/- 1 sigma	+/- 2 sigma (cal yr BP)	$\delta^{13}\text{C}$ ‰	mg C
AMD-0212	D-AMS 006994	11-12	Plant remains	335	23	312-468	-28.1	1.05*
AMD-0212	D-AMS 006995	15.5-16.5	Plant remains	590	22	541-646	-20.7	1.10*
AMD-0212	D-AMS 006996	20-21	Plant remains	1006	20	835-963	-21.9	1.35*
AMD-0212	D-AMS 006997	31-32	Plant remains	1778	24	1617-1808	-21.1	1.00*
AMP-112	Ua-48155	4-5	Plant remains	1481	30	1307-1411	-19.7	1.11
AMP-112	Ua-48156	6-7	Plant remains	1638	31	1416-1612	-21	0.66
<i>AMP-112</i>	<i>Ua-48156</i>	<i>6-7</i>	<i>Chironomid head capsules</i>	-	-	-	-	-
AMP-112	Ua-48157	11.5-12.5	Plant remains	1432	30	1295-1376	-19.1	0.74
AMP-112	Ua-48158	17.5-18.5	Plant remains	1860	30	1720-1869	-21.2	1.39
AMP-112	Ua-48159	22.5-23.5	Plant remains	1895	30	1737-1897	-22.1	1.29
AMP-112	Ua-48160	25.5-26.5	Plant remains	1925	31	1816-1947	-20.8	1.09
AMP-112	Ua-48161	31.5-32.5	Plant remains	2025	31	1896-2099	-21.3	1.07
AMP-112	Ua-48162	35-36	Plant remains	2100	30	1997-2144	-20.4	1.17
<i>AMP-112</i>	<i>ETH-49504</i>	<i>38-39</i>	<i>Chironomid head capsules</i>	-	-	-	-	-
AMP-112	Ua-48163	45-46	Plant remains	2564	30	2506-2754	-21.3	1.09
AMP-112	Ua-48164	50.5-51.5	Plant remains	2589	30	2545-2767	-19.2	1.07
AMP-112	Ua-48165	60.5-61.5	Plant remains	2859	30	2879-3064	-20.5	1.06
AMP-112	Ua-48166	73-74	Plant remains	3458	30	3641-3828	-21.6	1.18
AMP-112	Ua-48167	77.5-78.5	Plant remains	3433	30	3608-3826	-21.1	1.33
AMP-112	Ua-48168	85.5-86.5	Plant remains	3783	34	4006-4284	-21.7	1.07
AMP-112	Ua-48169	98.5-99.5	Plant remains	4293	33	4826-4959	-23.6	1.10
AMP-112	Poz-70631	104.5-105.5	Plant remains	4575	35	5055-5446	-17.4	1.10
AMP-112	ETH-49505	110-111	Plant remains	7107	56	7827-8023	-46.3	0.13
AMP-112	Ua-48170	121-122	Plant remains	7823	51	8455-8770	-25.1	0.006
AMP-112	Ua-48171	132-133	Plant remains	8236	50	9032-9399	-25	0.25
AMP-112	Ua-48172	141-142	Plant remains	7934	60	8610-8988	-25	0.05
AMP-112	ETH-49506	144-145	Plant remains	8718	52	9550-9887	-38.2	0.28
AMP-112	Ua-48173	156-157	Plant remains	10968	61	12719-12991	-25.9	1.44
<i>AMP-112</i>	<i>ETH-49507</i>	<i>158-159</i>	<i>Plant remains</i>	-	-	-	-	-
AMP-112	ETH-49508	162-163	Plant remains	10835	86	12614-12943	-63.5	0.11
AMP-112	ETH-49509	167-168	Plant remains	11008	55	12735-13014	-24.0	0.16

3.3 Multivariate analysis

Principal Component Analysis (PCA) was applied in order to explore the multi-proxy dataset from Hakluyvatnet, including LOI, variations in the 90th percentile of the grain size distribution (GSD90) and 10 geochemical elements (Al, K, Ca, Rb, Ti, Fe, Si, Mg, Mn, Sr) obtained from the ITRAX XRF scan. Regression analyses revealed a logarithmic relationship between many of the variables, which warranted a log transformation of all data before running the PCA, as the analysis assumes linearity between the included variables (e.g. Bakke et al., 2013). All of the data were then standardized before running the PCA in Canoco for Windows (v. 4.5; Lepš and Šmilauer, 2003).

RESULTS

4.1 Geomorphic mapping

An exposed seaward section of the beach sequence damming Hakluyvatnet has previously been studied by Landvik et al. (2003) and was interpreted as a succession of marine and glacial proximal sediments underlying glaciolacustrine sediments, capped by subglacial till containing large angular boulders. The section was dated by Landvik et al. (2003), with optically stimulated luminescence (OSL) ages clustering around 50 ka BP in the sub-till section, and correlated with the Kapp Ekholm interstadial (Mangerud et al., 1998). Here we interpret the topmost part of the ridge (16 m a.s.l.) as a marginal moraine (Fig. 1C). There are two outlets from Hakluyvatnet cutting down and through the ridge; in the east and in the west. GPR measurements across the ridge showed that the ridge is composed only of unconsolidated sediments, meaning that there is no bedrock threshold within the landform damming Hakluyvatnet.

Ridge-shaped lobate landforms consisting of large angular blocks with only sparse vegetation cover are present in large parts of the catchment area. These follow the mountain sides as a continuation of talus (Fig. 1C) and terminate in the sea on the north side of the catchment. These landforms are interpreted as rock glaciers (e.g. Swett et al., 1980), a feature frequently observed in polar regions like Svalbard. The rock glaciers are ice-cored and appear to be talus-derived (Shakesby et al., 1987). Two sets of smaller ridges in the southern cirque valley are interpreted as two generations of recessional moraines (Fig. 1C). The remainder of the valley floor is draped by a thin or discontinuous cover of till.

4.2 Lake core lithostratigraphy

The AMP-112 core was divided into 5 main stratigraphic units: A, B, C, D and E, based on visual logging (Fig. 2). A grain-size distribution (GSD) surface plot (Fig. 3) shows the main grain-size mode changing accordingly between the lithostratigraphic units. A cumulative plot of the GSD (Fig. 3) highlights the silt-sized grains constituting the background sediment in the AMP-112 record; where on average ~80% of the sediment is 63 μm or smaller.

Unit A (170-159 cm) consists of a grey to olive brown matrix-rich diamict. The unit is massive, over-consolidated, and poorly sorted. The organic content (LOI) is low (~5% for most of the unit), water content is close to zero (~4 %) whereas the density (DBD) values are relatively high (~1.1 g/cm³). The X-ray image (Fig. 2) shows the dense character of the unit, reflected by the dark colouring. Geochemical elements reflecting minerogenic content (e.g. Ti, Al, Ca, K) hold their highest values throughout the core in unit A. Unit A is the only unit where MS shows high amplitude fluctuations from 6 up to 22 (Si 10⁻⁵) (MS results not shown in Fig. 2 due to near-zero values throughout the rest of the core). Grain sizes range from clay to gravel, with clasts >2.5 cm and a matrix dominated by sand (~50%) and silt (~48%) (Fig.

3). Sub-rounded to sub-angular clasts $>2500\ \mu\text{m}$ are scattered throughout the unit, and these large clasts were removed before GSD analysis. Small amounts of terrestrial macrofossils were present and 2 samples from unit A were sent for radiocarbon dating (Table 1). From 159.3-159 cm depth, a pale yellow to grey horizon consisting mainly of clay, silt and very fine sand is visually prominent (Fig. 2). This horizon is considered to represent an ‘event’ layer, i.e. a layer of instantaneous deposition. The transition between units A to B is sharp.

Unit B (159-155 cm) consists of olive/dark brown laminated silty sediments, with mosses intertwined. Laminations range from $<1\ \text{mm}$ up to 2 mm. The transitions below and above are sharp. The layering of this 4-cm thick section is chaotic, and it contains a mix of grain sizes from clay and silt ($\sim 72\%$) to sand ($\sim 24\%$). LOI increases from the low values in Unit A to an average of $\sim 12\%$, whereas DBD decreases to average $\sim 0.7\ \text{g/cm}^3$. Because the geochemistry (sulphur peak in Fig. 2) indicated that that Unit B potentially represented a marine-brackish transition, we performed diatom analyses in order to investigate the potential for a marine impact on lake sedimentation. Diatom results (cf. Section 4.3 below) revealed that Hakluytvatnet holds a terrestrial and (freshwater) aquatic signal throughout the whole record.

Unit C (155-109 cm) consists of olive brown to very dark greyish brown laminated silty gyttja. Laminations are finest in the lowermost part (155-142.5 cm), which is also detected in X-ray imagery (Fig. 2). LOI ranges from $\sim 13\%$ to $\sim 35\%$, with a mean of $\sim 26\%$ and a trend of increasing organic content upwards where the highest values are found between 142 and 119.5 cm. DBD values range from 0.15 to $0.60\ \text{g/cm}^3$, with a mean value of $\sim 0.22\ \text{g/cm}^3$. Grain sizes vary in range from clay to coarse sand (Fig. 3), with most of the sediment being silt-sized, on average $\sim 77\%$. A small, minerogenic light yellowish brown horizon from 142.5-142 cm with sharp transitions above and below is characterised by a drop in organic content and a peak in DBD, which is also reflected in the X-radiographic image. Clay and very fine

silt also peaks at this depth, as well as increased Ti count rates indicating more detrital input. We consider that this thin layer might represent an instantaneous depositional event; however, it is not omitted from age-depth modelling. At 120.5-119.5 cm depth a light-coloured minerogenic horizon can be seen, which is characterized by greater clay and silt content (~84%) than the section below. Density increases are reflected in both DBD and X-ray imagery, and organic content drops to <15%. As with the above-mentioned light-coloured horizon at 142.5-142 cm, we acknowledge that this layer might represent an event, however; the gradual transitions to this layer indicates that it might represent normal sedimentation, and it is therefore not omitted from the age-depth modelling.

Unit D (109-105 cm) consists of massive, olive brown gyttja silt with an irregular transition to Unit C below. LOI averages ~16% and DBD averages 0.34 g/cm³. The higher density in this unit compared to unit C below can also be seen in the X-radiographic image. The geochemical detrital parameters increase (Ti, Ti/Al) as well as Si/Ti indicating a potential increase in lake productivity (Fig. 2). Small amounts of macrofossils are present. GSD (Fig. 3) shows that this section contains less clay (averaged ~2.9%) than the sections above and below, and that it consists mainly of silt (~71%) and sand (~26%), with most of it belonging in the range of medium silt to very fine sand.

Unit E (105-0 cm) consists of organic olive brown and very dark brown gyttja, where aquatic mosses are abundant throughout the unit. Weak laminations displaying different colouring and minerogenic content than the dominant dark brown organic-rich facies are visible, and are also reflected in the varying density seen in the X-ray image (Fig. 2). Water content is high (>96% at certain depths) throughout the unit, and some of the geochemical minerogenic indicators reflect this by yielding lower count rates in this section (Ti count rates in Fig. 2) (Tjallingii et al., 2007). LOI is on average ~29%, ranging from ~16 to ~43%. Sediments are predominantly silt-sized, with the highest averaged silt values in the core

~80%, ranging from ~65-86%. Sand content is on average ~17%; ranging from ~11-33% with most of it ranging from very fine to fine sand. From 66-62 cm depth and from 7-3 cm depth a relative increase in grain size is observed (Fig. 3).

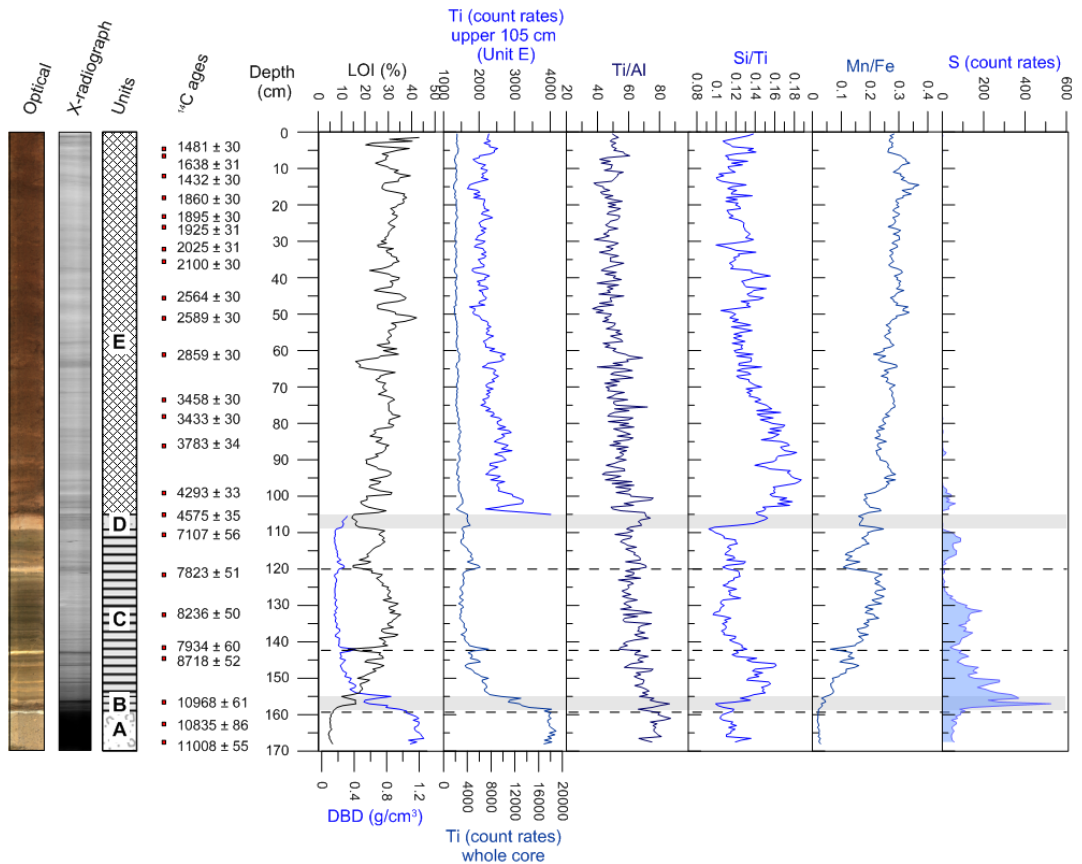


Figure 2: Compiled selected sedimentological parameters from AMP-112. Optical line-scan image and radiographic image show the sediment colour and density (darker colours represent denser sediment), respectively. Lithological log shows unit division (also indicated in horizontal light grey bars). All XRF data are smoothed to 0.5 cm resolution. Ti count rates are plotted for both the whole core length, and also zoomed in for the upper 105 cm due to change in count rates in Unit C (note change in scale). Ti count rates co-vary with Ti/Al ratio. Si/Ti is often used as an indicator of biological silica (productivity) (e.g. Balascio et al., 2011; Melles et al., 2012), and also co-varies with Ti/Al. Mn/Fe indicates increasingly oxic conditions (e.g. Naehler et al., 2013) towards the top of the core. Horizons of inferred instantaneously deposited sediments (cf. section 4.2) are highlighted with dashed lines.

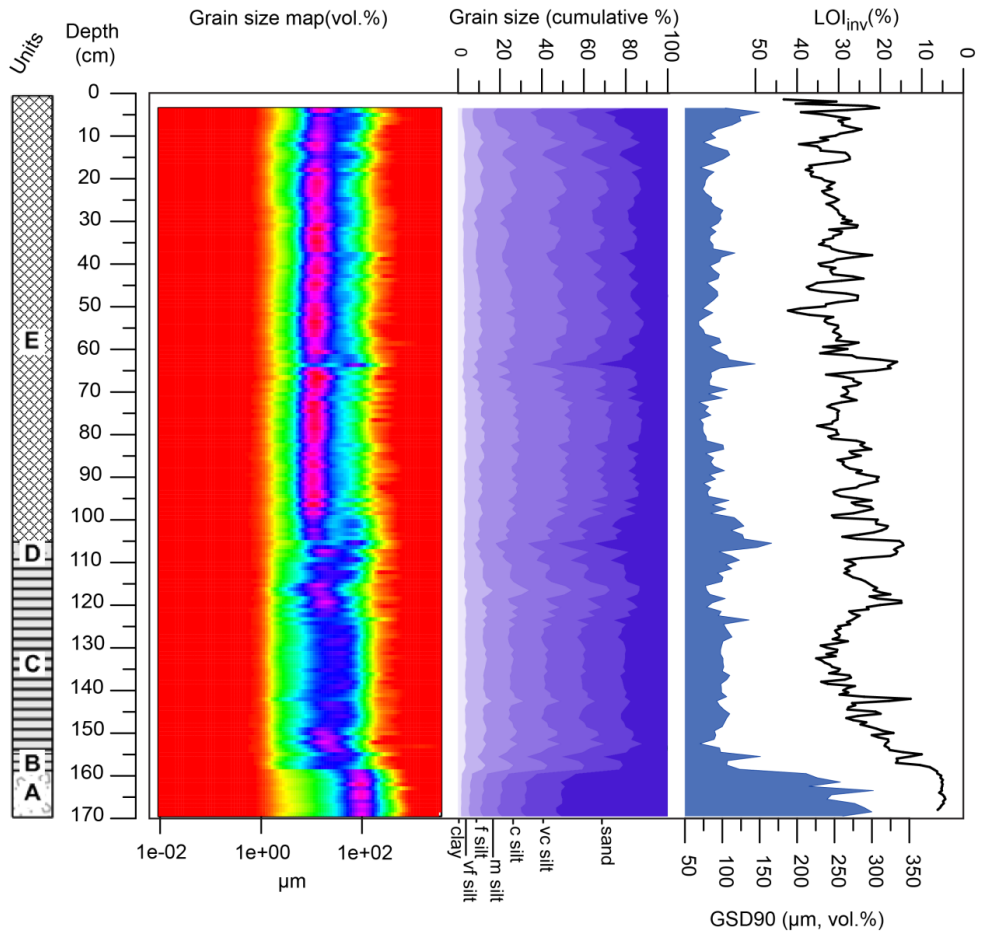


Figure 3: GSD (volume %) plotted as a surface diagram, with darker blue/purple colour where the frequency of particular grain sizes is highest (plotted using software 'EMMAgeo'; Dietze and Dietze, 2013). The well-sorted, fine-grained Unit E is easily visually distinguishable from the coarser-grained units A-D. Cumulative plot highlights the background sediment with silt making up most of the sediment. 90 percentile GSD reveals that the volume of Unit A contains coarser-grained particles, and the more similar variance in grain sizes throughout units B-E. LOI (%) is plotted on inverted scale, reflecting varying organic content throughout the core, co-varying inversely with GSD90 ($R=-0.5$). Note rapid drops in organic content during intervals of larger GSD.

4.3 Environmental evolution of Hakluytvatnet- inferences from diatom analyses

The main findings from the diatom analyses are presented in Fig. 4, and placed in environmental context below.

Two significantly different environments are identified from the diatom analysis: an early unstable, silt- and clay-dominated environment (units A-C), and a later, more productive clear water lake environment (units D-E). Initially, in samples from Unit A (160.5 cm), the diatom flora is characterized by the presence of species of *Muelleria*, *Diadesmis*, *Luticola* which are associated with polar subaerial environments, including cryoconite, soils, and microbial mats (cf. Johansen, 2010; van de Vijver et al., 2014). *Pinnularia* spp. and *Stauroneis gracilis* complex = cf. *S. gracilis*, *S. pax*, *S. vandevijveri*) are also present, the latter of which have been found in very shallow pools/seepages in elsewhere in the high Arctic (van de Vijver et al., 2004). Together, these suggest that Hakluytvatnet was not yet a lake, but a terrestrial landscape with a nascent soil and biofilm microbial community. This unit transitions to Unit B (sampled at 158 cm), where the soil diatoms have largely disappeared, and are replaced by *Navicula digitulus*, as well as small pioneering *Fragilaria s.l.* species (*Stauroneis pinnata*, *Pseudostauroneis pseudoconstruens*), a community characteristic of cold, oligotrophic, postglacial lake environments with high sedimentation rates (cf. Perren et al., 2012; Wojtal et al., 2014). In two samples from Unit C (150 and 130 cm), small fragilarioids continue to dominate (*S. pinnata*, *P. pseudoconstruens*, *S. exiguiformis*) as well as very small *Navicula*. cf. *submuralis*, suggesting a typically nutrient-poor, high-arctic lake, where suspended sediment load still precludes the development of a planktonic diatom community. Samples from units D (108 cm) and E (98 cm) record a fundamental shift to a more productive lake environment that supports a higher diversity of benthic as well as planktonic taxa (e.g. *Aulacoseira distans*). In these last units, most of the clay is gone, improving the light quality, and allowing for colonization and enhanced biological activity in all parts of the lake. This is

in agreement with the observed increase in Si/Ti at the transition to Unit E, which also suggests an increased production of biogenic silica (Fig 2).

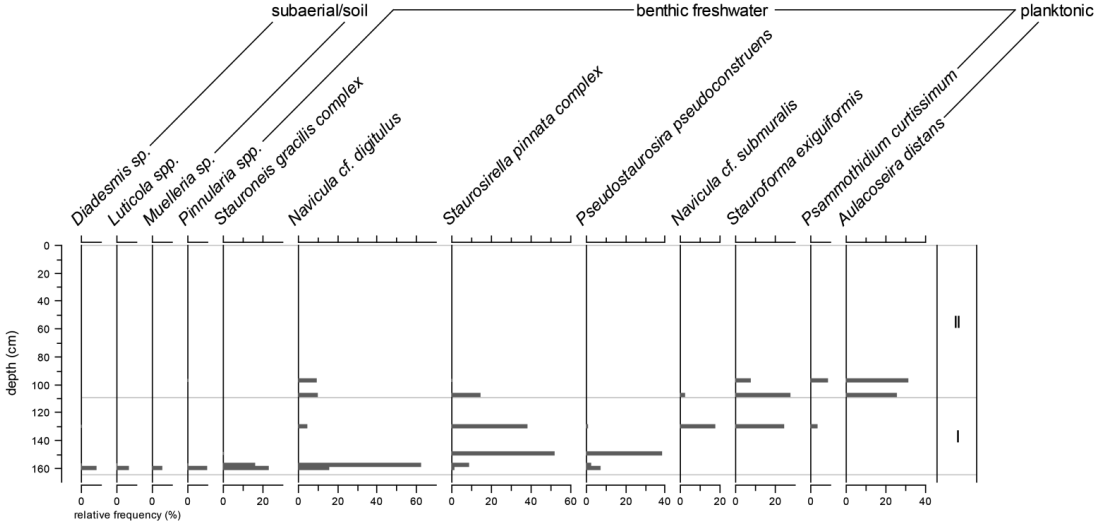


Figure 4: Percent abundance of diatom taxa that indicate environmental evolution of the lake and landscape. The two significant zones in the core stratigraphy are highlighted.

4.4 Principal component analysis

Ordination with PCA returned one significant Principal Component (PC) axis; explaining 49% of the variability in the dataset from the upper 105 cm of AMP-112. Most of the geochemical elements, except Sr and Mg, align closely with PCA1, with Mn correlating positively with LOI and the remaining elements correlating inversely with LOI (Si, K, Ca, Ti, and Fe). The second PC axis captures mainly the variability of GSD90 and Mg, although this axis may not be significant, explaining only 11% of the total variability. This shows that variations in grain size are not correlated with general changes in geochemistry, although there is a weak inverse correlation with Mg. Visually it is apparent that large GSD perturbations often occur at the same time as large fluctuations in the XRF data, but there is

no clear relationship in the direction of change, and additionally there is a long-term trend in the geochemical elements that is not observed in GSD. A linear detrending of the dataset increases the correlation between GSD90 and LOI, whereas it decreases the correlation between LOI and the geochemical elements. This could indicate that the long-term trend in the XRF-data is driven by LOI and water content through dilution of the XRF signal, which means that geochemistry and LOI are not governed by the same process(es) on shorter timescales. After detrending, the strongest correlation is found between GSD90 and LOI ($R=0.50$), suggesting some common driver of these signals.

4.5 Chronology and sedimentation rates

Compaction during piston coring caused loss of the sediment-water interface in core AMP-112, and pressed the upper soft sediments together. Intra-basin correlation between the short cores (AMD-0212 and AMD-0112) and AMP-112 was done based on XRF Ti count rates in order to construct a common depth scale for the cores and produce a composite age-depth model. In Fig. 5A the radiocarbon-based AMP-112 age-depth model produced in 'Bacon' is stippled with the 95% uncertainty range derived from the radiocarbon ages highlighted in grey. Also plotted in Fig. 5A is the PSV-synchronized age-depth relationship constructed from radiocarbon dates from both Hakluytvatnet and Lake Hajeren along with several PSV-synchronized tie points between the lakes. The individual control points are colour-coded for each source of origin (Fig. 5A).

Sediment accumulation rate (SAR) at Hakluytvatnet (Fig. 5B) changed significantly throughout the core. Periods of non-deposition, or extremely low SAR, <0.01 (cm/yr), are found at two intervals; $\sim 12,700 - \sim 9700$ cal yr BP and from $\sim 8400 - \sim 5300$ cal yr BP. Between these two periods, a significant increase in SAR (up to ~ 0.05 cm/yr) is seen around

9500 cal yr BP. After 5300 cal yr BP, the SAR gradually increases and varies more frequently and with larger amplitudes than in the lower sediment sequence. Several short-lived spikes in SAR are found centred at ~4800, ~3800, ~2900, ~1900 and ~350 cal yr BP (Fig. 5B).

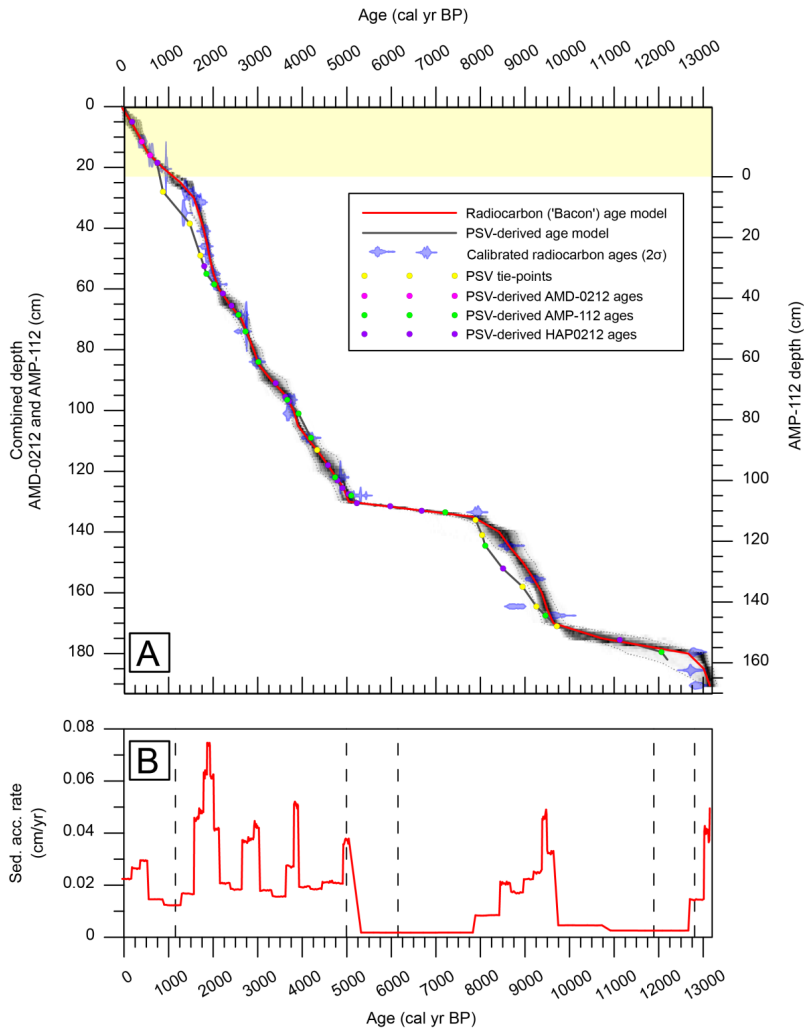


Figure 5: A) Age-depth relationship for AMP-112 and AMD-0112. Radiocarbon (‘Bacon’) age-model in grey shaded area (95% confidence interval); transparent blue points denote individual calibrated ^{14}C ages. ‘Best’ age-depth relationship (red solid line) is based on the weighted mean age for each depth. The PSV-corrected age-depth model is marked as a dark grey line including colour-coded PSV-derived radiocarbon ages from AMP-112 and AMD-0212, PSV tie-points (Ólafsdóttir et al., 2016), and radiocarbon ages from HAP0212 (van der Bilt et al., 2015). PSV-derived age model is truncated at transition to Unit A (159 cm depth AMP-112 depth scale; c.f. sections 4.5/5.2). Depth scales are shown both as the combined

depth scale coupling AMD-0212 and AMP-112 (left) and as individual AMP-112 depth scale (right) (+23 cm [yellow shaded area] added to AMD-0212; c.f. section 4.5. B) Sediment accumulation rate calculated from 'Bacon'-derived age-depth relationship. Dashed lines denote lithological unit divisions of AMP-112 (core top age: ~1150 cal yr BP).

4.6 Equilibrium-line altitude reconstruction

Modern-day regional equilibrium-line altitude (ELA) is situated above the highest point of the catchment area, i.e. above ~400 m a.s.l. (regional ELA overview in: Hagen et al., 2003). We estimated the ELA of the glacier that deposited the moraine ridge NW of the lake (Fig. 1C) based on a simple cartographic reconstruction of the palaeo-glacier's hypsometry. Calculating palaeo-ELAs can be done in several ways, but due to the few constraints available to define the glacier geometry (e.g. lateral moraines), we have chosen to apply the Accumulation Area Ratio (AAR) and the Area-Altitude Balance Ratio (AABR) methods (e.g. Benn and Lehmkuhl, 2000; Osmaston, 2005).

The AAR method assumes that the accumulation area constitutes a fixed ratio of the total glacier area, and the ratio applied for cirque and valley glaciers (as here) is normally ~0.6 (Benn and Evans, 1998; Rea, 2009), whereas the AABR method takes into account both glacier hypsometry and the difference between the accumulation and ablation gradients (Rea, 2009). We calculated ELAs for the palaeo-glacier using a range of AAR values between 0.65 and 0.45, which returned ELAs ranging from 50-180 m a.s.l.; with a mean of 60 and 125 m a.s.l. for AAR of 0.6 ± 0.5 and 0.5 ± 0.5 , respectively (Table 2). As such, we find that the hypsometry of the palaeo-glacier, which includes a steep and narrow part between 150 and 250 m a.s.l., makes it very sensitive to small changes in accumulation area within the likely AAR range investigated here. The AABR ratios applied are calculated from the regional Svalbard range (2.13 ± 0.52) from the compilation in Rea (2009) and are also presented in Table 2. The palaeo-ELAs calculated applying the AABR method display a narrower range

from 150-175 m a.s.l., which is within the wider AAR range. With the limited data available, we conclude that the ELA of the Hakluytvatnet palaeo-glacier was situated somewhere between 50 – 180 m a.s.l. when the moraine ridge north of Hakluytvatnet was deposited. Although there are large uncertainties in our ELA estimate, it highlights that the regional ELA does not have to be lowered very much to allow glaciation in the catchment, i.e. in the range of 100-200 m (Hagen et al., 2003).

Table 2: ELA's calculated for the reconstructed palaeo-glacier covering Hakluytvatnet.

Ratio	AAR ELA (m a.s.l.)		Balance ratio ELA (m a.s.l.)	
	0.45	0.65	1.61	2.65
Palaeo-glacier Hakluytvatnet	180	50	150	175

DISCUSSION

The main objective of this study has been to reconstruct the Late Glacial and Holocene climate history of Amsterdamøya based on sediments deposited in lake Hakluytvatnet. Below we discuss the deglaciation history, the large environmental changes observed in the Early- and Mid-Holocene, and finally, late Holocene changes in hydroclimate, based on interpretations of the lake record.

5.1 Chronology

The results from PSV-synchronizing between the lakes Hakluytvatnet and Hajeren highlight the potential of applying this methodology on high-Arctic lakes where robust radiocarbon chronologies are usually challenging to construct due to a general lack of organic detritus. However, due to two intervals in the core showing relatively large offsets in age between the two age-modelling approaches, as well as the large number of radiocarbon ages obtained for the Hakluytvatnet lake record ($n=28$), we have chosen to simply use the ‘Bacon’-derived age-depth relationship for plotting our lake proxies against age.

5.2 Late Glacial ELA reconstruction

The massive diamicton constituting Unit A in core AMP-112 from Hakluytvatnet is interpreted as a basal till deposited just prior to the final deglaciation of the Hakluytvatnet catchment. Two radiocarbon dates within the till, and one directly overlying it, returned overlapping ages (see Table 1) centred around 12,800 cal yr BP. From the geomorphological mapping our interpretation is that the moraine ridge deposited outside Hakluytvatnet (Fig. 1C) was formed by a local cirque glacier occupying the catchment covering the lake, and the basal till in AMP-112 is therefore interpreted to be related to this local glacier re-advance and not the Barents Sea Ice Sheet (BSIS). During the Last Glacial Maximum (LGM) ice extended to the shelf break some 8 km northwest of Amsterdamøya (Ingólfsson and Landvik, 2013), leaving most of the Hakluytvatnet catchment covered by a glacier, although the highest areas of Amsterdamøya were probably ice-free (Landvik et al., 2003). The Hakluytvatnet catchment might therefore have become more-or-less ice-free when the BSIS first retreated from the northwest Spitsbergen area around ~13,800 cal yr BP (~12 ^{14}C ka BP) (Ingólfsson and Landvik, 2013), and from our interpretation a local cirque glacier then formed and advanced

across Hakluytvatnet, before finally retreating in the early Younger Dryas (~12,800 cal yr BP). This could imply that this glacier advance commenced sometime during the warmer Bølling-Allerød period, and that it was initiated by increased precipitation and favourable wind conditions in the form of prevailing polar easterlies (Birgel and Hass, 2004). During the transition to the colder YD, moisture starvation induced by increased sea-ice cover (e.g. Müller et al., 2009) likely caused the demise of the cirque glacier, and the Hakluytvatnet lake has not been covered by a glacier ever since. OSL and radiocarbon ages centred around 50 ka of the sediment ('valley-fill') below the moraine ridge (Landvik et al., 2003) indicate that the stratigraphically younger moraine was deposited sometime after 50 ka. Thus, we acknowledge that the moraine ridge might be older than the glacier event detected in the sediment core, but our interpretation that Unit A is a subglacially deposited diamict implies that the glacier at least covered the part of the lake where the core was retrieved and the ridge acts as a maximum estimate of the palaeo-glacier extent. As there are no indications of marine sedimentation in Hakluytvatnet, sea level must have remained at below the top part of this ridge at 16 m a.s.l. ever since deglaciation and it is therefore not necessary to adjust our estimated palaeo-ELA due to changes in relative sea level. Relative to the highest point of the present-day snowfield (~400 m a.s.l.; Fig. 1C), the reconstructed ELA lowering is on the order of ~220 – 350 m (AAR) and from 225 – 250 m (AABR) (Table 2). This is comparable with YD ELA lowering in Northern Norway of ~370 m (Rea and Evans, 2007) and a recent study from Northern Norway showing 220 and 130 m ELA lowering during the Late Glacial and the YD, respectively (Wittmeier et al., submitted).

Our ELA estimate is the first YD ELA estimate from NW Svalbard, whereas in western Svalbard glacier extent has generally been thought to be larger during the LIA than during YD (Mangerud and Landvik, 2007). This may reflect that the west coast glaciers were located in the precipitation shadow from possible prevailing YD easterlies (Birgel and Hass, 2004),

thereby reducing accumulation on these glaciers. The Hakluytvatnet catchment receives snowdrift from the plateau, though mostly from snow that accumulates from N-NE winds, which could further support the idea that YD atmospheric conditions (e.g. Mayewski et al., 1993) could support a glacier in the Hakluytvatnet catchment for a short while before it started retreating.

5.3 Early and Mid-Holocene depositional environment

During the early- and mid-Holocene, the depositional environment changed significantly for Hakluytvatnet, which can be easily seen from the lithostratigraphy of AMP-112. Large shifts in the environment are reflected in changing SAR and geochemical properties, as well as environmental shifts detected in diatom assemblages when the lake was transitioning from a dry polar soil/biofilm environment to an oligotrophic lake (section 4.3).

During deposition of Unit B (~12,800 – ~11,900 cal yr BP), the diatom assemblage indicates that the sedimentary environment was likely a cold postglacial lake environment (cf. section 4.3), and this is further supported by low Si/Ti values (Fig. 2), which reflect low production of biogenic silica (e.g. Balascio et al., 2011; Melles et al., 2012). Unit C represents the early-Holocene depositional environment in lake Hakluytvatnet (~11,900 – ~6150 cal yr BP), and is clearly distinguishable from Units A and B below. The diatom assemblage is typical of a nutrient-poor, high-Arctic lake where not much is living in the photic zone. Unit C is suggested to reflect an anoxic depositional environment (as indicated by high sulphur counts and low Mn/Fe ratios; Fig. 2) and this might, combined with the nutrient-poor environment indicated by the diatom analyses, suggest that the lake was covered by lake ice for a longer period of the year than what is presently the case. Freshwater forcing by meltwater pulses originating from the decaying ice sheets in the North Atlantic induced enhanced seasonality

and unstable climatic conditions during the Early Holocene (e.g. Beck et al., 1997; Stager and Mayewski, 1997; Renssen et al., 2002), and we suggest that the more extreme seasonality during the Early Holocene (e.g. Haug et al., 2001) could have acted as a driver for stratification of the lake during the HTM, with more severe winters inducing a longer ice cover season. Additionally, shallowing lake levels could have progressed until the aquatic mosses were able to establish on the bed of the succeeding clearer lake waters (~5000 cal yr BP), in conjunction with turnover by wind on the smaller surface area of the lake preventing any strong stratification ever since.

Unit D (~6150 – ~5000 cal yr BP) either represents a period of very low sedimentation rate, or a hiatus in deposition when the lake might even have disappeared completely as a result of the warmer and drier climate of the Mid-Holocene on Svalbard, as is recorded in terrestrial (Birks, 1991) and marine records (Salvigsen, 2002). We can only speculate as to why the lake dried out, but conclude that there was a large shift in depositional environment at the time of Unit D being deposited, which is also reflected in the diatom assemblages with a shift to a more diverse lake environment and improved light quality. Increased productivity is also reflected in the large increase in Si/Ti (Fig. 2). At this point we make no conclusions about what caused this transition, and we have chosen to focus mainly on the last ~5000 years for the remainder of this discussion, because it reflects a stable depositional environment in Hakluytvatnet, and because this period is particularly interesting with respect to the Neoglacial period on Svalbard (e.g. Røthe et al., 2015). Furthermore, our age-model is well constrained for this time period.

5.4 Neoglacial runoff and productivity changes in Hakluytvatnet

The late-Holocene part of the sediment record from AMP-112 represented by Unit E covers the time period from ~5000 cal yr BP to ~1100 cal yr BP. Based on our geomorphological mapping and understanding of active earth surface processes in the catchment, we interpret changes in detrital input to Hakluytvatnet during the last 5000 cal yr BP (i.e. the Neoglacial) as primarily reflecting precipitation- or meltwater-induced sediment transport from the surrounding catchment area, as the flat topography surrounding the lake does not promote mass-wasting processes. Changes in grain size (GSD90) might therefore reflect changes in the intensity of precipitation events. The fairly strong (negative) correlation ($R=-0.5$) between GSD90 and detrended LOI suggests that periods of more intense precipitation and runoff is also an important driver for increased minerogenic sedimentation in the lake. Based on the GSD90 record, increased runoff intensity at Hakluytvatnet is observed during four distinct intervals: between ~1600 – ~1350 (top of runoff record) cal yr BP; between ~2250 – ~2150 cal yr BP; between ~3150 – ~3000 cal yr BP; and between ~5000 – ~4800 cal yr BP (grey vertical bars in Fig. 6).

The diatom analysis provides snapshots of detailed environmental information for Hakluytvatnet (Fig. 4), and it shows a distinct change to a more productive clear-water environment around 5000 cal yr BP. At the same level we observe a strong increase in the XRF Si/Ti ratio, which in some cases can act as a proxy for biogenic silica (e.g. Balascio et al., 2011; Melles et al., 2012), and thereby reflect internal productivity in the lake. This is based on the argument that Ti can only be provided to the lake sediments through detrital input while Si can be provided both through detrital input and through diatom growth in the lake. Seeing that the sharp increase in Si/Ti around 5000 cal yr BP coincides with a change in diatom flora that reflects increased productivity, we suggest that the Si/Ti ratio does reflect production of biogenic silica in Hakluytvatnet, thereby providing a high-resolution record of

productivity change for the entire Neoglacial period on Svalbard. The highest productivity is indicated between 5000-4000 cal yr BP, after which a gradual decrease is seen (Fig. 6). This pattern follows the general trend of decreasing insolation at high northern latitudes; however, the maritime setting of Hakluytvatnet should also make this site highly sensitive to oceanic influence. When initiation of modern oceanographic conditions in the eastern Fram Strait occurred ~5200 cal yr BP (Werner et al., 2013) this allowed for the WSC to transport heat and moisture up to NW Svalbard. This adjustment in oceanic configuration could explain the change in boundary conditions in the Hakluytvatnet catchment around the same time. During the Neoglacial, the decreasing trend in summer insolation (Huybers, 2006) (Fig. 6C) is also reflected in increasing sea ice extent (Müller et al., 2012) (Fig. 6C). Productivity in Hakluytvatnet (Fig. 6B and C) displays similar trends as changes in sea-ice extent in the Fram Strait, indicating that the distribution of sea ice greatly impacts lake productivity. Reduced sea ice thereby seems to promote lake productivity, reflecting milder and wetter (i.e. more maritime) conditions. The Si/Ti record from Hakluytvatnet could therefore provide a high-resolution record of local sea ice conditions around Amsterdamøya. As sea ice cover is a key factor in controlling the moisture availability for Svalbard, particularly for the very northernmost coast where Hakluytvatnet is situated, it should also impact runoff from the Hakluytvatnet catchment. Looking at the GSD90 record, we observe that there seems to be an increase in runoff-induced sedimentation to Hakluytvatnet during periods of decreasing sea ice extent, as reflected in higher Si/Ti values (Fig. 6C). We therefore suggest that the runoff record reflects the atmospheric moisture supply to the Hakluytvatnet catchment, which is highly dependent on the prevailing sea-ice conditions. There might also be a component related to atmospheric circulation in the runoff record, reflecting changes in for instance the Arctic Oscillation (AO). In instrumental data, a link is seen between increased snow-depth in SW Svalbard and a more negative AO index (Luks et al., 2011), making it possible that this

large-scale circulation feature might affect runoff to Hakluytvatnet. Though, variability in sea level pressure caused by AO changes might affect sea ice configuration that in turn affect moisture supply to the Hakluytvatnet catchment. However, as our runoff record does not overlap with instrumental data, we cannot establish a firm connection between atmospheric circulation and our lake data.

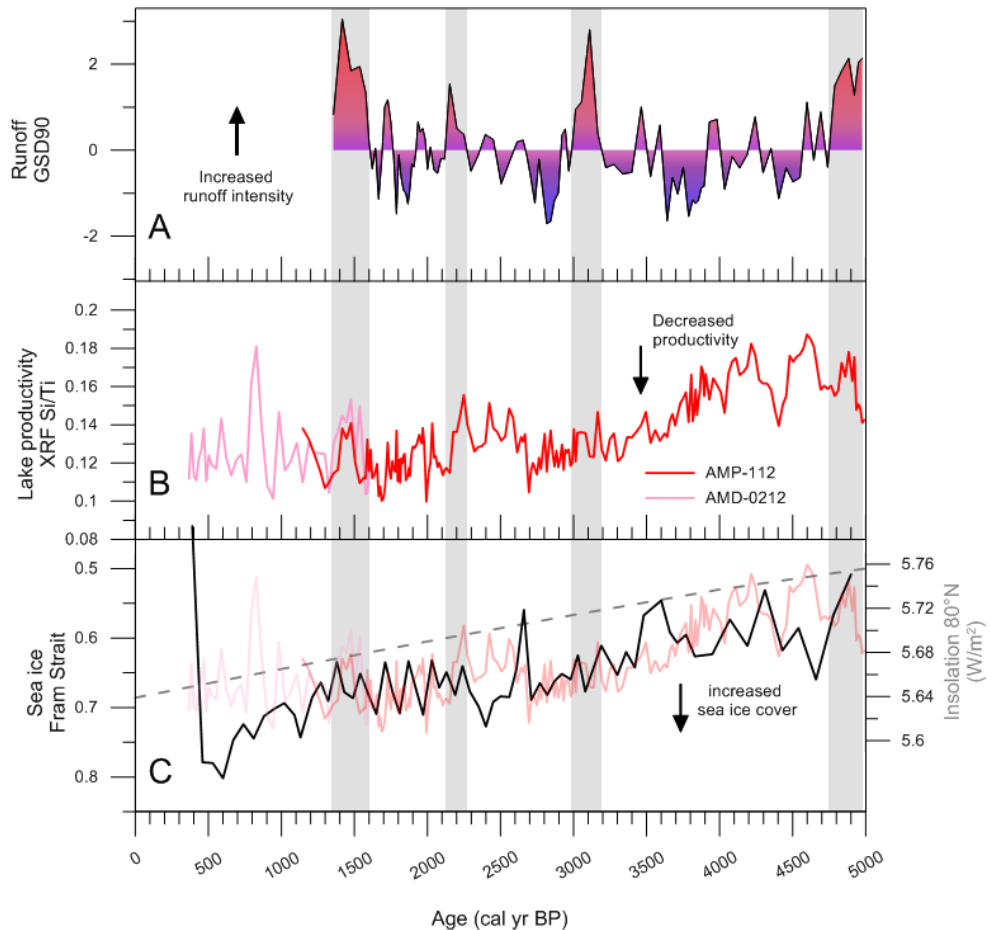


Figure 6: A) Runoff record from Hakluytvatnet (standardized and detrended GSD90); B) lake productivity record (XRF Si/Ti ratios, coupling AMP-0212 and AMP-112 [cf. section 4.5 and Fig. 5]); C) total solar insolation (dashed line) at 80°N (Huybers, 2006) and reconstructed sea ice variability in the Fram Strait from sea ice biomarker proxy IP_{25} (sediment core MSM5/5-712-2) (Müller et al., 2012). Also plotted in C) are Si/Ti XRF ratios as in B) to highlight covariance. Grey vertical bars denote periods with relatively large runoff.

CONCLUSIONS

- Fundamental changes in the depositional environment represented by the sediments reveal large changes in the hydrology of northwest Svalbard during the Holocene and the Hakluyvatnet record gives insight into these large changes
- We present the first (terrestrial?) evidence for a larger YD glacier extent on Svalbard than during the LIA and propose that the glacier extent was governed by favourable winds and precipitation before subsequent YD cooling and sea-ice expansion led to glacier starvation. The glacier retreated rapidly up-valley 12,800 cal yr BP
- Between 12,800 – 11,900 cal yr BP dry conditions precluded the formation of a lake or cold conditions led to a shallow lake that was frozen to the bottom. Sediment accumulated very slowly
- Between 11,900 – 6150 cal yr BP increased moisture led to a lake in the basin. In-wash of silt from the catchment made it a murky lake and restricted the growth of aquatic mosses
- Between 6150 – 5000 cal yr BP the lake completely dried up at this time and no sediment was deposited, likely as a result of the warm Holocene Thermal Optimum
- The onset of Neoglacial conditions ~5000 cal yr BP resulted in a positive moisture balance for the site and allowed the lake to form. Clear water allowed aquatic moss to grow. Punctuated episodes of clastic in-wash point toward rapid snowmelt events or high summer precipitation events that carried minerogenic material into the lake
- The sedimentary signal in the lake since ~5000 cal yr BP reflects extreme runoff from the catchment, and we constructed a time-series of runoff at NW Svalbard
- Further, we have constructed a time-series reflecting productivity that seems highly influenced by sea ice variability, thereby showing the potential of applying

productivity changes in Hakluytvatnet as a high-resolution proxy for sea ice variability at the northwesternmost corner of Svalbard

ACKNOWLEDGEMENTS

Permission to perform field work in the national park during both expeditions was granted by the Governor of Svalbard (RIS ID 5155, ref.: 2012/00753-11 a.512). We thank Bjørn C. Kvisvik, Rob D'Anjou and Greg de Wet for assistance during field work, and acknowledge funding by Svalbard Science Forum (AFG project no. 235919) as well as funding from the Norwegian Research Council via the SHIFTS project. Atle Nesje is thanked for giving constructive comments on the manuscript, and Gunhild Rosqvist is thanked for commenting an earlier draft of the manuscript. Eivind Støren is thanked for technical assistance with settings of the Mastersizer. Anne Bjune helped identify multiple macrofossil samples. PSV scan supervised by Joseph Stoner, Oregon State University. Micha Dietze is thanked for help with coding in EMMAgeo software. Radiocarbon dating was conducted in: Uppsala, Sweden (supervised by Göran Possnert and Elisabet Petterson); Poznan, Poland (supervised by Thomas Goslar), ETH, Switzerland, Direct AMS, USA (supervised by Ugo Zoppi).

REFERENCES

- Aagaard, K., Foldvik, A., Hillman, S., 1987. The West Spitsbergen Current: disposition and water mass transformation. *Journal of Geophysical Research: Oceans* (1978–2012) 92, 3778-3784
- ACIA, 2004. *Impacts of a Warming Arctic: Arctic Climate Impact Assessment, Impacts of a Warming Arctic*, Cambridge, UK, p. pp. 144.
- Antoniades, D., Hamilton, P., Douglas, M.S.V., Smol, J.P., 2008. Freshwater diatoms of the Canadian High Arctic Islands: Ellef Ringnes, northern Ellesmere and Prince Patrick islands, *Iconographia Diatomologica*. A.R.G. Gantner Verlag, Ruggell, p. 649.
- Bakke, J., Trachsel, M., Kvisvik, B.C., Nesje, A., Lyså, A., 2013. Numerical analyses of a multi-proxy data set from a distal glacier-fed lake, Sørsendalsvatn, western Norway. *Quaternary Science Reviews* 73, 182-195
- Balascio, N.L., Zhang, Z., Bradley, R.S., Perren, B., Dahl, S.O., Bakke, J., 2011. A multi-proxy approach to assessing isolation basin stratigraphy from the Lofoten Islands, Norway. *Quaternary Research* 75, 288-300
- Beck, J.W., Récy, J., Taylor, F., Edwards, R.L., Cabioch, G., 1997. Abrupt changes in early Holocene tropical sea surface temperature derived from coral records. *Nature* 385, 705-707
- Benn, D.I., Evans, D.J., 1998. *Glaciers and glaciation*, London.
- Benn, D.I., Lehmkuhl, F., 2000. Mass balance and equilibrium-line altitudes of glaciers in high-mountain environments. *Quaternary International* 65, 15-29
- Birgel, D., Hass, H.C., 2004. Oceanic and atmospheric variations during the last deglaciation in the Fram Strait (Arctic Ocean): a coupled high-resolution organic-geochemical and sedimentological study. *Quaternary Science Reviews* 23, 29-47
- Birks, H.H., 1991. Holocene vegetational history and climatic change in west Spitsbergen-plant macrofossils from Skardtjørna, an Arctic lake. *The Holocene* 1, 209-218
- Birks, H.J.B., Monteith, D.T., Rose, N.L., Jones, V.J., Peglar, S.M., 2004. Recent environmental change and atmospheric contamination on Svalbard as recorded in lake sediments—modern limnology, vegetation, and pollen deposition. *Journal of Paleolimnology* 31, 411-431
- Blaauw, M., Christen, J.A., 2011. Flexible paleoclimate age-depth models using an autoregressive gamma process. *Bayesian Analysis* 6, 457-474
- Boulton, G.S., Rhodes, M., 1974. Isostatic uplift and glacial history in northern Spitsbergen. *Geological Magazine* 111, 481-500.[doi:10.1017/S0016756800041546](https://doi.org/10.1017/S0016756800041546)

- Croudace, I.W., Rindby, A., Rothwell, R.G., 2006. ITRAX: description and evaluation of a new multi-function X-ray core scanner. *Special Publication - Geological Society Of London* 267, 51
- Dean, W.E., 1974. Determination of carbonate and organic matter in calcareous sediments and sedimentary rocks by loss on ignition: comparison with other methods. *Journal of Sedimentary Research* 44
- Dietze, M., Dietze, E., 2013. EMMAgeo: End-member modelling algorithm and supporting functions for grain-size analysis, R package version 0.9. 0.
- Førland, E.J., Benestad, R., Flatøy, F., Hanssen-Bauer, I., Haugen, J., Isaksen, K., Sorteberg, A., Ådlandsvik, B., 2009. Climate development in North Norway and the Svalbard region during 1900–2100.
- Førland, E.J., Benestad, R.E., Flatøy, F., Hanssen-Bauer, I., Haugen, J.E., Isaksen, K., Sorteberg, A., Ådlandsvik, B., 2010. Klimautvikling i Nord-Norge og på Svalbard i perioden 1900–2100: klimaendringer i norsk Arktis: NorACIA delutredning 1.
- Hagen, J.O., Melvold, K., Pinglot, F., Dowdeswell, J.A., 2003. On the net mass balance of the glaciers and ice caps in Svalbard, Norwegian Arctic. *Arctic, Antarctic, and Alpine Research* 35, 264-270
- Haug, G.H., Hughen, K.A., Sigman, D.M., Peterson, L.C., Röhl, U., 2001. Southward migration of the intertropical convergence zone through the Holocene. *Science* 293, 1304-1308
- Heiri, O., Lotter, A.F., Lemcke, G., 2001. Loss on ignition as a method for estimating organic and carbonate content in sediments: reproducibility and comparability of results. *Journal of Paleolimnology* 25, 101-110
- Hjelle, A., Ohta, Y., 1974. Contribution to the geology of north western Spitsbergen, In: SKRIFTER, N.P. (Ed.), Nr 158, pp. 1-107.
- Hormes, A., Gjermundsen, E.F., Rasmussen, T.L., 2013. From mountain top to the deep sea—deglaciation in 4D of the northwestern Barents Sea ice sheet. *Quaternary Science Reviews* 75, 78-99
- Huybers, P., 2006. Early Pleistocene glacial cycles and the integrated summer insolation forcing. *Science* 313, 508-511
- Ingólfsson, Ó., Landvik, J.Y., 2013. The Svalbard–Barents Sea ice-sheet—Historical, current and future perspectives. *Quaternary Science Reviews* 64, 33-60

- Johansen, J.R., 2010. Diatoms of aerial habitats, In: Smol, J.P., Stoermer, E.F. (Ed.), *The diatoms: applications for the environmental and earth sciences*. Cambridge University Press, Cambridge, UK, pp. 287-308.
- Jørgensen, C.J., Johansen, K.M.L., Westergaard-Nielsen, A., Elberling, B., 2015. Net regional methane sink in High Arctic soils of northeast Greenland. *Nature Geoscience* 8, 20-23
- Kattsov, V.M., Walsh, J.E., Chapman, W.L., Govorkova, V.A., Pavlova, T.V., Zhang, X., 2007. Simulation and projection of Arctic freshwater budget components by the IPCC AR4 global climate models. *Journal of Hydrometeorology* 8, 571-589
- Landvik, J.Y., Bondevik, S., Elverhøi, A., Fjeldskaar, W., Mangerud, J., Salvigsen, O., Siegert, M.J., Svendsen, J.-I., Vorren, T.O., 1998. The last glacial maximum of Svalbard and the Barents Sea area: ice sheet extent and configuration. *Quaternary Science Reviews* 17, 43-75
- Landvik, J.Y., Brook, E.J., Gualtieri, L., Raisbeck, G., Salvigsen, O., Yiou, F., 2003. Northwest Svalbard during the last glaciation: Ice-free areas existed. *Geology* 31, 905-908
- Lepš, J., Šmilauer, P., 2003. *Multivariate Analysis of Ecological Data using CANOCO*. Cambridge University Press, Cambridge.
- Luks, B., Osuch, M., Romanowicz, R.J., 2011. The relationship between snowpack dynamics and NAO/AO indices in SW Spitsbergen. *Physics and Chemistry of the Earth, Parts A/B/C* 36, 646-654
- Löwemark, L., Chen, H.-F., Yang, T.-N., Kylander, M., Yu, E.-F., Hsu, Y.-W., Lee, T.-Q., Song, S.-R., Jarvis, S., 2011. Normalizing XRF-scanner data: a cautionary note on the interpretation of high-resolution records from organic-rich lakes. *Journal of Asian Earth Sciences* 40, 1250-1256
- Mangerud, J., Dokken, T., Hebbeln, D., Heggen, B., Ingólfsson, Ó., Landvik, J.Y., Mejdahl, V., Svendsen, J.I., Vorren, T.O., 1998. Fluctuations of the Svalbard–Barents Sea Ice Sheet during the last 150 000 years. *Quaternary Science Reviews* 17, 11-42
- Mangerud, J., Landvik, J.Y., 2007. Younger Dryas cirque glaciers in western Spitsbergen: smaller than during the Little Ice Age. *Boreas* 36, 278-285
- Mayewski, P.A., Meeker, L.D., Whitlow, S., Twickler, M.S., Morrison, M.C., Alley, R.B., Bloomfield, P., Taylor, K., 1993. The atmosphere during the Younger Dryas. *Science* 261, 195-197
- Melles, M., Brigham-Grette, J., Minyuk, P.S., Nowaczyk, N.R., Wennrich, V., DeConto, R.M., Anderson, P.M., Andreev, A.A., Coletti, A., Cook, T.L., 2012. 2.8 million years of Arctic climate change from Lake El'gygytyn, NE Russia. *Science* 337, 315-320

- Merrill, R.T., McElhinny, M., McFadden, P.L., 1996. The magnetic field of the earth: paleomagnetism, the core, and the deep mantle. Academic Press, San Diego, CA.
- Müller, J., Massé, G., Stein, R., Belt, S.T., 2009. Variability of sea-ice conditions in the Fram Strait over the past 30,000 years. *Nature Geoscience* 2, 772-776
- Müller, J., Werner, K., Stein, R., Fahl, K., Moros, M., Jansen, E., 2012. Holocene cooling culminates in sea ice oscillations in Fram Strait. *Quaternary Science Reviews* 47, 1-14
- Naeher, S., Gilli, A., North, R.P., Hamann, Y., Schubert, C.J., 2013. Tracing bottom water oxygenation with sedimentary Mn/Fe ratios in Lake Zurich, Switzerland. *Chemical Geology* 352, 125-133
- Ohta, Y., Hjelle, A., Dallmann, W.K., 2007. Geological map Svalbard 1:100 000, sheet A4G, Vasahalvøya., Temakart nr. 40. ed. Norsk Polarinstitutt
- Osmaston, H., 2005. Estimates of glacier equilibrium line altitudes by the Area× Altitude, the Area× Altitude Balance Ratio and the Area× Altitude Balance Index methods and their validation. *Quaternary International* 138, 22-31
- Perren, B.B., Anderson, N.J., Douglas, M.S., Fritz, S.C., 2012. The influence of temperature, moisture, and eolian activity on Holocene lake development in West Greenland. *Journal of Paleolimnology* 48, 223-239
- R Development Core Team, 2012. R: A language and environment for statistical computing. R Foundation for Statistical Computing. R Foundation for Statistical Computing, Vienna, Austria.
- Rea, B.R., 2009. Defining modern day Area-Altitude Balance Ratios (AABRs) and their use in glacier-climate reconstructions. *Quaternary Science Reviews* 28, 237-248. <http://dx.doi.org/10.1016/j.quascirev.2008.10.011>
- Rea, B.R., Evans, D.J., 2007. Quantifying climate and glacier mass balance in north Norway during the Younger Dryas. *Palaeogeography, Palaeoclimatology, Palaeoecology* 246, 307-330
- Reimer, P.J., Bard, E., Bayliss, A., Beck, J.W., Blackwell, P.G., Ramsey, C.B., Buck, C.E., Cheng, H., Edwards, R.L., Friedrich, M., 2013. IntCal13 and Marine13 radiocarbon age calibration curves 0–50,000 years cal BP. *Radiocarbon* 55, 1869-1887
- Renberg, I., 1990. A procedure for preparing large sets of diatom slides from sediment cores. *Journal of Paleolimnology* 4, 87-90
- Renssen, H., Goosse, H., Fichefet, T., 2002. Modeling the effect of freshwater pulses on the early Holocene climate: The influence of high-frequency climate variability. *Paleoceanography* 17, 10-11-10-16

- Rubensdotter, L., Rosqvist, G., 2009. Influence of geomorphological setting, fluvial-, glaciofluvial-and mass-movement processes on sedimentation in alpine lakes. *The Holocene* 19, 665-678
- Ryżak, M., Bieganski, A., 2011. Methodological aspects of determining soil particle-size distribution using the laser diffraction method. *Journal of Plant Nutrition and Soil Science* 174, 624-633
- Røthe, T.O., Bakke, J., Vasskog, K., Gjerde, M., D'Andrea, W.J., Bradley, R.S., 2015. Arctic Holocene glacier fluctuations reconstructed from lake sediments at Mitrahalvøya, Spitsbergen. *Quaternary Science Reviews* 109, 111-125
- Salvigsen, O., 1977. Radiocarbon datings and the extension of the Weichselian ice-sheet in Svalbard. *Norsk Polarinstitutt Årbok* 1976, 209-224
- Salvigsen, O., 1979. The last deglaciation of Svalbard. *Boreas* 8, 229-231
- Salvigsen, O., 2002. Radiocarbon-dated *Mytilus edulis* and *Modiolus modiolus* from northern Svalbard: climatic implications. *Norsk Geografisk Tidsskrift-Norwegian Journal of Geography* 56, 56-61
- Shakesby, R.A., Dawson, A.G., Matthews, J.A., 1987. Rock glaciers, protalus ramparts and related phenomena, Rondane, Norway: a continuum of large-scale talus-derived landforms. *Boreas* 16, 305-317
- Sperazza, M., Moore, J.N., Hendrix, M.S., 2004. High-resolution particle size analysis of naturally occurring very fine-grained sediment through laser diffractometry: research methods papers. *Journal of Sedimentary Research* 74, 736-743
- Stager, J., Mayewski, P., 1997. Abrupt early to mid-Holocene climatic transition registered at the equator and the poles. *Science* 276, 1834-1836
- Stoner, J., St-Onge, G., 2007. Magnetic stratigraphy in paleoceanography: reversals, excursions, paleointensity and secular variation. *Proxies in Late Cenozoic Paleoclimatology*. Elsevier, 99-137
- Swett, K., Hambrey, M.J., Johnson, D.B., 1980. Rock glaciers in northern Spitsbergen. *The Journal of Geology*, 475-482
- Thomson, J., Croudace, I., Rothwell, R., 2006. A geochemical application of the ITRAX scanner to a sediment core containing eastern Mediterranean sapropel units. *Geological Society, London, Special Publications* 267, 65-77
- Tjallingii, R., Röhl, U., Kölling, M., Bickert, T., 2007. Influence of the water content on X-ray fluorescence core-scanning measurements in soft marine sediments. *Geochemistry, Geophysics, Geosystems* 8

- van de Vijver, B., Beyens, L., Lange-Bertalot, H., 2004. The genus *Stauroneis* in the Arctic and (Sub-) Antarctic-Regions.
- van de Vijver, B., Zidarova, R., Kopalova, K., 2014. New species in the genus *Muelleria* (Bacillariophyta) from the Maritime Antarctic Region. *Fottea* 14, 77-90
- van der Bilt, W.G., Bakke, J., Vasskog, K., D'Andrea, W.J., Bradley, R.S., Ólafsdóttir, S., 2015. Reconstruction of glacier variability from lake sediments reveals dynamic Holocene climate in Svalbard. *Quaternary Science Reviews* 126, 201-218
- Werner, K., Spielhagen, R.F., Bauch, D., Hass, H.C., Kandiano, E., 2013. Atlantic Water advection versus sea-ice advances in the eastern Fram Strait during the last 9 ka: Multiproxy evidence for a two-phase Holocene. *Paleoceanography* 28, 283-295
- Wittmeier, H.E., Schaefer, J.M., Bakke, J., Rupper, S., Paasche, Ø., Schwartz, R., Finkel, R.C., Interhemispheric mountain glacier fluctuations during the Late Glacial period indicate synchronous summer temperature change, submitted to *Geology*.
- Wojtal, A.Z., Ognjanova-Rumenova, N., Wetzel, C.E., Hinz, F., Piatek, J., Kapetanovic, T., Ector, L., Buczko, K., 2014. Diversity of the genus *Genkalia* (Bacillariophyta) in boreal and mountain lakes-taxonomy, distribution and ecology. *Fottea* 14, 225-239

Paper III

Gjerde, M., Bakke, J.: Increased storminess at Andøya (Arctic Norway) during the Little Ice Age reconstructed from lake sediments. Submitted to Quaternary Research.

Increased storminess at Andøya (Arctic Norway) during the Little Ice Age reconstructed from lake sediments

Gjerde, Marthe¹ and Bakke, Jostein¹

¹ Department of Earth Science and Bjerknes Centre for Climate Research, University of Bergen, Allégaten 41, 5007 Bergen, Norway

Corresponding author: Marthe Gjerde, Department of Earth Science, University of Bergen, Allégaten 41, NO-5007 Bergen, Norway. E-mail: Marthe.gjerde@uib.no. Phone: +47 55 58 81 10.

Keywords: Lake sediments; Sediment trap; Late-Holocene; Aeolian; Storminess; Grain-size; Arctic Norway

Abstract

A novel record of storminess in Arctic Norway is reconstructed from aeolian sediment input into the coastal lake Måvatnet, Andøya island. The study site is situated at the extreme west coast of Arctic Norway; a sensitive location for changes in North Atlantic westerly winds. We have combined sediment trap monitoring with a multi-proxy lake sediment study for detecting the aeolian member deposited in the lake. The high-resolution record reveals an abrupt increase in storminess synchronously with the onset of the Little Ice Age (LIA), ca. 600 cal yr BP, coeval with increased winter precipitation in western Norway and a strengthening of the persistent low-pressure west of Iceland (Icelandic Low) that exerts a strong effect on North Atlantic storm tracks. Further, the timing of the LIA onset along the coast of Norway appears to be linked to the dynamics of the large-scale atmospheric circulation systems in the North Atlantic, and we propose that the position of the Intertropical Convergence Zone (ITCZ) holds the key to explaining LIA precipitation patterns along the coast of Norway, reflected in the strength and position of the westerlies.

Introduction

In order to disentangle relative importance between natural and anthropogenic forcing on projected climate warming (IPCC, 2013), elucidating the contribution from natural climate variability is crucial. As instrumental climate data only extends at most a couple of centuries back in time, applying natural archives for palaeoclimatic reconstructions offer the possibility to extend earth system observations beyond the instrumental time period and enable a perspective on the range of climate variability (e.g. Bradley, 2000). The northeastern (NE) North Atlantic is a key area for climate research as the dynamic nature of the prevailing atmospheric and oceanic systems found here can change in a rapid pace, both spatially and temporally, and have done so in the past (e.g. Bianchi and McCave, 1999). The Arctic Oscillation (AO) and the North Atlantic Oscillation (NAO) constitute the most prominent modes of winter climate variability in the northern hemisphere (NH) (Wanner et al., 2001), transporting atmospheric masses from the mid-latitudes to high-latitudes in the North Atlantic with a shared winter storm track between the NE North Atlantic and the Arctic (Rogers and McHugh, 2002). The AO/NAO modes are quantified by variations in the sea level pressure gradient, which is reflected in the strength and position of the westerly winds. As the storm tracks are projected to shift poleward in near-future climate (Yin, 2005), surface wind stress and precipitation (mostly during NH winter rather than summer) accompany the storm tracks, modulating *inter alia* precipitation patterns along the coast of Norway. By investigating a site with the potential to record high-resolution shifts in extreme wind activity (i.e., storminess) we opt to reconstruct the variability of the westerlies at Andøya island, Arctic Norway. A beach situated west of the lake constitutes a source area for possible aeolian-transported sediments. This setting enables us to test past westerly wind strength variability as the northwestern coastal area of Norway is situated directly in an area sensitive to changes in the NAO (Lehner et al., 2012), and consequently, the westerlies.

Typically, wind-transported (aeolian) sediments fall in the range between the finer silt fractions to very fine sand, as these grain-sizes are most readily picked up and transported by wind (e.g. Pye, 1987). The potential for reconstructing aeolian activity reflecting atmospheric circulation variability has hitherto been shown mostly in ice core dust records and in marine sediment archives (e.g. Rea, 1994; Gingele et al., 2007; Steffensen et al., 2008; De Deckker, 2014; Stuut et al., 2014). Also, peat and mire deposits where the relative fraction of wind-blown dust is distinguishable from the organic background sediment have been investigated for aeolian content (e.g. Björck and Clemmensen, 2004; de Jong et al., 2006; De Jong et al., 2007; Marx et al., 2011). Lake sediments, offering insight on past climate fluctuations on a wide range of age scales and proxies, however, are more sparsely applied as records of past aeolian activity although an increasing number of lake studies are published that include wind-driven sedimentation events (e.g. Lewis et al., 2002; An et al., 2012; Dietze et al., 2012; Krawiec and Kaufman, 2014).

Here, we present a late-Holocene lake record from Andøya in Arctic Norway, a sensitive site to changes in North Atlantic wind climate (Møller, 1995). The site is in close proximity to a west-facing beach, providing abundant source material for aeolian entrainment during (westerly) storms. By integrating monitored present-day sedimentation from sediment traps with lake sediments for palaeo-aeolian influx, our aim is to reconstruct late-Holocene storminess for Andøya. In the following we focus on: 1) Reconstructing storminess at lake Måvatnet, Andøya, based on multi-proxy analyses of lake sediments in combination with aeolian sediment fingerprinting of sediment trap content; and 2) climatic implications of our findings in relation to North Atlantic late Holocene climate. We further assess our storminess record as a proxy for variability in the North Atlantic westerlies and propose an age constraint for the onset of the Little Ice Age at Andøya.

Study area

Andøya island ('øya'=island) (69°N, 15°E) is situated in Arctic coastal Norway, and is the northernmost island of the Lofoten-Vesterålen Islands (Fig. 1). Alpine mountains characterize the islands, and the close proximity to the shelf break (~10 km) (Laberg et al., 2000) prevented vertical build-up of ice caps due to the calving effect. Because of this Andøya was early deglaciated, and constitutes lake records spanning back to immediately after the Last Glacial Maximum (c. 20 ka) (e.g. Vorren, 1978; Vorren et al., 1988; Alm and Birks, 1991; Møller et al., 1992; Alm, 1993; Vorren and Plassen, 2002; Nesje et al., 2007). However, due to palaeoclimate studies focusing mainly on deglaciation and Late Glacial ages, the Holocene history of Andøya is not constrained equally well (Vorren and Alm, 1999; Vorren et al., 2007).

Geomorphological setting

Måvatnet (6 m a.s.l, 69°12.48'N; 15°52.28'E) is a shallow (~1 m deep) lake in the outermost part of the Stavedalen valley in the northwest corner of Andøya. The lake is situated on the Norwegian strandflat; a relatively flat foreland stretching along large parts of the Norwegian coast with an origin linked to glacial erosion in conjunction with marine abrasion and sea level changes (e.g. Nansen, 1922; Holtedahl, 1998). The bedrock in the catchment area consists of Archean migmatite gneisses and Early Proterozoic gabbro intruded by granites (Henningsen and Tveten, 1998). Måvatnet is located approximately 300 m inland of the present coastline, at a distance of minimum 300 m from any cliffs framing the valley (Fig. 1). The catchment area is characterised by sandy and silty wave-reworked glacial deposits, with peat and moss deposits draped over the Stavedalen valley. Though the reworked silts and sands are present in all directions in the catchment, they are only presently exposed and

accessible for aeolian transport at the beach. West of Måvatnet three undulating terraces mark the altitude of former shorelines (at 12; 10 and 8 m a.s.l.). The beach ridge (i.e., old shoreline) impounding the lake at maximum 12 m a.s.l. and the relatively younger shoreline levels (10 and 8 m a.s.l.) are all fluvially incised by a channel of unknown age indicating previous exchange with sea water and/or possible drainage of the lake. A presently vegetated (relict) dune field west of Måvatnet and north of the channel is suggested to have been more active during the Little Ice Age, and it probably acted as a source area for aeolian sediment influx to Måvatnet (cf. Discussion below). Also, certain areas in Stavedalen valley were exposed for peat cutting in the past with the consequence that some areas of the peat have been drained. Our geomorphological mapping around Måvatnet concludes that slope processes are not affecting the lake sediments and that fluvial processes have restricted effect on the lake environment since the competence and the capacity of the small inlets meandering their way to the lake indicates that transport of large clasts into the lake is unlikely, i.e.: larger clasts are deposited before reaching the lake bed.

Climate

The climate at Andøya is strongly affected by its downwind position of the westerlies, and it is characterised by relatively warm winters despite its geographic location north of the Arctic Circle (Fig. 1A). From the meteorological station at Andenes (station no. 87110; Norwegian Meteorological Institute; NMI) the normal period (1961-1990) winter temperatures (DJF) were -1.8°C , summer temperatures (JJA) 10.2°C , and average precipitation was 1060 mm/yr with the majority of precipitation occurring during autumn/winter. Total summer precipitation (JJA) for the normal period is 205 mm. Måvatnet is almost every winter covered by snow and/or lake ice, however, due to its close proximity to sea (300 m) we expect that the lake is

not frozen solid. Wind speed distribution from the closely located Trolltinden station (station no. 87120; NMI) covering 2013-2015 (i.e., the monitoring years; comparable to the normal for Andøya St.) show that prevailing winds are from the southwest, with largest wind speeds predominantly from the west (Fig. 1C). The highest mean maximum gusts (>30 m/s) are found from October-March; highlighting the potential of severe winter-storms to facilitate (coarser-grained) sediment movement.

During the sediment-trap monitoring period (08/16/13 – 06/24/15), two ‘extreme weather’ events occurred bringing strong winds and precipitation to Andøya (NMI). On 11 March 2014, extreme weather ‘Kyrre’ brought strong winds and precipitation from the SW to northern Norway, with the highest median wind speeds measured at Andøya (Trolltinden Station) of 33.1 m/s, and strongest gust of 44.8 m/s, also at the Trolltinden Station. On 7 February 2015, extreme weather ‘Ole’ brought strong winds from WNW, with highest median winds (over 10 minutes) at 24.8 m/s (Andøya St.) and 30.5 m/s (Trolltinden St.), and wind gusts were measured at 34.4 and 49.4 m/s, respectively, corresponding to whole gale and hurricane strength (NMI).

Methods

Andøya island was formerly inundated by the sea, and the marine limit (ML) is found between 35-40 m a.s.l. (Vorren, 1978). Piston cores collected in 2007 (MÅP-107: 180 cm; MÅP-207: 222.5 cm; and MÅP-307: 177.5 cm; Supplementary Figures 1 and 2) indicate that the Tapes Transgression (Vorren and Moe, 1986) mark the last period (~6100 cal yr BP) where Måvatnet was inundated by the sea (Supplementary Table 1, Supplementary Figure 3). We cannot accurately constrain the maximum transgression level, but infer that maximum wave exposure was at least 12 m a.s.l. (cf. max. beach ridge elevation). Following the Tapes

maximum at 6100 cal yr BP, a sea level regression of ~4 m (Møller, 1986) is also recorded in a lake core from Lofoten, south of Andøya (Balascio et al., 2011) and the relative sea level has thereafter dropped until present-day level (Supplementary Figure 3). In this study, we wish to focus on the late Holocene part of the lake record and therefore extracted 3 short gravity cores using a UWITEC corer in the spring of 2013 (MAD-113: 24.5 cm; MAD-213: 25 cm; MAD-313: 35 cm), avoiding any marine influence on sedimentary properties. Further, the UWITEC coring system allowed the pristine sediment-water interface to be obtained. The uppermost 11.5 cm ($n=23$) of MAD-113 (the core extracted closest to the already ^{14}C -dated MÅP-207, Supplementary Table 1) was sampled for ^{210}Pb age profile. Unfortunately, this attempt was unsuccessful. In August 2013, three sediment traps (©Reidar Løvlie) each consisting of connected PVC tubes capped in the bottom with mooring weights attached were deployed in the lake for monitoring sediment influx (Fig. 2). The three sediment traps (ST22, ST44, and ST88) were constructed using 3 different tube lengths (22, 44 and 88 cm length, respectively). Unfortunately, two of the sediment traps (ST22 and ST88) tore off the weights by the time of collection in June 2015, so only the content of ST44 remained in the water and could be further analysed. See Figure 3 for bathymetry, coring locations of piston cores, gravity cores and location of the sediment traps. All laboratory work was conducted at EARTH LAB, Department of Earth Science, University of Bergen

Sediment traps

Sediment traps were deployed in Måvatnet for monitoring of present sedimentation. By placing the sediment traps directly below the lake level surface (Fig. 2F) we circumvented the problem of underflows/ bottom current sedimentation and disturbances such as e.g. event layers. Because only 1 of the sediment traps (ST44) survived the monitoring period, we

sampled bulk samples from the (surprisingly full) gyttja-filled tubes in ST44, where noticeable amounts of minerogenic sediment had accumulated in the lower part of the tubes. We assess that any minerogenic content in the tubes must be derived from aeolian sedimentation, and attribute the largest grain sizes in the tubes to the extreme weather events ‘Kyrre’ and ‘Ole’.

A total of $n=5$ bulk sediment samples $\sim 0.5 \text{ cm}^3$ each from ST44 (tubes 1-5) were heated with 35% hydrogen peroxide (H_2O_2) for $\sim 1-4$ hours until organic material was dissolved. The sediments were thereafter examined for grain-size distribution (GSD) analysis (averaged over 5 runs of each sample; weighted residual $<1\%$ for all samples), using the Mastersizer 3000 from Malvern Instruments Ltd. connected to the Hydroseries wet dispersion unit allowing for laser diffraction measurement of particle sizes (Ryzak and Bieganski, 2011). Grains >2 mm were picked out before each sample was decanted into the wet dispersion unit containing water with 0.05% Calgon (sodium hexametaphosphate) and analysed for grain-size by measuring the scattered laser beam on measured grains. Particle absorption index was set to 0.01; particle refractive index to 2.0, and the pump speed was 2500 rpm. 60% ultra-sonication was applied for 60 s before analysis for all samples, and each measurement was set to 25 s counting time (Sperazza et al., 2004; Ryzak and Bieganski, 2011). The Mie scattering model was applied as it offers more accurate data on smaller fractions. Each of the 5 runs was visually inspected for consistency. Nomenclature and definitions of grain-sizes used are adapted from Blott and Pye (2001).

Lake sediment records

The sediment cores were split lengthwise in the laboratory and one half of each core was stored for reference. Core surfaces were then carefully cleaned and photographed. Lithofacies

and sedimentological structures and textures were described in detail before scanning and sub-sampling was initiated.

Geochemical data and radiographic images were obtained using an ITRAX x-ray fluorescence (XRF) scanner (Croudace et al., 2006). A molybdenum (Mo) x-ray tube was used for radiographic measurements, whereas XRF analyses were performed applying a chromium (Cr) tube, with a down-core resolution of 200 μm . Power settings of 30kV and 55 mA were used with a 10 s counting time. Down-core variations in surface magnetic susceptibility (MS) were measured on the split cores at 0.5 cm resolution using a Bartington MS2E point sensor. Standard procedures for estimating weight loss-on-ignition (LOI, %), dry bulk density (DBD, g/cm^3) and water content (WC, %) were followed (Dean, 1974; Heiri et al., 2001), and MAD-113 and MAD-313 were sampled for this purpose every 0.5 cm (MAD-113: $n=48$; MAD-313: $n=70$) using a syringe for fixed volume extraction (1 cm^3). The samples were weighed and dried overnight at 105°C before being weighed again for DBD and WC. Following subsequent ignition at 550°C for one hour, the samples were cooled in a desiccator and reweighed for LOI.

MAD-313, holding the longest core length of the 3 short cores, was sampled every cm down-core (from 0-35 cm depth; $n=35$) for GSD analysis. $\sim 0.5 \text{ cm}^3$ wet samples were extracted from the core and heated with 35% hydrogen peroxide (H_2O_2) for $\sim 1-4$ hours until organic material was dissolved. The same procedure as for the sediment trap samples was thereafter followed, and the same settings were applied when running the samples in the Mastersizer 3000.

Chronology

Six samples containing terrestrial plant remains were extracted from MAD-313 and submitted for accelerator mass spectrometry (AMS) radiocarbon dating at the Poznan Radiocarbon Laboratory in Poland (Table 1). 1-cm sediment slices were extracted at selected depths and wet-sieved, after which terrestrial plant macrofossils were handpicked, dried overnight at 50°C and placed in sterilized glass vials before submission to AMS dating.

An age-depth relationship was established applying the OxCal (v. 4.2) software (Bronk Ramsey, 2008), implementing the radiocarbon calibration curve from IntCal13 (Reimer et al., 2013). The mathematical framework in OxCal is a Bayesian approach. The deposition process in Måvatnet is described as random in terms of a Poisson process where only the order of dated events is known. The P_{sequence} deposition model was therefore applied, allowing for fluctuating sediment accumulation rates which was found most likely for the sediments in the Måvatnet basin based on lithostratigraphy (see Results below). We allowed the model to determine a variable k parameter from $(-2) - 2$, and set the interpolation rate at 2.

Multivariate analysis

Principal Component Analysis (PCA) was applied in order to explore the multi-proxy dataset from MAD-313, including LOI and DBD, $n=9$ geochemical elements (Al, Si, K, Ca, Ti, Mn, Fe, Rb, Sr) obtained from the ITRAX XRF scan, and GSD data ($n=10$ grain-size intervals). To reduce the effect of the closure problem, the compositional grain-size data were log-ratio transformed before being included in the PCA (Aitchison, 1983). All of the data were then standardized before running the PCA in Canoco for Windows (v. 4.5; Lepš and Šmilauer, 2003).

Results

Sediment trap grain-size distribution

The GSD results from the sediment trap tubes 1-5 are shown in Figure 4. A bimodal distribution is observed in all tubes, with the exception of tube no. 4 (Fig. 4D) displaying a normal distribution. We attribute this anomaly to sample preparation, where incomplete decanting of the sample may have led to the finer fraction being erroneously underrepresented. 4 out of 5 of the tubes revealed a strikingly similar bimodal distribution, and we therefore argue that the main signal from the sediment trap is bimodal and from here on we discuss the sediment trap tubes no. 1, 2, 3, and 5 as representative and omit tube no. 4 from the dataset as an anomaly. This bimodal distribution is split into two populations, where the smallest population holds a mode of $\sim 12.7 \mu\text{m}$. The largest population holds a mode between $88.1\text{-}94.7 \mu\text{m}$ (Fig. 4A-F).

Lithostratigraphy

As MAD-313 holds the longest sediment record out of the three UWITEC cores, we discuss this record in detail (selected results from MAD-113 and MAD-213 are compiled in Supplementary Figure 4). Visual correlation supported by geochemical indices from XRF scanning allowed for intra-basin correlation of MAD-113, MAD-213 and MAD-313 (Supplementary Figure 5), revealing the similar detrital signal in the records. MAD-313 was divided into 4 lithostratigraphic units, A-D, based on a combination of visual, physical and geochemical properties. A compilation of selected sediment variables are shown in Figure 5 combined with optical image, radiographic image and unit division of the core as well as

depths with their corresponding ^{14}C ages indicated. Grain-size properties are shown in Figure 6.

Unit A (35-24 cm) consists of very dark brown gyttja, with silty/sandy lenses intertwined. DBD values are relatively low, averaging $\sim 0.29 \text{ g/cm}^3$, whereas LOI averages $\sim 14.5\%$. X-radiographic image reveals layers of varying density throughout the unit. Detrital parameters such as Ti and Si (XRF count rates) show low variability throughout the unit. The grain size distribution mode is relatively fine-grained (Fig. 5), with most of the sediment from very coarse silt up to medium sand (Fig. 6).

Unit B (24-20 cm) consists of dark greyish brown gyttja silt and sand, and the unit appears massive. Unit B obviously differs from the underlying unit, with higher DBD (on average $\sim 0.60 \text{ g/cm}^3$) and lower LOI (averaging $\sim 5.1\%$). The transition between Unit A and Unit B appears erosive. Geochemical detrital parameters such as Ti, Si, Ca and K XRF count rates all increase (Fig. 5). GSD mode shows a peak in Unit B, with most ($>53\%$) of the sediment situated within very fine and fine sand. The massive nature of the unit and the properties discussed indicate that this layer is likely deposited instantaneously, i.e. an ‘event’ layer and it is therefore omitted during age-depth modelling.

Unit C (20-11 cm) consists of very dark brown gyttja with small silty/sandy lenses interlayered. LOI increases to the highest values in the core (up to $>35\%$), averaging $\sim 22.9\%$. DBD drops to an average of $\sim 0.25 \text{ g/cm}^3$. The detrital geochemical parameters (e.g. Si, K) decrease. The X-radiographic image shows lighter density of the unit compared to Unit B. Grain-sizes show a shift to finer distribution than below (Fig. 6).

Unit D (11-0 cm) consists of very dark greyish brown gyttja silt, with frequent silty/sandy layers detected in the alternating lighter and darker colours of the X-radiographic image in Figure 5. A small twig ($\sim 3 \text{ cm}$ length) was found at 9-10.5 cm depth. LOI averages

~9.8% and DBD ~0.47 g/cm³. The unit is characterized by large fluctuations in detrital parameters (e.g. DBD, Ti, Si), and possibly represents a shift in depositional environment to more frequent detrital sedimentary input and/or more variable internal lake productivity (reflected in LOI). The grain-size mode holds the largest values throughout the core.

Statistics

Principal component analysis returned one significant axis (PC axis 1) capturing ~55% of the variance in the dataset. PC axis 1 captures the balance between fine-grained and coarse-grained sediments and between LOI and DBD. Several of the geochemical elements show high scores along PC axis 1, such as Si (0.87) and K (0.93) (Supplementary Table 2), and it is therefore possible to apply these elements as high-resolution proxies of changes in grain-size. While the individual GSD classes above medium sand shows a somewhat more erratic behaviour (Supplementary Figure 6), the total volume % of sand and sediment >125 µm correlates well with both Si and K (Supplementary Figure 7), suggesting that these elements may reflect influx of coarse-grained sediments to the lake.

Chronology

The resulting age-depth relationship produced in OxCal (Bronk Ramsey, 2008) for MAD-313 (Table 1) is shown in Figure 7. Figure 7A shows the original output from OxCal including full core length in the age model. Radiocarbon ages directly above and below Unit B (Poz-74067 and Poz-74068; Table 1) indicate that the unit (which is detected in all three short cores; cf. Supplementary Figures 4 and 5) represents a relatively long time period. The erosive lower boundary and the massive change in lithological parameters indicate that this

unit represents an event layer (marked with red ellipse in Fig. 7A). Subsequently, we omitted the unit when constructing the final age-depth relationship but retained the radiocarbon ages extracted directly above and below Unit B (Fig. 7B) and denoted the boundary at 20 cm (colour change), and subsequently attributed new depths for the radiocarbon ages below this point when running the model.

Discussion

The main object of this study was to identify aeolian sediments transported by extreme winds into lake Måvatnet. Our approach has been to investigate aeolian sediments collected in sediment traps deployed in the lake and compare the content of the sediment traps with the sediments deposited in the lake. Below, we assess the validity of our methodological approach and implications of our findings, and further discuss our results in a palaeoclimatic context.

Chronology

Arguably, the most critical part of establishing proxy records of past climate is the interpretation of age-depth relationships. Unfortunately, the attempt on establishing a ^{210}Pb profile from the upper section of MAD-113 was unsuccessful, and we could therefore not relate modern-day sediment accumulation to instrumental meteorological data. Instantaneously deposited layers are important to exclude from age-depth modelling since they may yield erroneous ages as well as perturbing accumulation rates (e.g. Rubensdotter and Rosqvist, 2009). Based on the radiocarbon ages directly above and below Unit B and the lithostratigraphical properties, we consider the sandy, massive sediment as deposited over a relatively short period of time and the erosional lower boundary support our interpretation of

Unit B as an event layer with a hiatus below. Precipitation-induced flooding in the catchment would likely not transport large grain-sizes into the lake because the lake level would rise slowly and the small streams and inlets would not increase their competence as the flat valley bed implies that larger (eroding) rivers could never form and the energy in the system would thus be too low to affect the lake bed. During time of erosion and subsequent deposition of Unit B (~1800-900 cal yr BP), the sea level was approximately 2 m higher than present (Supplementary Figure 3), and if highest astronomical tide was similar to present (~2.5 m) (Tidevannstabeller, 2014), this implies that sea inundation during a storm surge event concurrent with extremely low pressure and higher sea level could reach substantially higher levels than mean sea level. The relict channel west of Måvatnet incising the old shoreline levels may have been inundated and/or eroded by the former higher sea level and this could have disturbed the lake bed. We propose that such an extreme event led sea water into Måvatnet via the channel sometime around 900 cal yr BP (top age of Unit B). As the unit holds an anomalous sedimentary signature (Fig. 5) present in all three short cores (Supplementary Figure 5), we attribute that the most likely explanation based on the discussion above is therefore that an extreme storm surge event eroded into the Måvatnet basin and subsequently deposited a sandy mass. In the other units of the core(s), the fluctuations detected in the sediment parameters reveal inferred similar boundary conditions prevailing during sediment accumulation, and we therefore assess that units A, C and D are representative of lake sedimentation and further discuss these units in a palaeoclimatic context.

Utilizing sediment traps to assess wind activity

In order to identify the sedimentary signature of the wind-transported material we equipped lake Måvatnet with three sediment traps. Because two of the sediment traps were expelled from the lake at some point during the monitoring period, we cannot assess differences in sediment influx at different sites in the lake. But, we argue that the placement of ST44 directly below the lake surface in order to avoid disturbances in sediment accumulation by potential bottom currents/suspended sediments and other processes except wind transport allows for an assessment of aeolian sediment influx to Måvatnet. The most probable source of the fine-grained component into the sediment traps (as well as background sedimentation in the lake sediments) is atmospheric transport of finer silt-sized sediment (i.e., dust) that can be transported both over shorter and longer distances in the atmosphere. Large grains could be transported into the sediment trap by lake ice entrainment of grains from the lake shore and subsequent deposition in the sediment trap after thawing could lead to erroneous inferences. However, if this is an important process in the lake we would expect coarser sand and gravel with the same properties as present day shoreline around lake Måvatnet to be represented in the sediment trap without any sorting (cf. similar GSD in Fig. 4). Because of the finite width of the beach (i.e., the source area), the wind direction is an important factor in aeolian transport to Måvatnet (e.g. Arens, 1996). As the strongest winds are mainly from the west (Fig. 1), the lake is downwind of the source area when the strongest winds prevail. As there were two major extreme weather events occurring during monitoring, we attribute the largest grain-sizes in the sediment trap to these two events. Though we cannot directly quantify the aeolian sediment transport during these two extreme events, they highlight the potential of strong winds to entrain and deposit large grain-sizes at the study site; in particular during winter storms which facilitate larger grain sizes by niveo-aeolian transport as the snow cover

smooths the otherwise irregular surfaces (e.g. Björck and Clemmensen, 2004; de Jong et al., 2006).

From the discussion above, we acknowledge that there exists potential sources of error that might complicate the identification of the aeolian sediment content from the sediment traps, however, we suggest that the majority of the sediment tubes (4 out of 5) do reflect aeolian sediment accumulation (in addition to internal lake productivity) and hence underscore the potential for using sediment trap monitoring in order to record wind-transported material at Andøya.

Extracting an aeolian sediment signal from lake sediments

Lakes act as sediment traps for all type of sediments delivered from various earth surface processes and it is important to be aware of potential sources of error when interpreting sediment properties in a climatic context. Impact of human activity around lake Måvatnet is visible as the locals have drained and cut peat for heating as well as cattle grazing. However, these factors have the potential to mainly influence the organic productivity in and around the lake and to less extent affect the inorganic sedimentation. We therefore rule out human impact as important for the boundary conditions for lake Måvatnet.

Historical sources from the Stave farm including Måvatnet assess more impact of aeolian sand flux and frost at least during the 1800's (source: Andøy Historielag). The presently vegetated (i.e., relict) dune field west of Måvatnet is inferred to have been more active during the LIA, and we tentatively suggest that this was an important source area for sand influx to Måvatnet during the LIA with active dune migration. Further, the colder conditions during the LIA could serve to facilitate increased niveo-aeolian transport of larger grain sizes. Niveo-aeolian processes are established as the main transport mode for grains $>125/200 \mu\text{m}$ to be deposited

in ombrotrophic bogs in SW Sweden (Björck and Clemmensen, 2004; de Jong et al., 2006; De Jong et al., 2007). In these studies, where the aeolian fraction is considered relatively easily distinguishable, the large grains are assumed to reflect winter season signal.

Based on the bimodal distribution of grain-sizes in the sediment trap, it was desirable to test if the two modes reflected an aeolian sediment signal in the lake sediments that could serve as an aeolian proxy. However, when examining all the grain-size intervals (clay-gravel; n=12 intervals) (Supplementary Figure 6), it is apparent that clay and silt-sized sediment intervals all show the same variability, co-varying with the smallest mode extracted from the sediment trap GSD (12.7 μm) probably reflecting atmospheric dust deposition into lake Måvatnet. The medium silt-sized aeolian sediment from the sediment trap is thus difficult to separate from background silt-sized (dust) sedimentation in Måvatnet, and we therefore investigated whether the larger mode (centred around 90 μm) (Supplementary Figure 6) could be used to represent the aeolian component in the Måvatnet sediment record. This mode seems to smooth out the fluctuating signal in the core in this 'transitional' grain-size (Supplementary Figure 6). Thus, we apply the previously established aeolian sediment influx grain-size >125 μm (Björck and Clemmensen, 2004; de Jong et al., 2006; De Jong et al., 2007; De Jong et al., 2009) as a proxy for aeolian sediment influx to Måvatnet. Although we interpret the fraction >125 μm to represent aeolian influx, aeolian sediments are likely also present as finer-grained material (cf. Fig. 4), however, these sediments can be indistinguishable from the matrix sediment (e.g. Lamoureux and Gilbert, 2004). We therefore assess that the fine-grained component likely represents continuous background sedimentation originating from atmospheric dust deposition. The fine-grained component may also originate from weathered clay and silt-sized grains produced by blockfield weathering (Paasche et al., 2006), however, it is difficult to explain the abundance of fine-grained material with the slow rates of weathering and transport of the weathered material.

Thus, we assess that the coarse-grained component ($>125\ \mu\text{m}$ and sand fraction) represents the extreme wind sediment component, i.e. storminess. As the XRF and DBD results are of higher time resolution than the GSD, we opted to test if it was possible to use elemental XRF count rates reflecting inorganic sedimentation (e.g. Kylander et al., 2011; Davies et al., 2015) as a proxy for the fraction $>125\mu\text{m}$ and the sand fraction. From the PCA results (Supplementary Table 2) and correlation of selected parameters indicative of detrital input (Supplementary Figure 7), we assess that there is a close relationship and co-variance between both K and Si with the physical detrital parameter DBD, as well as a medium-good relationship with grains $>125\ \mu\text{m}$ and the sand fraction. Thus, we tentatively apply the higher-resolution Si and K count rates as proxies for aeolian sediment influx (i.e., storminess) to Måvatnet.

Måvatnet storminess record in a climatic context

Our record suggests a significant shift of increased storminess from around 600 cal yr BP until present, with more rapid and larger-amplitude fluctuations than seen in the first part of the Måvatnet record. Interestingly, this shift in storminess occurs around the onset of the LIA (from ~ 600 -100 cal yr BP), and the palaeoclimatic implications of this are discussed below.

In Figure 8, we compare our storminess record with different proxy records tracking shifts in major atmospheric circulation systems. Comparing the Måvatnet record with a reconstruction of the Icelandic Low from a compilation of Greenland ice core records (Meeker and Mayewski, 2002) (Fig. 8F), the onset of the LIA at Andøya ~ 600 cal yr BP occurs simultaneously as a deepening (strengthening) of the Icelandic Low. This could explain increased westerlies reaching Måvatnet by a strengthened south-north pressure gradient, thereby forcing increased meridional (westerly) wind strength. Further, reconstructed winter

precipitation at the west coast of Norway (Gjerde et al., 2016) shows a similar pattern with a relatively abrupt onset of larger fluctuations and more precipitation during the onset of the LIA (Fig. 8E). In SW Sweden, reconstructions of storminess from aeolian sediment influx into peat bogs in Sweden; the Boarps Mosse (Björck and Clemmensen, 2004) and the Store Mosse (de Jong et al., 2006; De Jong et al., 2007) (Fig. 8D and 8C, respectively), also indicate an increase in storminess during the LIA; however, in this region the relative importance of the westerlies on storm climate remains unclear. Marine sediments from the Cariaco Basin (Haug et al., 2001) indicate a southward migration of the Intertropical Convergence Zone (ITCZ) during the Holocene as reflected in lower titanium content from less riverine terrigenous input (Haug et al., 2001) (Fig. 8B). This southward displacement of the ITCZ is detected in several other records, including a lake record from Lake Edward, central equatorial Africa (Russell and Johnson, 2007) (Fig. 8A), where the magnesium content in calcite is a proxy for drought periods. A shared feature in all of the records discussed above reflecting atmospheric circulation patterns is that a major shift started ~600 cal yr BP (AD 1350) and terminated ~400 years later, at ~100 cal yr BP (AD 1850). This interpretation is based on a qualitative evaluation of the presented data.

Compiling all of the above-discussed proxy series enable us to assess inferences on larger-scale atmospheric circulation patterns, and, in particular, to focus on the position of the westerlies and the relationship between storminess and precipitation. We suggest that the LIA represents a period of large reconfiguration of atmospheric circulation patterns, where the southward migration of the ITCZ is linked to an increased strength of the westerlies in northeastern North Atlantic. Finally, we posit that this time interval (600-100 cal yr BP/AD 1350-1850) delimits the LIA climate anomaly at our site at Andøya based on our novel storminess record from Måvatnet.

Conclusions

- We have reconstructed a novel storminess record from Andøya, Arctic Norway, employing a methodological approach combining sediment trap monitoring with multi-proxy analyses of lake sediments
- By detecting the aeolian component, we are able to construct a proxy record reflecting wind-transported material into lake Måvatnet
- We have compared our storminess record with other records reflecting atmospheric variability in the North Atlantic as well as records reflecting the position of ITCZ
- The onset of the Little Ice Age in Måvatnet is remarkably similar to other records from the North Atlantic as well as other records in equatorial Africa and offshore Venezuela, and we propose that the position of the ITCZ holds the key to explaining LIA precipitation patterns along the coast of Norway, reflected in the strength and position of the westerlies as a source of moisture

Acknowledgements

Atle Nesje is thanked for commenting the manuscript, and Anne Hormes provided helpful comments on an earlier draft. Kristian Vasskog performed principal component analysis. Field work conducted over three seasons was assisted by: Tom Thorsen, Bjørn C. Kvisvik, Lisa Larsen, Kjersti Moe, Trygve Snøtun, Svein Olaf Dahl, and Willem van der Bilt. Late Prof. Reidar Løvlie designed the sediment traps, and supervised magnetic analyses. Jozef Kusior helped constructing the sediment traps. Jo Brendryen assisted with settings in OxCal, and Eivind W. N. Støren is thanked for assistance with appropriate Mastersizer settings.

Micha Dietze is thanked for providing codes for EMMAgeo. Svante Björck is thanked for sharing ASI data from bogs in Sweden.

References

- Aitchison, J., 1983. Principal component analysis of compositional data. *Biometrika* 70, 57-65
- Alm, T., 1993. Øvre Æråsvatn-palynostratigraphy of a 22,000 to 10,000 BP lacustrine record on Andøya, northern Norway. *Boreas* 22, 171-188
- Alm, T., Birks, H.H., 1991. Late Weichselian flora and vegetation of Andøya, Northern Norway-macrofossil (seed and fruit) evidence from Nedre Æråsvatn. *Nordic Journal of Botany* 11, 465-476
- An, Z., Colman, S.M., Zhou, W., Li, X., Brown, E.T., Jull, A.T., Cai, Y., Huang, Y., Lu, X., Chang, H., 2012. Interplay between the Westerlies and Asian monsoon recorded in Lake Qinghai sediments since 32 ka. *Scientific reports* 2
- Arens, S., 1996. Rates of aeolian transport on a beach in a temperate humid climate. *Geomorphology* 17, 3-18
- Balascio, N.L., Zhang, Z., Bradley, R.S., Perren, B., Dahl, S.O., Bakke, J., 2011. A multi-proxy approach to assessing isolation basin stratigraphy from the Lofoten Islands, Norway. *Quaternary Research* 75, 288-300
- Bianchi, G.G., McCave, I.N., 1999. Holocene periodicity in North Atlantic climate and deep-ocean flow south of Iceland. *Nature* 397, 515-517
- Björck, S., Clemmensen, L.B., 2004. Aeolian sediment in raised bog deposits, Halland, SW Sweden: a new proxy record of Holocene winter storminess variation in southern Scandinavia? *The Holocene* 14, 677-688
- Blott, S.J., Pye, K., 2001. GRADISTAT: a grain size distribution and statistics package for the analysis of unconsolidated sediments. *Earth surface processes and Landforms* 26, 1237-1248
- Bradley, R.S., 2000. Past global changes and their significance for the future. *Quaternary Science Reviews* 19, 391-402
- Bronk Ramsey, C., 2008. Deposition models for chronological records. *Quaternary Science Reviews* 27, 42-60
- Croudace, I.W., Rindby, A., Rothwell, R.G., 2006. ITRAX: description and evaluation of a new multi-function X-ray core scanner. *Special Publication - Geological Society Of London* 267, 51
- Davies, S.J., Lamb, H.F., Roberts, S.J., 2015. Micro-XRF Core Scanning in Palaeolimnology: Recent Developments, *Micro-XRF Studies of Sediment Cores*. Springer, pp. 189-226.
- De Deckker, P., 2014. Fingerprinting aeolian dust in marine sediment: examples from Australia. *Past global changes magazine (PAGES)* 22, 80-81
- de Jong, R., Björck, S., Björkman, L., Clemmensen, L.B., 2006. Storminess variation during the last 6500 years as reconstructed from an ombrotrophic peat bog in Halland, southwest Sweden. *Journal of Quaternary Science* 21, 905

- De Jong, R., Hammarlund, D., Nesje, A., 2009. Late Holocene effective precipitation variations in the maritime regions of south-west Scandinavia. *Quaternary Science Reviews* 28, 54-64
- De Jong, R., Schoning, K., Björck, S., 2007. Increased aeolian activity during humidity shifts as recorded in a raised bog in south-west Sweden during the past 1700 years. *Climate of the Past* 3, 411-422
- Dean, W.E., 1974. Determination of carbonate and organic matter in calcareous sediments and sedimentary rocks by loss on ignition: comparison with other methods. *Journal of Sedimentary Research* 44
- Dietze, E., Hartmann, K., Diekmann, B., Ijmker, J., Lehmkuhl, F., Opitz, S., Stauch, G., Wünnemann, B., Borchers, A., 2012. An end-member algorithm for deciphering modern detrital processes from lake sediments of Lake Donggi Cona, NE Tibetan Plateau, China. *Sedimentary Geology* 243, 169-180
- Dietze, M., Dietze, E., 2013. EMMAgeo: End-member modelling algorithm and supporting functions for grain-size analysis, R package version 0.9. 0.
- Gingele, F., De Deckker, P., Norman, M., 2007. Late Pleistocene and Holocene climate of SE Australia reconstructed from dust and river loads deposited offshore the River Murray Mouth. *Earth and Planetary Science Letters* 255, 257-272
- Gjerde, M., Bakke, J., Vasskog, K., Nesje, A., Hormes, A., 2016. Holocene glacier variability and Neoglacial hydroclimate at Ålfotbreen, western Norway. *Quaternary Science Reviews* 133, 28-47. <http://dx.doi.org/10.1016/j.quascirev.2015.12.004>
- Haug, G.H., Hughen, K.A., Sigman, D.M., Peterson, L.C., Röhl, U., 2001. Southward migration of the intertropical convergence zone through the Holocene. *Science* 293, 1304-1308
- Heiri, O., Lotter, A.F., Lemcke, G., 2001. Loss on ignition as a method for estimating organic and carbonate content in sediments: reproducibility and comparability of results. *Journal of Paleolimnology* 25, 101-110
- Henningsen, T., Tveten, E., 1998. Geologisk kart over Norge. Berggrunnskart ANDØYA, M 1:250 000. Norges Geologiske Undersøkelse.
- Holtedahl, H., 1998. The Norwegian strandflat-a geomorphological puzzle. *Norsk geologisk tidsskrift* 78, 47-66
- IPCC, 2013. *Climate Change 2013: The Physical Science Basis*. Contribution of Working Group I to the Fifth Assessment Report of the Intergovernmental Panel on Climate Change, In: Stocker, T., Qin, D., Plattner, G., Tignor, M., Allen, S., Boschung, J., Nauels, A., Xia, Y., Bex, V., Midgley, P. (Eds.). Cambridge Univ Press, Cambridge, United Kingdom and New York, NY, USA, p. 1555.
- Krawiec, A.C., Kaufman, D.S., 2014. Holocene storminess inferred from sediments of two lakes on Adak Island, Alaska. *Quaternary Research*
- Kylander, M.E., Ampel, L., Wohlfarth, B., Veres, D., 2011. High-resolution X-ray fluorescence core scanning analysis of Les Echets (France) sedimentary sequence: new insights from chemical proxies. *Journal of Quaternary Science* 26, 109-117

- Laberg, J.S., Vorren, T.O., Dowdeswell, J.A., Kenyon, N.H., Taylor, J., 2000. The Andøya Slide and the Andøya Canyon, north-eastern Norwegian–Greenland Sea. *Marine Geology* 162, 259-275. [http://dx.doi.org/10.1016/S0025-3227\(99\)00087-0](http://dx.doi.org/10.1016/S0025-3227(99)00087-0)
- Lamoureux, S.F., Gilbert, R., 2004. Physical and chemical properties and proxies of high latitude lake sediments, Long-term Environmental Change in Arctic and Antarctic Lakes. Springer, pp. 53-87.
- Lehner, F., Raible, C.C., Stocker, T.F., 2012. Testing the robustness of a precipitation proxy-based North Atlantic Oscillation reconstruction. *Quaternary Science Reviews* 45, 85-94
- Lepš, J., Šmilauer, P., 2003. *Multivariate Analysis of Ecological Data using CANOCO*. Cambridge University Press, Cambridge.
- Lewis, T., Gilbert, R., Lamoureux, S.F., 2002. Spatial and temporal changes in sedimentary processes at proglacial Bear Lake, Devon Island, Nunavut, Canada. *Arctic, Antarctic, and Alpine Research*, 119-129
- Marx, S.K., Kamber, B.S., McGowan, H.A., Denholm, J., 2011. Holocene dust deposition rates in Australia's Murray-Darling Basin record the interplay between aridity and the position of the mid-latitude westerlies. *Quaternary Science Reviews* 30, 3290-3305
- Meeker, L.D., Mayewski, P.A., 2002. A 1400-year high-resolution record of atmospheric circulation over the North Atlantic and Asia. *The Holocene* 12, 257-266
- Møller, J.J., 1986. Holocene transgression maximum about 6000 years BP at Ramså, Vesterålen, North Norway.
- Møller, J.J., 1995. Sandy beaches as records of changes in relative sea level and storm frequency. *Journal of Coastal Research*, 169-172
- Møller, J.J., Danielsen, T.K., Fjalstad, A., 1992. Late Weichselian glacial maximum on Andøya, north Norway. *Boreas* 21, 1-13
- Nansen, F., 1922. The strandflat and isostasy. I kommission hos J. Dybwad.
- Nesje, A., Dahl, S.O., Linge, H., Ballantyne, C.K., Mccarroll, D., Brook, E.J., Raisbeck, G.M., Yiou, F., 2007. The surface geometry of the Last Glacial Maximum ice sheet in the Andøya-Skånland region, northern Norway, constrained by surface exposure dating and clay mineralogy. *Boreas* 36, 227-239
- Paasche, Ø., Strømsøe, J.R., Dahl, S.O., Linge, H., 2006. Weathering characteristics of arctic islands in northern Norway. *Geomorphology* 82, 430-452
- Pye, K., 1987. *Aeolian dust and dust deposits*. Elsevier.
- R Development Core Team, 2012. *R: A language and environment for statistical computing*. R Foundation for Statistical Computing. R Foundation for Statistical Computing, Vienna, Austria.
- Rea, D.K., 1994. The paleoclimatic record provided by eolian deposition in the deep sea: The geologic history of wind. *Reviews of Geophysics* 32, 159-196

- Reimer, P.J., Bard, E., Bayliss, A., Beck, J.W., Blackwell, P.G., Ramsey, C.B., Buck, C.E., Cheng, H., Edwards, R.L., Friedrich, M., 2013. IntCal13 and Marine13 radiocarbon age calibration curves 0–50,000 years cal BP. *Radiocarbon* 55, 1869-1887
- Rogers, J., McHugh, M., 2002. On the separability of the North Atlantic oscillation and Arctic oscillation. *Climate Dynamics* 19, 599-608
- Rubensdotter, L., Rosqvist, G., 2009. Influence of geomorphological setting, fluvial-, glaciofluvial- and mass-movement processes on sedimentation in alpine lakes. *The Holocene* 19, 665-678
- Russell, J., Johnson, T., 2007. Little Ice Age drought in equatorial Africa: intertropical convergence zone migrations and El Niño–Southern Oscillation variability. *Geology* 35, 21-24
- Ryzak, M., Bieganski, A., 2011. Methodological aspects of determining soil particle-size distribution using the laser diffraction method. *Journal of Plant Nutrition and Soil Science* 174, 624-633
- Sperazza, M., Moore, J.N., Hendrix, M.S., 2004. High-resolution particle size analysis of naturally occurring very fine-grained sediment through laser diffractometry: research methods papers. *Journal of Sedimentary Research* 74, 736-743
- Steffensen, J.P., Andersen, K.K., Bigler, M., Clausen, H.B., Dahl-Jensen, D., Fischer, H., Goto-Azuma, K., Hansson, M., Johnsen, S.J., Jouzel, J., 2008. High-resolution Greenland ice core data show abrupt climate change happens in few years. *Science* 321, 680-684
- Stuut, J.-B.W., Temmesfeld, F., De Deckker, P., 2014. A 550 ka record of aeolian activity near North West Cape, Australia: inferences from grain-size distributions and bulk chemistry of SE Indian Ocean deep-sea sediments. *Quaternary Science Reviews* 83, 83-94
- Tidevannstabeller, 2014. Tidevannstabeller for den norske kyst med Svalbard samt Dover, England
2015. Sjøkartverket, Statens kartverk.
- Vorren, K., Moe, D., 1986. The early Holocene climate and sea-level changes in Lofoten and Vesterålen, North Norway. *Norsk geologisk tidsskrift* 66, 135-143
- Vorren, K.D., 1978. Late and middle Weichselian stratigraphy of Andøya, north Norway. *Boreas* 7, 19-38
- Vorren, K.D., Alm, T., 1999. Late Weichselian and Holocene environments of lake Endletvatn, Andøya, northern Norway: as evidenced primarily by chemostratigraphical data. *Boreas* 28, 505-520
- Vorren, K.D., Blaauw, M., Wastegård, S., Plicht, J.v.d., Jensen, C., 2007. High-resolution stratigraphy of the northernmost concentric raised bog in Europe: Sellevollmyra, Andøya, northern Norway. *Boreas* 36, 253-277
- Vorren, T.O., Plassen, L., 2002. Deglaciation and palaeoclimate of the Andfjord-Vågsfjord area, North Norway. *Boreas* 31, 97-125
- Vorren, T.O., Vorren, K.D., Alm, T., Gulliksen, S., Løvlie, R., 1988. The last deglaciation (20,000 to 11,000 BP) on Andøya, Northern Norway. *Boreas* 17, 41-77

Wanner, H., Brönnimann, S., Casty, C., Gyalistras, D., Luterbacher, J., Schmutz, C., Stephenson, D.B., Xoplaki, E., 2001. North Atlantic Oscillation—concepts and studies. *Surveys in geophysics* 22, 321-381

Yin, J.H., 2005. A consistent poleward shift of the storm tracks in simulations of 21st century climate. *Geophysical Research Letters* 32

Table 1: Radiocarbon ages from MAD-313, calibrated in OxCal (using the IntCal13 calibration curve).

Lab. no.	Depth (cm)	Material	¹⁴ C age	Error (+/-)	δ ¹³ C ‰	2 sigma cal yr BP	Note
Poz-74065	0.5-1.5	Terrestrial plant remains	75	30	-37.6	25-260	0.3 mgC
Poz-74066	9.5-10.5	Terrestrial plant remains	445	30	-26	464-534	
Poz-74067	19.5-20.5	Terrestrial plant remains	940	40	-26.1	766-931	
Poz-74068	23.5-24.5	Terrestrial plant remains	1855	30	-19.7	1716-1868	
Poz-74069	29.5-30.5	Terrestrial plant remains	2320	30	-29.4	1622-3140	
Poz-74070	34-35	Terrestrial plant remains	2495	30	-36.1	2466-2732	

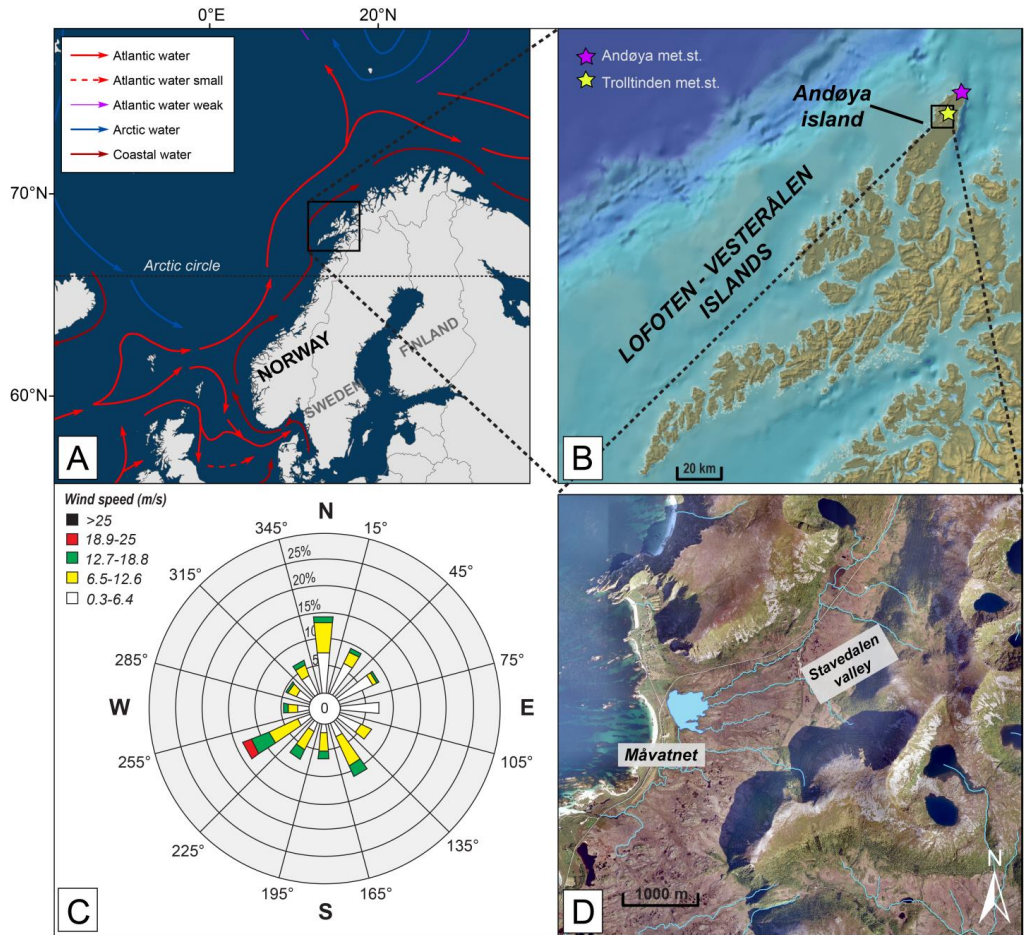


Figure 1: A) Study site in the North Atlantic. B) Zoom-in on the study site in the northernmost part of the Lofoten-Vesterålen islands. Climate stations mentioned in the text highlighted in asterisks. C) Frequency distribution (%) of wind speed at Trolltinden climate station (over the sediment trap monitoring years 2013-2015). D) Orthophoto of study site, water lines highlighted in blue. Base maps: Norwegian Mapping Authority. Ocean currents: Institute of Marine Research, Bergen, Norway. Meteorological data: NMI.

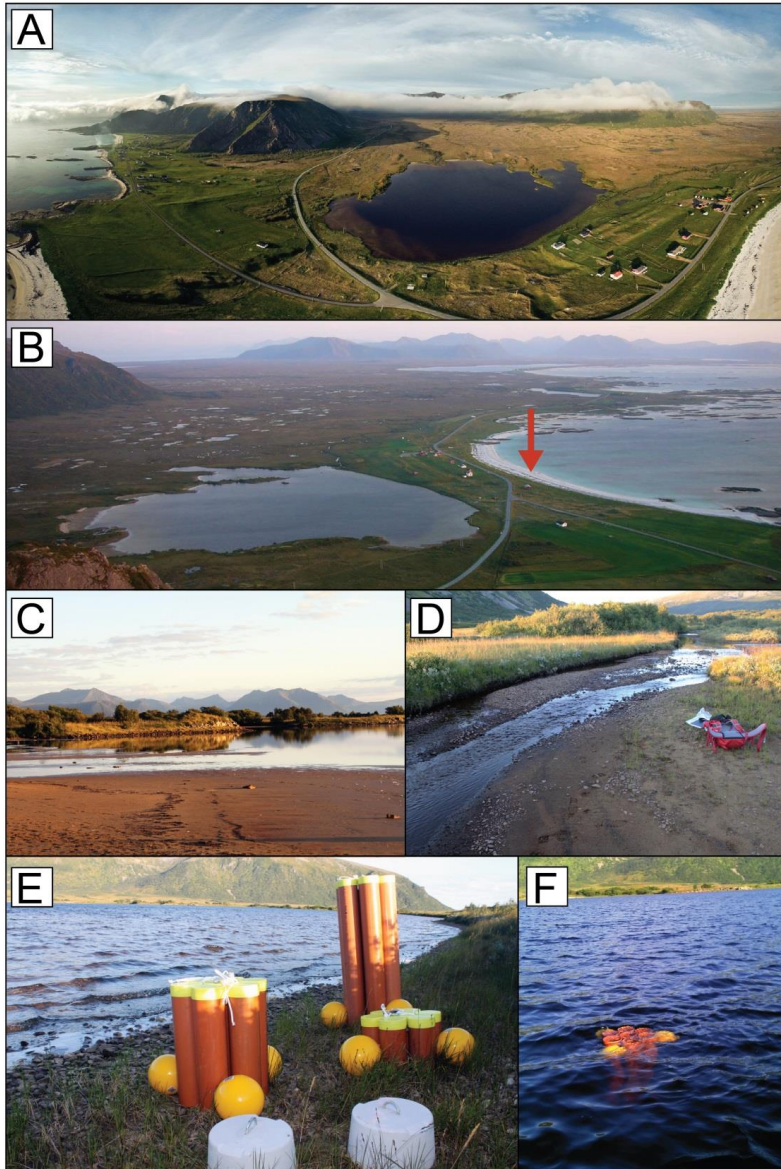


Figure 2: A) Fish-eye view of the catchment area looking northeast, into Stavedalen valley (Photo: Roy Samuelson). B) Panoramic view of study site, looking southwest. Note beach sediment source area west (right) of the lake indicated with a red arrow. C) Flat bed surrounding the east side of Lake Måvatnet, looking south. D) Inlet to Måvatnet. E) Sediment traps mounted (upside down with yellow bottom caps up) before deployment, mooring weights in the front. F) Sediment trap deployed in the lake, bordering the lake water surface.

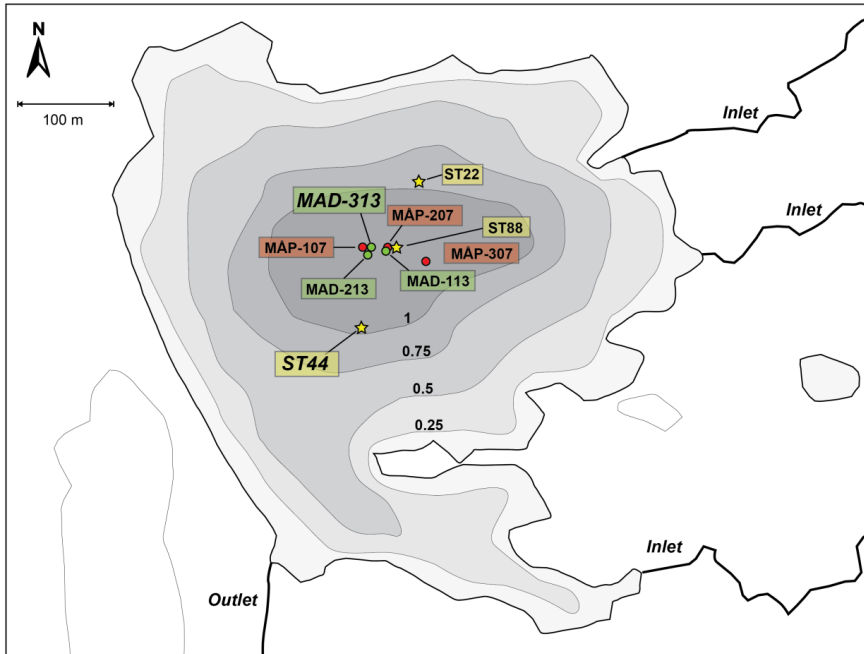


Figure 3: Bathymetry of Måvatnet with coring sites and sediment trap deployment sites labelled and colour-coded. Green circles: short ‘MAD’ cores. Red circles: longer piston ‘MÅP’ cores. ‘ST’: Sediment traps (yellow asterisks).

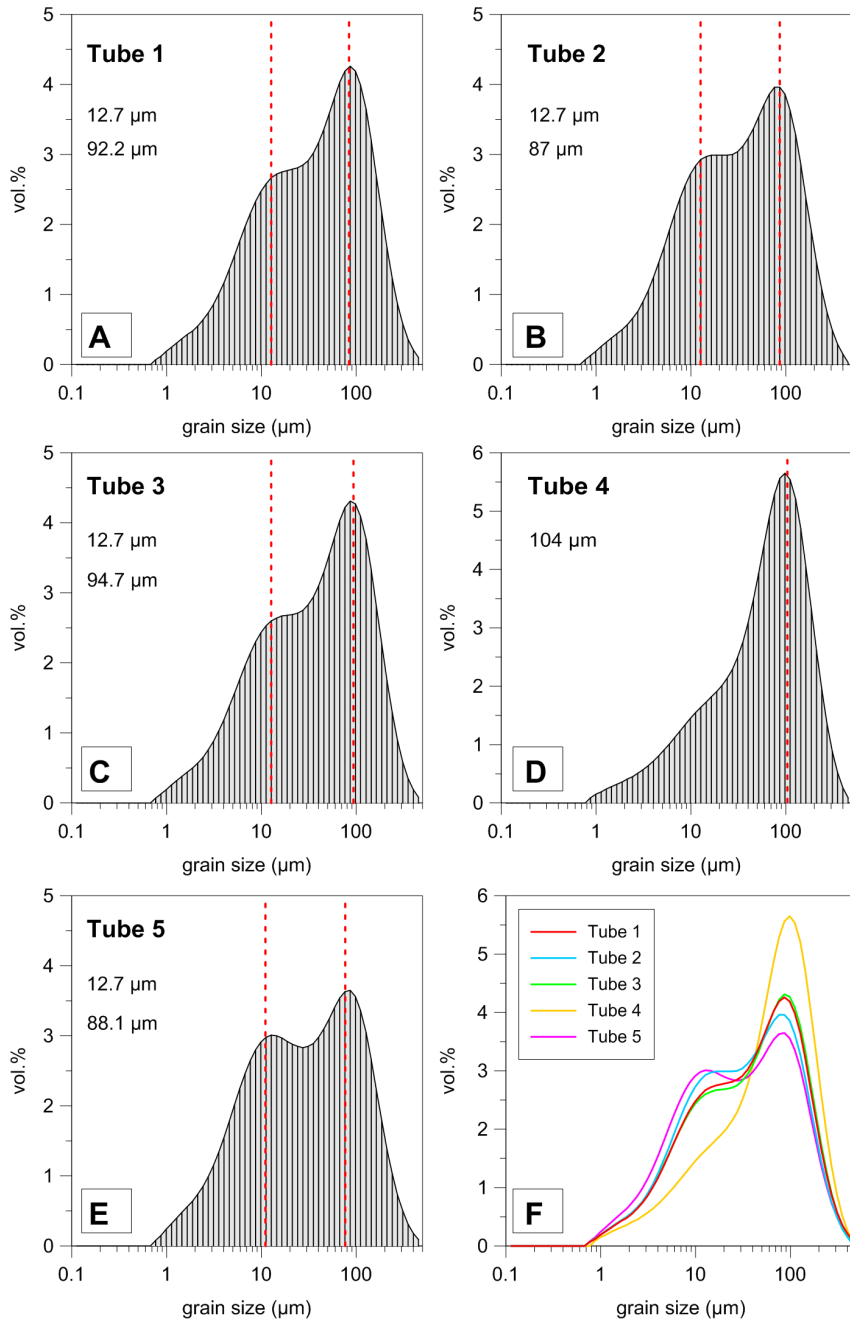


Figure 4: GSD results from sediment trap samples, labelled Tube no. 1-5 (A-E). Red dashed lines indicate modes. F) All distributions plotted. A bimodal distribution is observed in all tube samples, with the exception of tube no. 4 (normal distribution). Note different y-axis scale in D) and F).

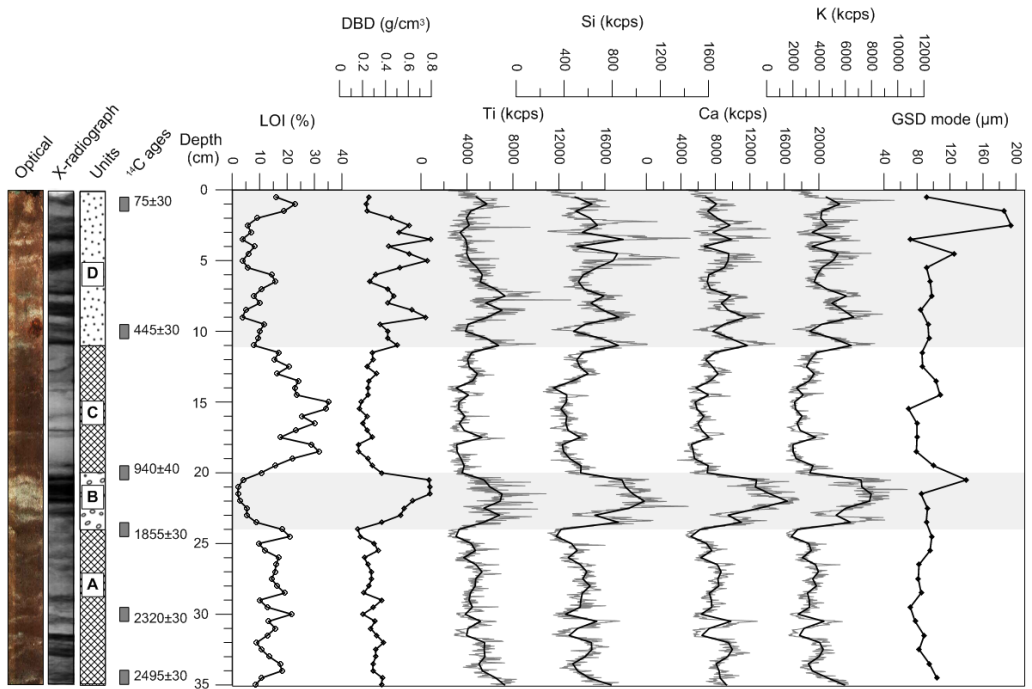


Figure 5: Selected sediment variables from MAD-313. Optical image and X-radiographic image shows sediment colour and density variations. Lithological log shows unit division, and units are also indicated in light grey horizontal bars. XRF results are shown in count rates, and are smoothed to 0.5 cm resolution (200µm increments shown as light grey). GSD mode (µm) is shown to the right. Visually, the minerogenic layers are easily distinguishable and correlate with DBD and peaks in geochemical detrital elements (e.g. Ti, Si, Ca, and K).

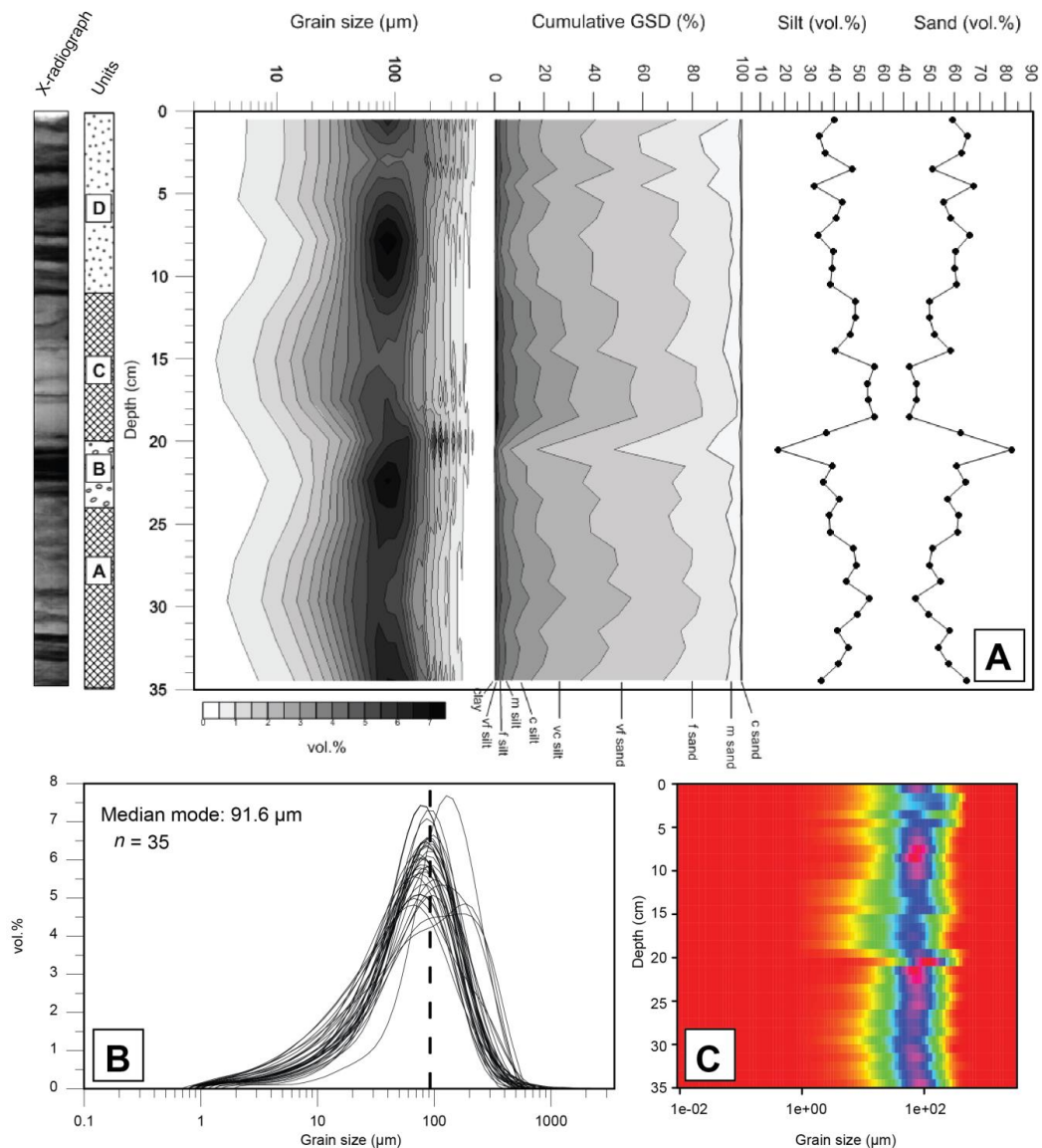


Figure 6: A) From left: GSD surface plot of MAD-313 (averages, $n=35$); cumulative plot; silt interval (2-63 μm); and sand interval (63-2000 μm). Note opposite trends between silt and sand. All values plotted as volume %. B) Grain-size frequency diagram of averages from all depths. Dashed line highlights median mode. Note normal distribution of the core GSD as opposed to the bimodal sediment trap distribution. C) Surface plot made in EMMAgeo package (Dietze and Dietze, 2013) implemented in the open-source statistical software R (R Development Core Team, 2012).

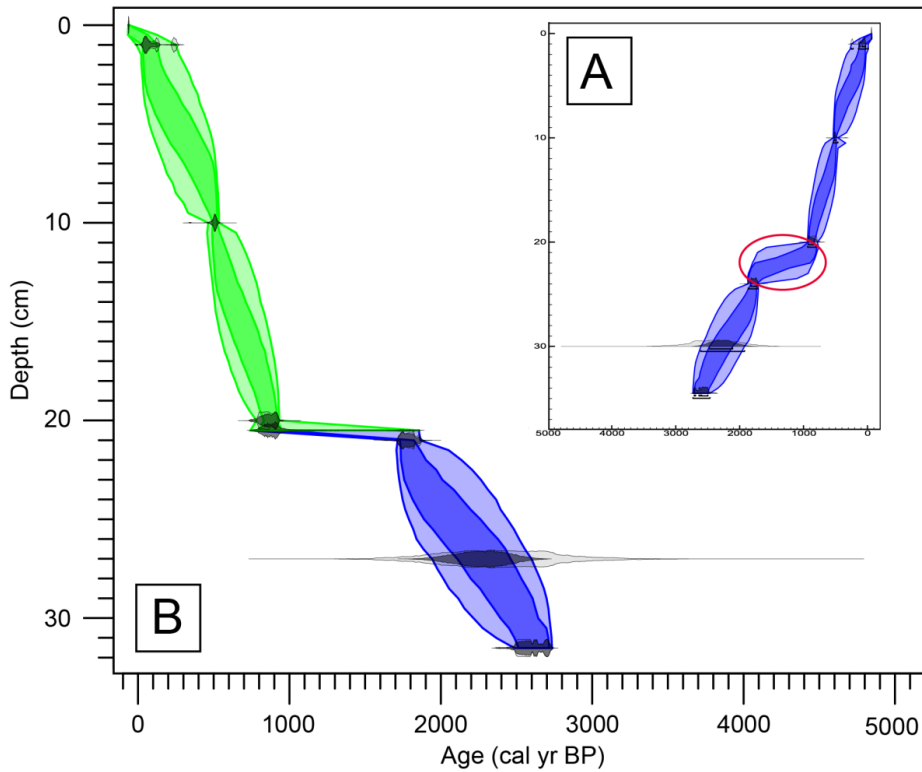


Figure 7: A) Original age-depth relationship for MAD-313. Individual calibrated ages distributions shown in grey shaded areas (1 and 2σ ; yielding darker and lighter grey shades, respectively). Red ellipse denotes Unit B and a change in sediment accumulation rates. B) Final age-depth relationship for MAD-113 constructed after omitting Unit B. The depth model curves are envelopes for the 1 and 2σ highest probability density ranges. Colour change indicates boundary between units C and A. Note reversed age-axis (x-axis) from A); depth scale is adjusted.

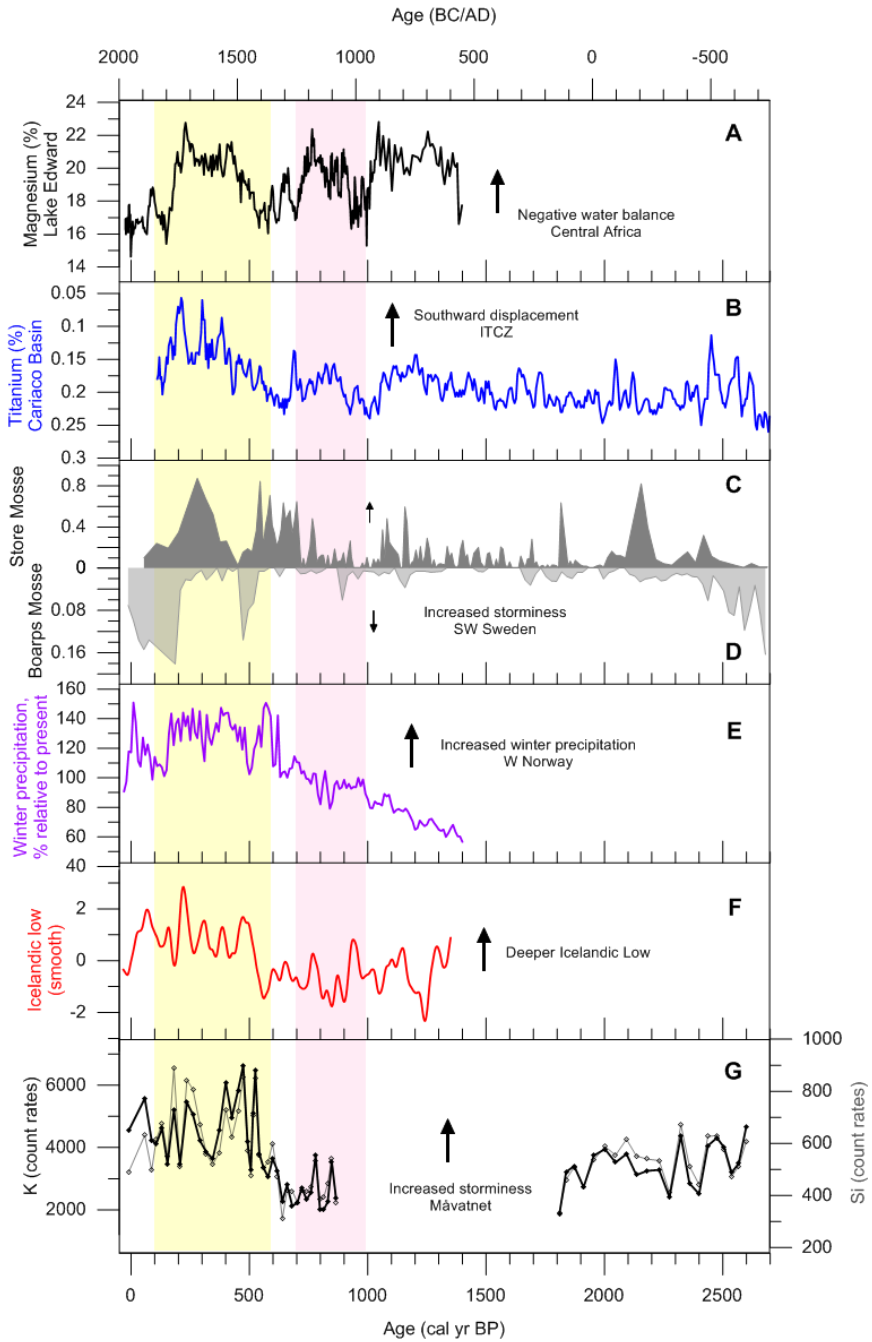


Figure 8: A) %Magnesium from Lake Edward, equatorial Africa (Russell and Johnson, 2007), B) %Titanium from the Cariaco Basin, offshore Venezuela (Haug et al., 2001), C) Aeolian sediment influx (ASI) at Store Mosse Bog, SW Sweden (De Jong et al., 2007) and D) ASI at

Boarps Mosse Bog, SW Sweden (Björck and Clemmensen, 2004) (data is clipped to y-axis maximum), E) Reconstructed winter precipitation, western Norway (Gjerde et al., 2016), F) Reconstructed strength of the Icelandic Low (Meeker and Mayewski, 2002), and G) Måvatnet storminess record (this study). The LIA (~600-100 cal yr BP) highlighted in yellow vertical bar; Medieval Climate Anomaly (MCA) (~1000-700 cal yr BP) highlighted in pink. BC/AD age scale on top.

Supplementary material

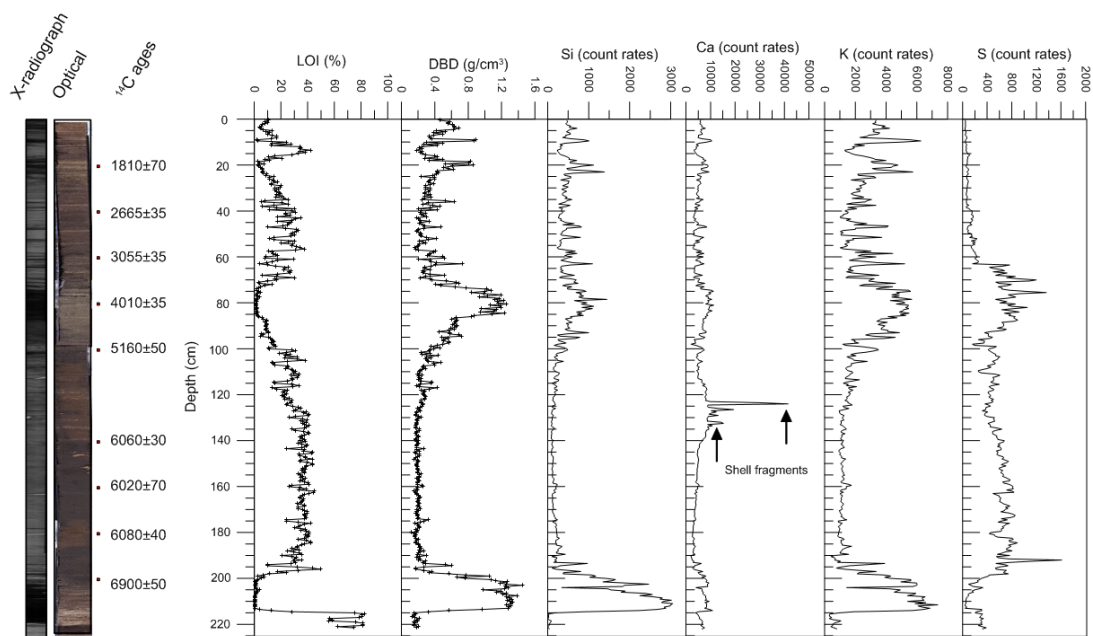
Laboratory analyses piston cores

The sediment cores MÅP-107, MÅP-207 and MÅP-307 were split lengthwise in the laboratory and one half of each core was stored for reference. Core surfaces were then carefully cleaned and photographed. Lithofacies and sedimentological structures and textures were described in detail before scanning and sub-sampling was initiated.

Standard procedures for estimating weight loss-on-ignition (LOI, %), dry bulk density (DBD, g/cm³) and water content (WC, %) were followed (Dean, 1974; Heiri et al., 2001), and MÅP-207 was sampled for this purpose every 0.5 cm ($n = 443$) using a syringe for fixed volume extraction (1 cm³). The samples were weighed and dried overnight at 105°C before being weighed again for DBD and WC. Following subsequent ignition at 550°C for one hour, the samples were cooled in a desiccator and reweighed for LOI. Down-core variations in surface magnetic susceptibility (MS) were measured on the split cores at 0.2 cm resolution using a Bartington MS2E point sensor.

Geochemical data and radiographic images were obtained using an ITRAX x-ray fluorescence (XRF) Scanner (Croudace et al., 2006) in EARTHLAB, Department of Earth Science, University of Bergen. Due to the core halves already being sub-sampled, we extracted core material from all core sections using u-channels prior to scanning. A molybdenum (Mo) x-ray tube was used for radiographic measurements, whereas XRF analyses were performed applying a chromium (Cr) tube, with a down-core resolution of 200 µm. Power settings of 30kV and 55 mA were used with a 10 s counting time.

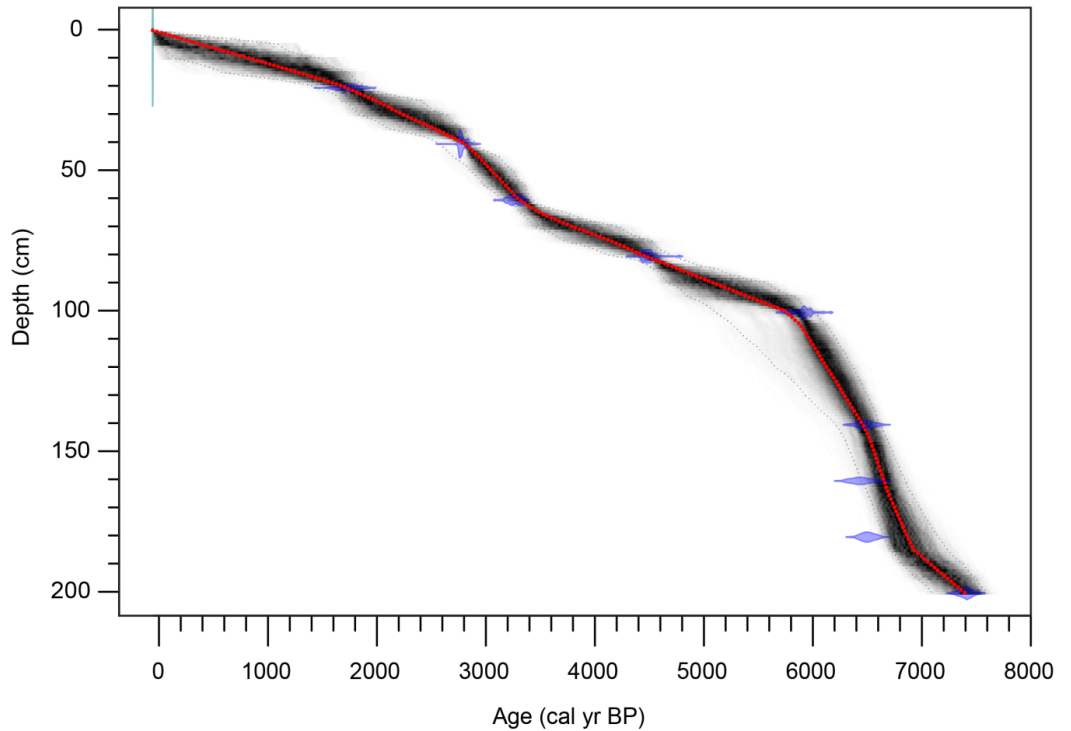
An age-depth relationship was established using the Bayesian framework calibration software code 'Bacon' (v. 2.2; Blaauw and Christen, 2011), applied into the open-source statistical software 'R' (v. 3.2.2; R Development Core Team, 2012). Radiocarbon ages are reported in calibrated radiocarbon years before present ('cal yr BP'; BP=1950) according to IntCal13 (Reimer et al., 2013).



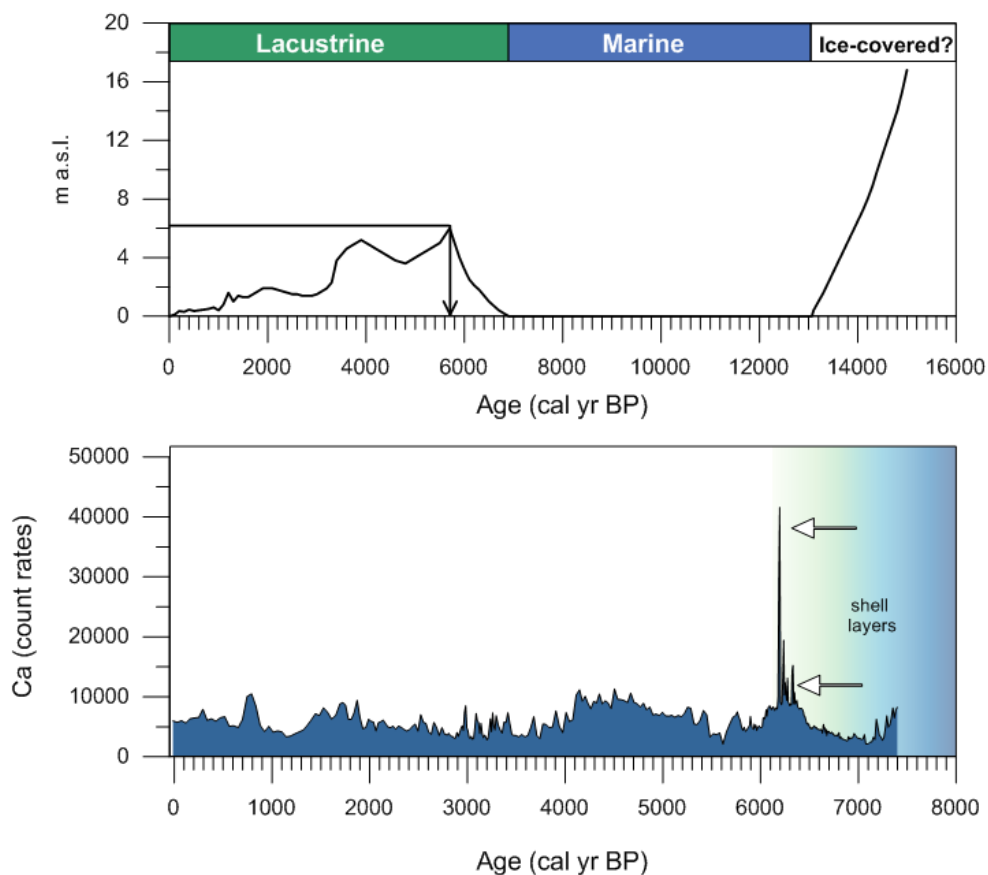
Supplementary Figure 1: Selected sediment variables for MÅP-207. XRF count rates are smoothed to 0.5 cm resolution. Arrows indicate spikes in Ca at depths with abundant shell fragments.

Supplementary Table 1: Radiocarbon ages MÅP-207. Lowermost 4 ages: marine.

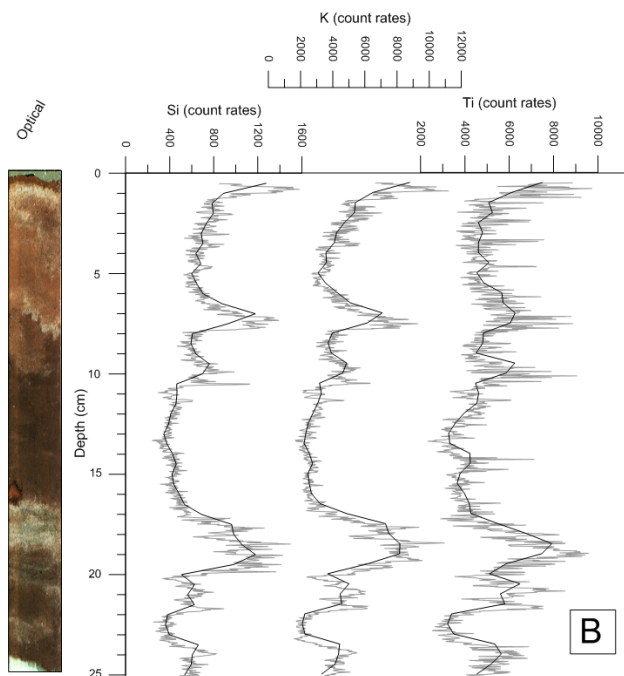
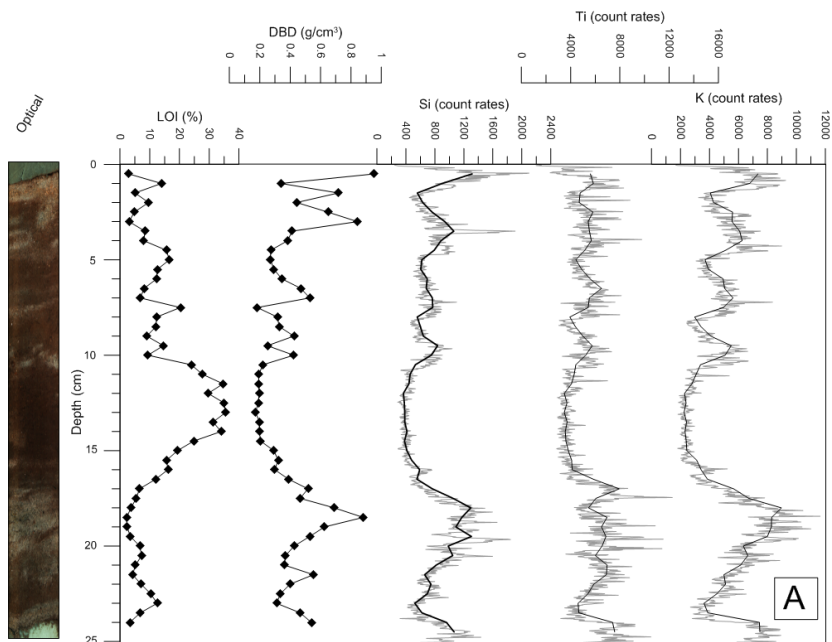
Lab. no.	Depth (cm)	Material	¹⁴C Age	Error (+/-)	Note
Poz-29125	20-21	Terrestrial plant remains	1810	70	0.18 mgC
Poz-29126	40-41	Terrestrial plant remains	2665	35	0.74 mgC
Poz-29127	60-61	Terrestrial plant remains	3055	35	
Poz-29128	80-81	Terrestrial plant remains	4010	35	
Poz-29119	100-101	Terrestrial plant remains	5160	50	0.59 mgC
Poz-29120	140-141	Terrestrial plant remains	6060	30	0.69 mgC
Poz-29121	160-161	Terrestrial plant remains	6020	70	0.28 mgC
Poz-29122	180-181	Terrestrial plant remains	6080	40	
Poz-29123	200-201	Terrestrial plant remains	6900	50	



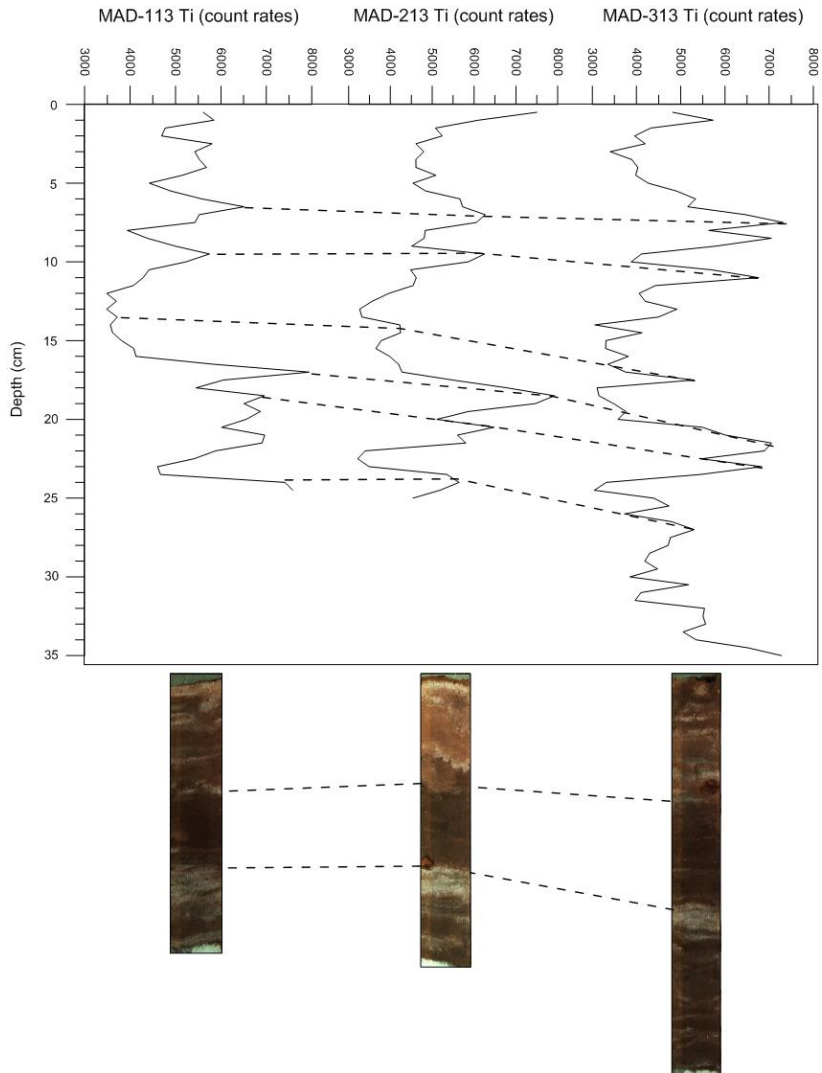
Supplementary Figure 2: Age-depth model for MÅP-207 constructed in ‘Bacon’. Ages are not extrapolated beyond the lowermost dated depth. As the 4 lowermost radiocarbon ages are extracted below shell-bearing layers (i.e., marine), these ages were corrected for reservoir effect applying the Marine13 calibration curve (Reimer et al., 2013). Individual calibrated ^{14}C dates in transparent blue, and ‘best’ age-depth model (red) is based on the weighted mean age for each depth (grey shaded area indicates 95% confidence interval).



Supplementary Figure 3: Top: sea-level displacement curve for Andøya (data compiled by: Møller, J. J., & Holmeslet, B. 1998 in software ‘Sealevel32, Sea Level change’, v. 3.51). Isolation age of Måvatnet indicated from shell-bearing layers (white arrows) reflected in MÅP-207 XRF Ca spikes (below). Blue shaded area denotes time of marine inundation. The uppermost shell-bearing layer likely reflects the Tapes transgression (Vorren and Moe, 1986), with an estimated age of ~6100 cal yr BP.



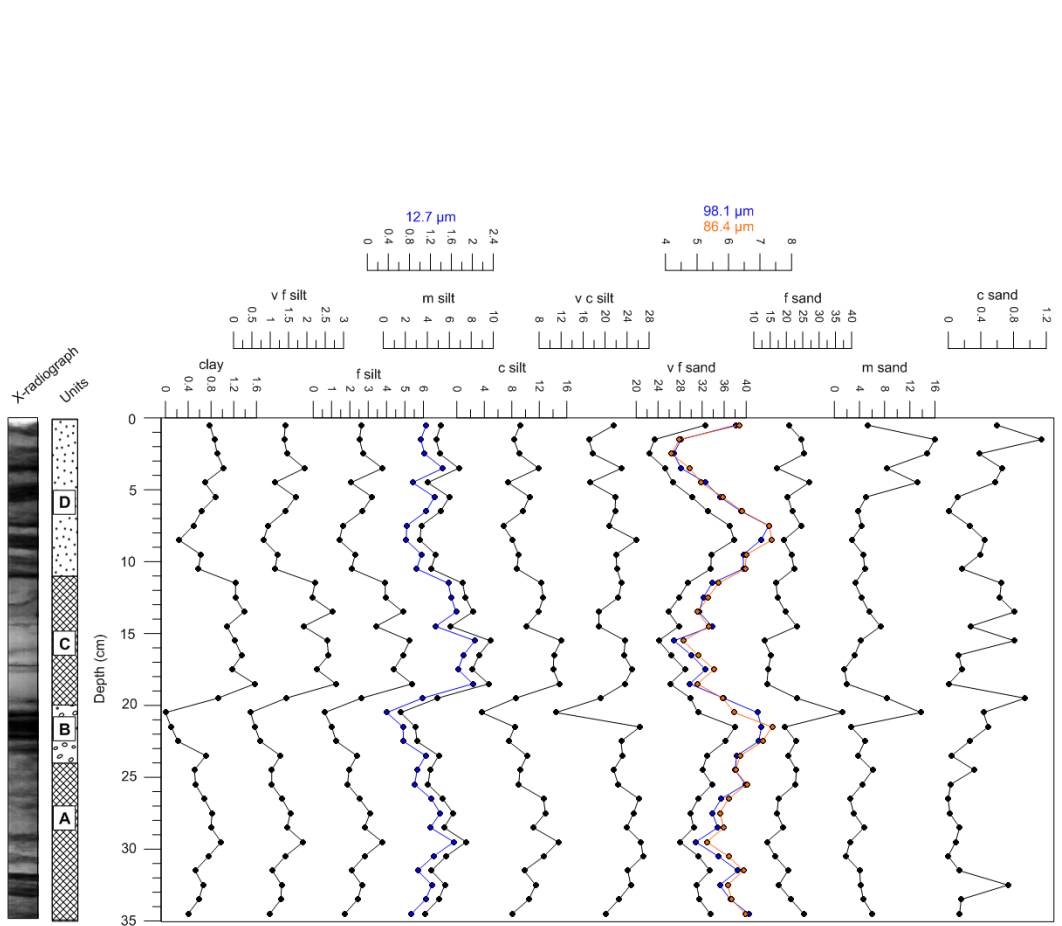
Supplementary Figure 4: A) Selected sediment variables from MAD-113. A) Selected sediment variables from MAD-213.



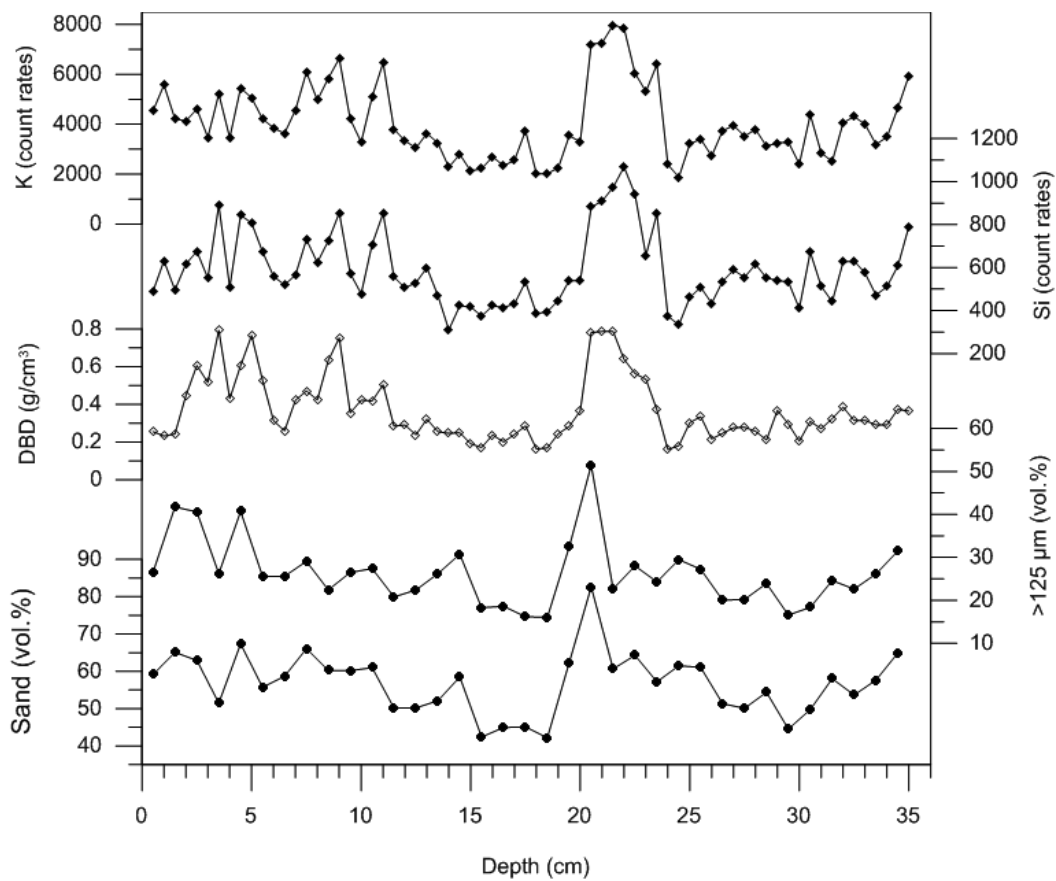
Supplementary Figure 5: Correlation of cores MAD-113, MAD-213 and MAD-313 based on visual and geochemical correlation (redox-insensitive XRF Ti count rates). MAD-313 displays the stratigraphically longest record, and is therefore chosen for GSD analysis. Further, it is apparent that all the short cores are relatively easily correlated, and we therefore assess that MAD-313 comprises the longest sedimentary record of sediment accumulation in Måvatnet and also is representative for sediment accumulation in Måvatnet.

Supplementary Table 2: PCA scores MAD-313.

	PCA 1	PCA 2	PCA 3	PCA 4
	55.4%	16.9%	11.9%	4.9%
LOI	-0.8866	0.0984	-0.2643	-0.2083
DBD	0.8785	-0.0142	0.3322	0.1449
Al	0.6699	-0.5089	0.1716	-0.1329
Si	0.873	-0.2285	0.3686	0.1168
K	0.9296	-0.2	0.2149	-0.1073
Ca	0.8877	-0.2425	0.2334	0.0931
Ti	0.7353	-0.4896	-0.2057	-0.2813
Mn	-0.6347	-0.0459	-0.6224	-0.2746
Fe	0.6565	-0.3969	-0.4157	-0.4102
Rb	0.8053	-0.2732	0.2151	-0.3313
Sr	0.8669	-0.024	0.3943	-0.0691
Clay	-0.6993	-0.3139	0.3074	-0.259
vf silt	-0.853	-0.0899	0.4174	-0.1957
f silt	-0.8709	-0.1422	0.4131	-0.1619
m silt	-0.8747	-0.2307	0.3908	-0.1265
c silt	-0.8198	-0.4754	0.2812	0.0477
vc silt	-0.3623	-0.8431	-0.0257	0.1506
vf sand	0.5359	-0.4361	-0.6206	0.0025
f sand	0.6814	0.6202	-0.235	-0.0718
m sand	0.3329	0.8456	0.261	-0.1343
c sand	0.1739	0.4954	0.2526	-0.5345



Supplementary Figure 6: Grain size distribution from MAD-313. The modes extracted from the sediment trap bimodal distribution are highlighted; 12.7 μm (blue) and 86.4 (orange)/98.1 (blue) μm. Very coarse sand and gravel are not plotted (very low values). All data plotted as volume %. Note that the majority of the sediment is situated within the very coarse silt – fine sand fraction, with very fine sand showing a smoothed signal.



Supplementary Figure 7: Comparison of K and Si XRF count rates, DBD (g/cm^3), grains $>125 \mu\text{m}$ and sand grains ($63\text{-}2000 \mu\text{m}$) (volume %) from MAD-313.

Supplementary Table 3: Correlation matrix of selected detrital parameters MAD-313.

	DBD	>125	sand	Si	K
DBD	1				
>125	0.451935	1			
sand	0.545141	0.879936	1		
Si	0.876854	0.321212	0.473986	1	
K	0.827536	0.397942	0.599034	0.927455	1

References Supplementary Material

- Blaauw, M., Christen, J.A., 2011. Flexible paleoclimate age-depth models using an autoregressive gamma process. *Bayesian Analysis* 6, 457-474.
- Croudace, I.W., Rindby, A., Rothwell, R.G., 2006. ITRAX: description and evaluation of a new multi-function X-ray core scanner. *Special Publication - Geological Society Of London* 267, 51.
- Dean, W.E., 1974. Determination of carbonate and organic matter in calcareous sediments and sedimentary rocks by loss on ignition: comparison with other methods. *Journal of Sedimentary Research* 44.
- Heiri, O., Lotter, A.F., Lemcke, G., 2001. Loss on ignition as a method for estimating organic and carbonate content in sediments: reproducibility and comparability of results. *Journal of Paleolimnology* 25, 101-110.
- R Development Core Team, 2012. R: A language and environment for statistical computing. R Foundation for Statistical Computing. R Foundation for Statistical Computing, Vienna, Austria.
- Reimer, P.J., Bard, E., Bayliss, A., Beck, J.W., Blackwell, P.G., Ramsey, C.B., Buck, C.E., Cheng, H., Edwards, R.L., Friedrich, M., 2013. IntCal13 and Marine13 radiocarbon age calibration curves 0–50,000 years cal BP. *Radiocarbon* 55, 1869-1887.
- Vorren, K., Moe, D., 1986. The early Holocene climate and sea-level changes in Lofoten and Vesterålen, North Norway. *Norsk geologisk tidsskrift* 66, 135-143.